Cells on Fire: Regulation of the NLRP3 inflammasome via endoplasmic reticulum and mitochondrial crosstalk

By

Denise Nicole Bronner

A dissertation submitted in partial fulfillment
of the requirements for the degree of
Doctor of Philosophy
(Microbiology and Immunology)
in the University of Michigan
2015

Doctoral Committee:

Associate Professor Mary X. D. O'Riordan, Chair
Associate Professor Yongqun He
Professor Gabriel Nuñez
Professor Malini Raghavan
Professor Michele S. Swanson

DEDICATION

I dedicate this dissertation to my parents, Shawn and Beatrice Bronner. Without them, I would have not pursued a life in science.

ACKNOWLEDGMENTS

First and foremost, I would like to thank my mentor, Dr. Mary O'Riordan for allowing me to join her lab after an awesome rotation during the summer of 2010. Over the past five years, Mary has been the most supportive and enthusiastic mentor. She has encouraged me to think critically by delivering criticism that was never sugar coated. Her unique mentoring style has served as a driving force that has led me to become a confident independent researcher. I thoroughly enjoyed being able to stop by her office and drop some data on her desk, talk about the latest movie or documentary, debate about the changes that need to happen in academia, or share a meal (hot wings were our favorite!). Even with her schedule becoming more and more hectic, Mary still allotted time for our one-on-one discussions. I hope that in the future I am at least half of the awesome scientist, mentor, and human being that Mary is.

I would also like to thank my thesis committee (aka Thesis League) for aiding in the development of my project and my growth as a scientist by providing thoughtful questions and comments. I want to thank Oliver for helping in the creation of this project and being an awesome co-mentor. I give thanks to Gabriel for reagents, cells, and great debate over whether the mitochondria are involved in inflammasome activation. I thank Malini for helping me think about immunology and cell biology in a meaningful way. I also would like to thank Michele for providing

insight into autophagy, and always giving great advice on presentation skills and career choices.

I want to give special thanks to my lab mates for they have had to put up with my crazy and energetic antics. Thanks to Basel for teaching new molecular techniques, for helping me with my mouse experiments, and having great debates on scientific papers as well as who is the most expensive in lab. Thanks to Karla for interesting conversations about life and providing great insight on my writing and presentations. Thanks to Marie-Eve for sharing her scientific knowledge and expertise with molecular techniques and writing. In addition, Marie-Eve helped with me keeping my lab bench clean (mostly through jokes) and sharing pictures of her beautiful children. I would also like to thank the most awesome undergraduate student ever, Jake. Jake you have grown so much and you have made mentoring extremely fun. I greatly appreciate you giving me insight into what it means to be a good mentor and for making me laugh a lot in lab. I do apologize for scaring you so much in the lab. I would also like to thank the Carruthers lab for sharing reagents, thoughts on experimental design, and for allowing me to be in your lab space. Mae, BigBean, Aric, Ou, and Olivia have been the best lab space mates ever. You all have listened to me tell jokes, share good news, and complain about the bad. In return, you guys have shared things about your life and made me feel welcomed and comfortable. I thoroughly enjoyed our conversations and I greatly appreciate you all showing me where I can buy ice cream. Vern would catch sometimes – thanks Vern for not throwing me out and letting me be me in your lab space as an *honorable Carrutherian* ☺.

I would also like to thank my collaborators (too many to list) who have provided mice, cells, reagents, insight into experiment design, and for providing comments on my manuscripts. I want to thank previous mentors for helping and encouraging me to pursue my dreams as well as providing critical assessments of my development. I would like to thank the lovely ladies in the Microbiology and Immunology Departmental office. Heidi, Margaret, Bonnie, Sheryl, and Marilyn, you guys are awesome and without you none of the administrative stuff would have happened. Additionally, you all have always made me feel welcomed and always put a smile on my face. I could tell that you all genuinely cared about my mental health and progression through this Ph.D. program. I want to thank my funding sources: Genetics Training Grant, ASM Robert D. Watkins Graduate Research Fellowship, Rackham Merit Fellowship, ASM student travel awards as well as Rackham graduate student travel awards. I want to also thank the individuals in ULAM technical services (Kaitlin Harvey and LaJuanda Carter) who provided technical assistance with some of my mouse experiments, Brian in the CLCI for helping me with 3-D reconstruction of mitochondrial networks, and Sasha at the MIL for training me in confocal microscopy. I would also like to thank PIBS, in particular Lori Isom, Michelle Melis, Josh Daniels, and Lisa Garber – you guys really helped me during my first year here at UM. I greatly appreciate all of your help and insight into resources on campus.

I am thankful for my friends who have provided the best support system a human being could ask for. Elizabeth (aka Lizbeth) you have been a great and beautiful friend who has provided amazing jokes, a shoulder to cry on, drinks, and

you were never afraid to tell me what I needed to fix. I like your rawness and it is great to see that another raw individual exists in the world. Olivia (aka The Big O), you have been an amazing friend – it has been hard trying to keep up with you when watching House of Cards but you are so good at not sharing information. Additionally, thanks for including me in your life and for helping me to understand my potential. Andrew (aka White Lightning/Captain America) and Jessica (aka Marquette Queen), you guys are awesome because you two have continued to be my friends even though you both know I have no filter. I greatly appreciate the happy hours and being able to share my life with you guys. To my girl Adele (aka Adele my Bell), I thank you for being my friend even though you are in another state – we have cried together as well as laughed together. We have shared many meals and I am so happy that even after all this time we are still in each other's life. I would also like to thank my friend Desmond (aka Dez) for providing jokes, great debates on movies and comics, as well as pushing me to pursue my dreams –now you are not the only Doctor!

Special thanks to my fiancé Nick (aka The Red Baron) – you have been my rock and greatest competitor in life. While pursuing your own Ph.D., you have provided me with support, laughs, and toxic fumes. With you, I have experienced great things and traveled to places I have never been before. Although we have our moments, we still are there for each other. We share the same values and passions in life. I love that we can play video games together and can be quite competitive without anyone getting their feelings hurt. I am lucky that our lives crossed and I hope you know that I *greatly appreciate and love you*. I want to thank

Nick's family (Melanie, Bruce, and Kyle) for welcoming me into the family. You guys have been awesome – from listening to me talk about my project to attending my talks at UM, and taking me on vacation to the Caribbean! I have never felt awkward in your home and I know that if I ever needed anything I could call on you guys. Kyle, you are the brother I never had and I greatly appreciate your jokes, especially the one about me having t-rex arms. Melanie and Bruce, I am so thankful that I will have you two as future in-laws!

Finally, I MUST acknowledge the contribution of two beautiful people – my mom and dad. Without you two, this work would not exist because I would not exist. You two made it possible for an inner city black girl to feel that anything is possible. From buying me science toys and books, to putting me in private school, you two sacrificed for me. You guys never made me feel that I could not be great especially in a field dominated by men. You guys have wiped my tears (and butt when I was a baby), bandaged my cuts/bruises, encouraged me, and provided constructive criticism over the years. Although you two are not scientists, you two still went above and beyond to get me into anything related to biology. You let me explore the world and be whatever I wanted to be. When I wanted a brother, you guys got me a dog (Pongo) and he was the best friend a child could have while growing up. Even though I disappointed you guys sometimes, you still told me that you were proud of me and still saw me as a star. My rawness, unwavering drive/passion for scientific endeavors, and stubbornness comes from you two. I am so fortunate to have parents like you because I did not choose you guys but

you two choose to have me. I love you guys and I hope that I can continue to make you proud.

TABLE OF CONTENTS

DEDICATION ii
ACKNOWLEDGMENTS iii
LIST OF TABLES xi
LIST OF FIGURES xii
ABSTRACT xiv

Chapter 1:
Endoplasmic reticulum and mitochondria: key regulators of cell fate and immunity 1
Endoplasmic Reticulum: central hub for signaling integration 2
UPR, the stress signaling headquarters 2
The ER integrates stress programs with host defense 5
Restoration of homeostasis via autophagy and apoptosis 7
Mitochondria: converting signaling into action 11
Cell fate hinges on mitochondrial membrane integrity 12
Mitochondria, one platform for inflammasome assembly 13
Mitophagy maintains the integrity of the mitochondrial network 17
Conclusions 20
References 24

Chapter 2:
Caspase-2 mediates a *Brucella abortus* RB51-induced hybrid cell death having features of apoptosis and pyroptosis 31
Abstract 31
Introduction 32
Results 36
Conclusions 47
Materials and Methods 53
References 59

Chapter 3:
ER stress activates the inflammasome via NLRP3-caspase-2 driven mitochondrial damage 64
Abstract 64

Introduction 65
Results 66
Conclusions 82
Materials and Methods 86
References 94

Chapter 4:
PERK suppresses inflammasome activity via Parkin-dependent mitophagy 99
Abstract 99
Introduction 99
Results 101
Conclusions 114
Materials and Methods 119
References 128

Chapter 5:
Perspective
Overview 132
Novel roles for non-inflammatory protein 133
Broader impact of these pathways in infectious and non-infectious conditions 134
Future Areas of Investigation
What is the fate of damaged mitochondria captured during mitophagy? 135
Why does mtROS increase when ROS-detoxifying mechanisms exist? 137
What role does calcium play in inflammation modulation? 138
What feature of HK RB51 is essential for PERK activation? 140
Conclusions and Significance of Thesis 142
References 144

Appendix 146

LIST OF TABLES

Table 2.1:
Cell death measurements in caspase-2 deficient and caspase-3 and -8 inhibited macrophages 37

Table 2.2:
Comparison of caspase-2-mediated cell death to classical apoptosis and pyroptosis 50

LIST OF FIGURES

Chapter 1:
1.1 Schematic of ER stress sensors ATF6, IRE1, and PERK 7
1.2 Illustration of the steps of autophagy 8
1.3 Mechanisms of mitochondrial outer membrane permeabilization 14
1.4 Mitophagy, the labeling and removal of damaged mitochondria 18
1.5 *Brucella* interacts with the ER 22

Chapter 2:
2.1 Caspase-2 drives both the intrinsic and extrinsic cell death pathways 39
2.2 Caspase-2 drives proinflammatory responses in RB51-infected macrophages 41
2.3 Pore formation does not contribute to RB51-induced cell death 44
2.4 Caspase-2 mediates caspase-3 and -8 activation in other contexts 46

Chapter 3:
3.1 IRE1 via TXNIP modulates RB51-induced inflammasome activation 68
3.2 ER stress-induced mitochondrial dysfunction drives IL-1β production 71
3.3 NLRP3 is required for RB51-induced release of mitochondrial contents 74
3.4 NLRP3 and caspase-2 are required for ER stress-induced inflammasome 76
3.5 NLRP3 controls mitochondrial dysfunction by a Bid dependent mechanism 78
3.6 NLRP3 and caspase-2 are required for caspase-1 activation during ER stress 81
3.7 Working model of IRE1-induced inflammasome activation 83

Chapter 4:
4.1 IL-1β processing, not priming, depends upon microbial viability 102
4.2 PERK suppresses IRE1-induced inflammasome activation 103
4.3 PERK inhibits IRE1-driven mitochondrial damage 106
4.4 PERK drives removal of damaged mitochondria via mitophagy 108
4.5 PERK-induced mitophagy is mediated by Parkin 111

4.6 PERK and Parkin mediate RSV-induced mitophagy 113
4.7 Mitophagy decreases RSV-induced inflammation *in vitro* and *in vivo* 115
4.8 PERK drives Parkin-mediated mitophagy to suppress the inflammasome 116

Appendix:

A1 Caspase-2 mediates RB51-induced macrophage cell death 147
A2 Caspase-3 and -8 are involved in RB51-induced cell death 148
A3 Caspase-1 aids in RB51-induced pore formation 149
A4 RB51 infection does induce IL-1β production but no cell death 150
A5 Chemical inhibitors do not affect bacterial uptake 151
A6 IRE1 is required for RB51-induced inflammasome activation 152
A7 IRE1 inhibition decreases bacterial killing *in vivo* 153
A8 IRE1 inhibition does not affect priming 154
A9 IRE1 is required for RB51-induced cytochrome *c* release 156
A10 Cyclosporin A treatment has no effect on bacterial uptake 157
A11 AIM2 is not required for ER stress-induced IL-1β production 158
A12 NLRP3, not ASC, is essential for RB51-induced mitochondrial dysfunction 159
A13 Inhibition of caspase-1 has no effect on bacterial uptake 160
A14 Caspase-2 mediated mitochondrial damage is triggered by IRE1 and NLRP3 161
A15 ER stress-induced caspase-2 mediates Bid truncation 162
A16 Bid is required for bacterial killing *in vivo* 163
A17 ER stress triggers weak priming of proIL-1β 164
A18 Amount of stress determines route of inflammasome activation 165
A19 Purity of mitochondrial fraction 166
A20 Both Live and HK RB51 induce IRE1 and ATF6 activation 167
A21 Deficiency in ATF4 leads to increased mitochondrial damage 168
A22 LC3b deficiency does not prevent fragmentation of the mitochondrial network 169
A23 PERK inhibition decrease Parkin transcription in RSV-infected BMDM 170
A24 PERK and Parkin suppress RSV-induced caspase-1 activation 171
A25 ATF4 knockdown efficiency in BMDM 172
A26 Damaged mitochondria are released into the extracellular space 173
A27 Sirt3 degradation occurs during infection 174
A28 PERK activation is not dependent upon microbial viability 175

ABSTRACT

Inflammation is a complex biological response to stress triggered by microbial infections. Although inflammation drives microbial clearance, if uncontrolled it leads to cellular damage and cell death. Previous studies have demonstrated that endoplasmic reticulum (ER) and mitochondrial stress programs can contribute to immunity by mediating production of inflammatory cytokines; however, the regulatory mechanisms are unclear. By utilizing *Brucella abortus* cattle vaccine strain RB51, we elucidated how ER and mitochondrial stress mediate inflammatory responses and the eventual fate of infected cells. Our initial findings revealed that RB51-induced programmed cell death (PCD), mediated by caspase-2-induced mitochondrial damage, led to activation of proapoptotic caspase-3 and -8. Notably, this caspase-2 mediated PCD was accompanied by the production of proinflammatory cytokines, TNFα and IL-1β, a phenomenon associated with pyroptosis, not PCD. These observations led us to further investigate how caspase-2 could regulate inflammation and proinflammatory cell death. As early as 2 hours post infection, RB51 triggered activation of ER stress sensor, IRE1, leading to increased ROS levels in the mitochondrial network. This sharp increase in mitochondrial ROS elicited the recruitment of inflammasome component NLRP3 and caspase-2 to the mitochondrial network, which triggered mitochondrial damage. Damage promoted release of mitochondrial danger signals

into the cytosol and the activation of the NLRP3-ASC-caspase-1 inflammasome, which processes the inflammatory cytokine, IL-1β. Damaged mitochondria are usually tagged for removal by a mitochondria-specific form of autophagy called mitophagy. We observed that killed RB51 activated a second ER stress sensor, PERK, which suppressed IL-1β production. Upon PERK activation, the downstream transcription factor ATF4 initiated transcription of Parkin, a key regulator of mitophagy, which decreased mitochondrial damage signals and activation of the inflammasome. We have discovered that the partnership between the ER and mitochondria is essential for mediating inflammatory responses and determining cell fate. By fine-tuning the immune response via selective activation of ER stress sensors, we have laid the groundwork for therapeutic targeting of these regulators in inflammatory diseases associated with cellular stress.

Chapter 1

Endoplasmic reticulum and mitochondria: key regulators of cell fate and immunity

Introduction

Exposure to microbial pathogens triggers contextual signals that result in host immune responses, defining the outcome of infection. Activation of cellular stress programs by infection can trigger the secretion of microbicidal effectors and inflammatory mediators. These cellular stress responses protect the cell against unfavorable conditions by minimizing damage and maintaining host tissue integrity. If cellular stress remains unresolved, these stress programs can initiate cell death, thus limiting microbial spread and replication. Two essential organelles, the endoplasmic reticulum (ER) and the mitochondrial network, are key platforms for sensing and signaling cellular stress. Unresolved or prolonged ER and mitochondrial stress are implicated in many inflammatory or degenerative diseases. Although key proteins in these stress pathways have been well characterized, their crosstalk with innate immune signaling and their role in the regulation of host defense are less clear. Recent studies, highlighted in this introductory chapter, emphasize the emerging importance of ER and mitochondrial stress in infection-induced inflammation.

Endoplasmic Reticulum: central hub for signaling integration

The endoplasmic reticulum (ER) is a dynamic organelle involved in lipid production, protein translational modification and protein folding. Stress stimuli such as nutrient deprivation or infection can perturb normal ER function and lead to an accumulation of misfolded proteins within the ER, triggering the Unfolded Protein Response (UPR) [1]. UPR activation begins with dissociation of the ER stress chaperone BiP (GRP78) from three UPR stress sensors: ATF6, IRE1, and PERK (Fig. 1.1). The unfolded proteins sequester BiP, allowing for the three stress sensors to activate signaling pathways aimed at relieving ER stress [2]. These three UPR sensors separately regulate the expression of chaperones, cytokines, cell death components, as well as translational attenuation. Malfunctions in the ER stress response caused by aging, mutations, or environmental factors (e.g., infection) can result in various pathologies such as inflammatory and neurodegenerative disorders.

UPR, the stress signaling headquarters

ATF6: an ER-responsive transcription factor

Activating transcription factor 6 (ATF6) is localized to the ER during unstressed conditions. Under stress conditions, BiP dissociation allows transport of ATF6 to the Golgi apparatus where it is processed by site 1 and 2 proteases (S1P and S2P) [3, 4]. Upon cleavage, ATF6 translocates to the nucleus resulting in the increased expression of endoplasmic reticulum associated protein degradation (ERAD) encoding genes as well as XBP1, a downstream target of

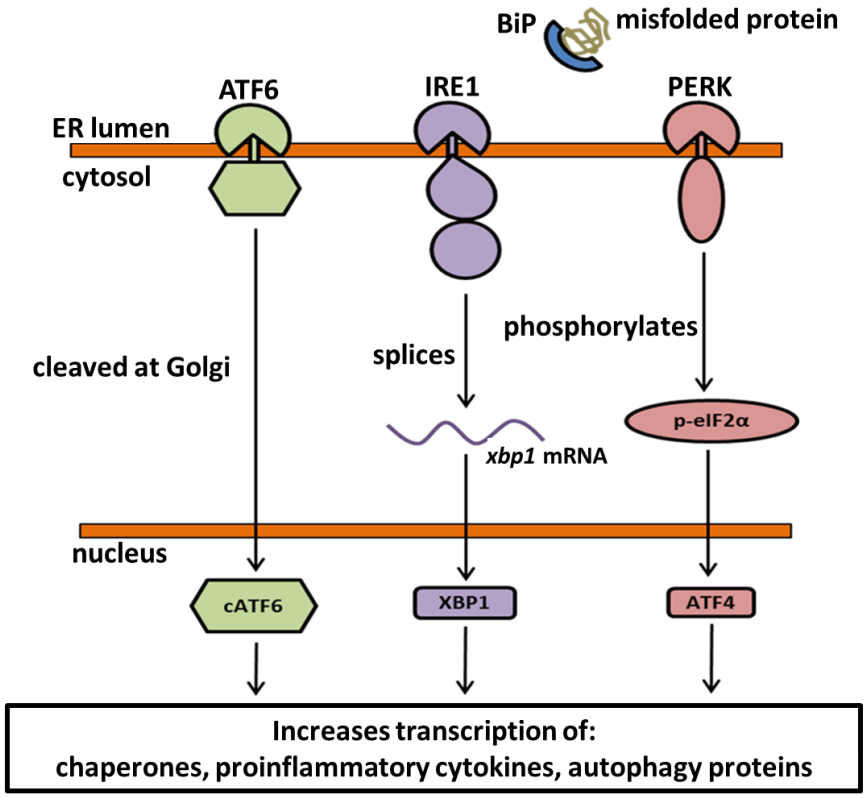

Figure 1.1: Schematic of ER stress sensors ATF6, IRE1, and PERK. Accumulation of misfolded or unfolded protein aggregates in the ER lumen, leads to activation of three ER transmembrane proteins, PERK, IRE1, and ATF6. BiP, an ER chaperone, normally is bound to the stress sensors and keeps them inactive. Accumulation of misfolded proteins triggers BiP dissociation from them to assist with protein folding thus triggering activation of the 3 stress pathways. Upon activation, PERK phosphorylates eIF2α which inhibits global protein synthesis and reduces the protein load in the ER lumen. ATF4 expression increases upon eIF2α phosphorylation and translocates to the nucleus allowing for transcription of UPR target genes. These genes include CHOP, a proapoptotic transcription factor that results in cell death if ER stress conditions persist, and GADD34, which acts as a negative regulator of the PERK pathway by dephosphorylating eIF2α. Active IRE1 splices XBP1, a mRNA encoding a transcription factor that can lead to upregulation of ER chaperones and other UPR target genes. ATF6 activation leads to its translocation to the Golgi where it is sequentially cleaved by site 1 and site 2 proteases. This leads to the release of the N-terminal ATF6 fragment which translocates to the nucleus and activates UPR target genes. In addition to UPR target genes, these three sensor can also increase expression of proinflammatory cytokines (e.g. IL-6 and TNF) as well as autophagy proteins – both of which contribute to infection resolution.

IRE1 [5]. The leucine-zipper domain of ATF6 allows for interaction with the ER stress response element (ERSE) located in the promoter of UPR-responsive genes.

IRE1: Regulator of mRNA and protein degradation

Upon BiP dissociation, Inositol-requiring Enzyme 1 (IRE1), located in the ER membrane, dimerizes and autotransphosphorylates, activating its kinase and endoribonuclease domains. The endoribonuclease domain splices an unusual cytoplasmic mRNA encoding X-box binding protein 1 (XBP1). This allows for translation of an active XBP1 transcription factor that upregulates UPR-related genes, e.g., that mediate the ER associated degradation pathway (ERAD) [6, 7]. Additionally, XBP1 also promotes ER membrane expansion by increasing expression of genes involved in phospholipid biosynthesis, thus relieving stress. Parallel to ERAD, IRE1 also triggers regulated IRE1-dependent decay, (RIDD) [8], a process that specifically degrades mRNAs encoding ER-localized proteins, which prevents protein delivery to the stressed ER. Basal RIDD is necessary for ER homeostatic maintenance; however, increased RIDD activity during stress conditions can induce pro-apoptotic pathways.

PERK: Suppressor of global translation

Protein kinase RNA-like ER kinase (PERK) autophosphorylates its cytoplasmic kinase domain when BiP dissociates. After activation, PERK phosphorylates eukaryotic translation-initiation factor 2 alpha (eIF2α), preventing the exchange of GDP for GTP that is necessary for eIF2α activation [9]. Preventing

eIF2α activation reduces global translation, allowing a subset of genes involved in ER stress response, autophagy, apoptosis, amino acid metabolism, and antioxidant responses to be preferentially regulated. A downstream target of eIF2α, activating transcription factor 4 (ATF4), mediates transcriptional induction of these genes [10]. Sustained PERK signaling upregulates the pro-apoptotic transcription factor C/EBP-homologous protein (CHOP). CHOP facilitates the decrease in expression of B-cell lymphoma 2 (Bcl-2), a protein that interacts with proapoptotic proteins (e.g., Bax and Bak), thus preventing cell death [11].

The transcriptional program controlled by these three stress sensors results in upregulation of stress chaperone proteins to aid in folding proteins, as well as to trigger protein and mRNA degradation to prevent further accumulation of misfolded proteins. The initial program triggered by these three sensors is pro-survival; however, if the stress is not resolved, these sensors can initiate a pro-apoptotic program leading to cell death. Recent advances have shown that, in addition to regulating cell survival, ER stress can promote innate immune responses to combat microbial infections.

The ER integrates stress programs with host defense

Recent evidence has revealed that ER stress is involved in inflammatory responses that aid in infection resolution, as well as tissue damage [12, 13]. All three ER stress sensors (IRE1, ATF6, and PERK) can participate in upregulating inflammatory processes. The UPR sensors enhance activation of NF-κB, a transcription factor that regulates expression of proinflammatory cytokines, via different mechanisms. Toll-like receptor activation of XBP1 increases transcription

of proinflammatory cytokines IL-6, TNFα, and IFNβ in response to LPS treatment [13]. Notably, transcription of the proinflammatory cytokine IL-1β is not dependent upon the IRE1-XBP1 axis. In contrast to IRE1, PERK increases cytokine levels by suppressing translation of IκB thus allowing NF-κB to translocate to the nucleus and induce transcription of proinflammatory cytokines [14]. Additionally, PERK-induced CHOP increases transcription of another proinflammatory cytokine, IL-23. Similar to IRE1 and PERK, ATF6 can also enhance NF-κB activation, although the mechanism is not currently known [15].

Although ER stress-induced inflammation can be protective and aids in the clearance of microbial pathogens, it can also be detrimental to the host and exacerbate some inflammatory diseases. For instance, ER stress can contribute to the progression of Type 2 diabetes by suppressing insulin receptor signaling [16]. ER stress can also induce cell death in intestinal epithelial cells, Paneth cells, and goblet cells, thus increasing inflammation in inflammatory bowel diseases (IBDs), such as Crohn's disease and ulcerative colitis [17, 18]. Furthermore, ER stress-induced inflammation has been implicated in the progression of cystic fibrosis and cigarette smoke-induced chronic obstructive pulmonary disease [19], both of which are chronic inflammatory airway diseases. There is evidence supporting the notion that ER stress-induced inflammation can promote the pathogenesis of some chronic diseases such as Type 1 and 2 diabetes, heart disease, Alzheimer's disease, and Parkinson's disease [20]. Although ER stress can aid in the progression of inflammation, ER stress has also been linked to autophagy, a cellular process that dampens inflammatory responses [21]. Thus,

further study of ER stress to tease out the complex mechanisms that link this program to inflammation is warranted.

Restoration of homeostasis via autophagy or apoptosis

The ER stress response is a major pivot point that determines whether a cell will survive or die in response to stress. During ER stress, the UPR program promotes restoration of ER homeostasis. If homeostasis cannot be restored, chronic UPR stress signaling eventually results in programmed cell death, in the form of apoptosis. To delay apoptosis, the UPR can trigger autophagy, a pro-survival dynamic process where cellular components are sequestered by double-membrane autophagosomes for lysosomal degradation (Fig. 1.2). These cellular components can include proteins, damaged organelles, and microbial pathogens. Efficient sequestration and clearance of damaged cellular or non-self components are crucial for cell survival as well as function.

Initiation of autophagy begins with the formation of the phagophore, a process mediated by the UNC51-like kinase (ULK1) and Beclin-1 initiation complex. The interaction between Beclin-1 and Bcl-2, an anti-apoptotic factor, prevents assembly of the phagophore, thus inhibiting autophagy [22]. Once initiation occurs, the Atg5-Atg12-Atg16L complex and LC3-II promote elongation and engulf the designated cargo. This new structure is called the autophagosome, which subsequently fuses with the lysosome, leading to degradation of the interior cargo.

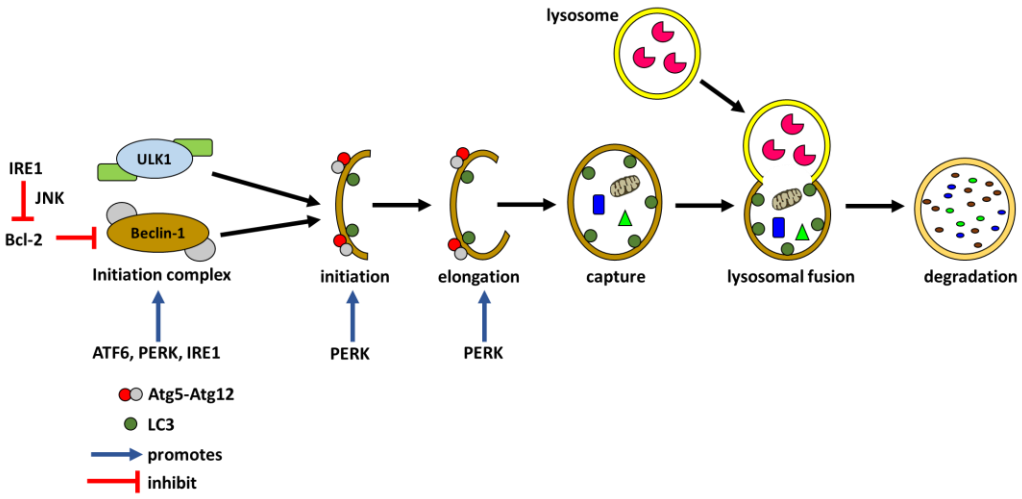

Figure 1.2: Illustration of the steps of autophagy. Activation of ULK1 and Beclin-1 complexes in response to certain signals initiates isolation membrane and the formation of phagophore. The Atg protein complex and LC3 promote the elongation and capture of cytosolic cargos (e.g. protein and organelles), leading to the formation of autophagosome. Subsequently, lysosome fuses with the autophagosome leading to degradation of the cytosolic cargo. Pro-apoptotic BCL-2 inhibits autophagy by interacting with Beclin-1. UPR sensors can trigger autophagy by promoting activation of the initiation and elongation complexes. IRE1 triggers autophagy by activating JNK thus leading to phosphorylation and dissociation of Bcl-2 from Beclin-1. Moreover, PERK and IRE1 mediate Beclin-1 and ULK1 transcription whereas ATF6 triggers phosphorylation of Beclin-1 thus triggering Beclin-1 dissociation from Bcl-2. PERK promotes elongation of the phagophore by inducing upregulation of Atg proteins and triggering LC3 conversion. This schematic was adapted from Kang et al. Cell Death Differ, 2011. 18(4):571-80.

The three UPR sensors regulate many of the autophagic proteins through different mechanisms. Activation of the PERK-eIF2α axis induces Atg12 upregulation, conversion of LC3-I to LC3-II, and subsequently facilitates autophagosome formation [23]. Moreover, PERK-induced ATF4 and CHOP regulate LC3, Atg5, and ULK1 transcription, further demonstrating a role for PERK in autophagy initiation and elongation [24]. IRE1 recruits tumor-necrosis factor receptor associated factor 2 (TRAF2), thus triggering JNK activation. JNK phosphorylates Bcl-2, which promotes its dissociation from Beclin-1 and leads to subsequent autophagy induction [25, 26]. Besides regulating activation, IRE1 can also modulate Beclin-1 expression through XBP1. Lastly, recent evidence has uncovered a role for ATF6 in autophagy induction through death-associated protein kinase 1 (DAPK1). DAPK1 promotes autophagy by phosphorylating Beclin-1, dissociating it from autophagy negative regulator Bcl-2 [27]. These data demonstrate an intricate redundancy in ER stress-induced autophagy. Autophagy occurs throughout the life of a cell, working to maintain or restore metabolic homeostasis, and may be a critical determinant in ER stress-induced cell survival or death.

If restoration of homeostasis is not achieved, IRE1-induced JNK activation triggers activation of the proapoptotic protein BIM while deactivating the antiapoptotic protein Bcl-2 [26], thus committing the cell to apoptosis. Phosphorylation of Bcl-2 triggers dissociation from BAX and BAK, two proapoptotic proteins. Upon release and activation, BAX and BAK form an oligomeric pore in the outer mitochondrial membrane, facilitating the release of cytochrome *c* into the

cytosol and activation of proapoptotic caspases [28]. Similar to IRE1, CHOP-induced apoptosis involves interaction with members of the Bcl-2 family of proteins. One such interaction involves transcriptional downregulation of Bcl-2, thus preventing the expression of apoptosis repressors. CHOP can also induce the transcription of BIM, which plays a role in mitochondrial-mediated apoptosis. BIM serves as a death ligand and specifically interacts with certain antiapoptotic Bcl-2 protein members, which leads to apoptosis induction [26].

A second mechanism of ER stress-induced apoptosis involves calcium signaling. ER stress is accompanied by alterations in calcium levels due to calcium leakage or efflux from the ER [29]. CHOP-dependent activation of the ER oxidase 1α triggers ER calcium release by activating the ER calcium channel IP_3R [30]. Cytoplasmic calcium activates the calcium-sensing enzyme CaMKII, which in turn triggers downstream signaling. Moreover, excess cytosolic calcium is absorbed into the matrix of mitochondria, leading to changes in membrane potential, as well as promoting the transfer of cardiolipin from the inner to outer mitochondrial membrane (a signal for targeted insertion of proapoptotic Bcl-2–family proteins Bid and Bax into membranes) [31]. Besides affecting mitochondria, ER-induced calcium release alters phospholipid scramblases that transfer phosphatidylserine, a lipid that serves as a signal for clearance of apoptotic cells by phagocytosis, to the outer leaflet of the plasma membrane.

Together, these studies illustrate that the ER can recruit mitochondria to aid in its apoptotic program. This is not surprising because (a) the ER and mitochondria share close contacts throughout the cytosol [32], and (b) many

apoptotic proteins between the ER and mitochondria overlap [33]. Due to the close proximity of these two organelles, crosstalk is quite frequent and can influence the stress level within each organelle. Communication between the ER and mitochondria takes place at specialized contact sites called mitochondrial associated membranes (MAMs) [33]. At the MAMs, calcium is released from the ER through the IP_3R channel and is taken up by the calcium channel VDAC located on the outer mitochondrial membrane [34, 35]. Calcium transfer [36] between these two organelles is important for cell metabolism and intracellular calcium signaling. Any alterations in calcium transfer (mitochondrial calcium overload, deficiency in ER calcium leakage, etc.) can have profound effects on the cell and can trigger cell death or autophagy [37]. Thus, the integration of mitochondrial signaling pathways appears to contribute to ER-mediated cell fate decisions.

Mitochondria: converting signaling into action

Cells activate multiple mechanisms to re-establish homeostasis and to repair stress-induced molecular damage. Mitochondria are involved in the response of cells to a wide number of perturbations including, but not limited to, oxidative stress and pathogen invasion. Furthermore, mitochondria can be both the substrate of autophagic degradation (mitophagy [38]) or spared by the autophagic machinery to ensure energy production during stress. Similar to the ER, mitochondria are particularly sensitive to endogenous stress and are another major sensor of environmental stress. During mitochondrial stress, the mitochondrial membrane depolarizes, reactive oxygen species (ROS) production increases, and mitochondrial contents can be released into the cytosol to act as

danger signals. Several human diseases, including neurodegenerative diseases and cancer, are associated with mitochondrial dysfunction and increased ROS damage [39-42]. To promote survival under such conditions, mitophagy prevents the accumulation of nonfunctional and damaged mitochondria that contribute to human pathologies.

Cell fate hinges on mitochondrial membrane integrity

Mitochondria are the main site of ATP production and are sensitive to conditions that might disturb membrane potential. In healthy mitochondria, a high proton gradient, or membrane potential ($\Delta\psi_m$), exists across the mitochondrial inner membrane due to protons pumped into the intermembrane space by the respiratory chain protein complexes located in the inner membrane [43]. The proton pumping occurs as a result of the electron transport chain (ETC), which provides free energy for transferring protons against their electrochemical gradient. In addition to proton pumping, the ETC also mediates ATP production and oxygen consumption in mitochondria, a process called oxidative phosphorylation [44]. Defective oxidative phosphorylation reduces metabolic capacity, which is a sign of mitochondrial stress. Perturbations in oxidative phosphorylation can lead to reduced ATP production, depolarization of the inner membrane, and excessive reactive oxygen species (ROS) production [44].

Inner mitochondrial membrane depolarization induces opening of the mitochondrial permeability transition pore (MPTP) [45]. This pore is a protein complex consisting of VDAC, cyclophilin D (CypD), and adenine nucleotide translocase that, when opened, allows small hydrophilic molecules (e.g., calcium

ions and ATP) to cross the mitochondrial membrane in response to membrane depolarization. The influx of calcium ions causes mitochondrial swelling, and eventually the outer membrane ruptures, allowing mitochondrial contents to leak into the cytosol [46, 47]. Alternatively, release of mitochondrial contents can be induced upon pore formation in the outer membrane.

Proapoptotic Bid mediates oligomerization of two pore forming proteins, BAK and BAX, in the outer mitochondrial membrane [28]. Activation of Bid can be triggered by several host proteases, including caspase-8, cathepsin, and calpain, with caspases predominantly cleaving Bid during apoptosis. Release of mitochondrial intermembrane space (IMS) proteins into the cytosol generally triggers cell death (Fig. 1.3) [47]. IMS proteins (e.g., cytochrome *c*, SMAC, OMI, APAF-1) can activate proapoptotic proteins in the cytosol leading to apoptosis. Notably, cytochrome *c* release drives the assembly of the apoptosome [48, 49], a multiprotein complex that cleaves and activates procaspase-9. Upon activation, caspase-9 cleaves procaspase-3, resulting in the execution of apoptotic cell death [48, 49]. These observations indicate that proper regulation of mitochondrial membrane potential is critical for viability of the cell as well as the organism as a whole.

Mitochondria, one platform for inflammasome assembly

Besides triggering cell death, outer membrane rupture can also trigger inflammation due to the release of mtROS and mtDNA. These two mtDAMPs can activate inflammasomes, large immune signaling machines that are responsive to microbial pathogens and endogenous stressors [50, 51] and that activate the

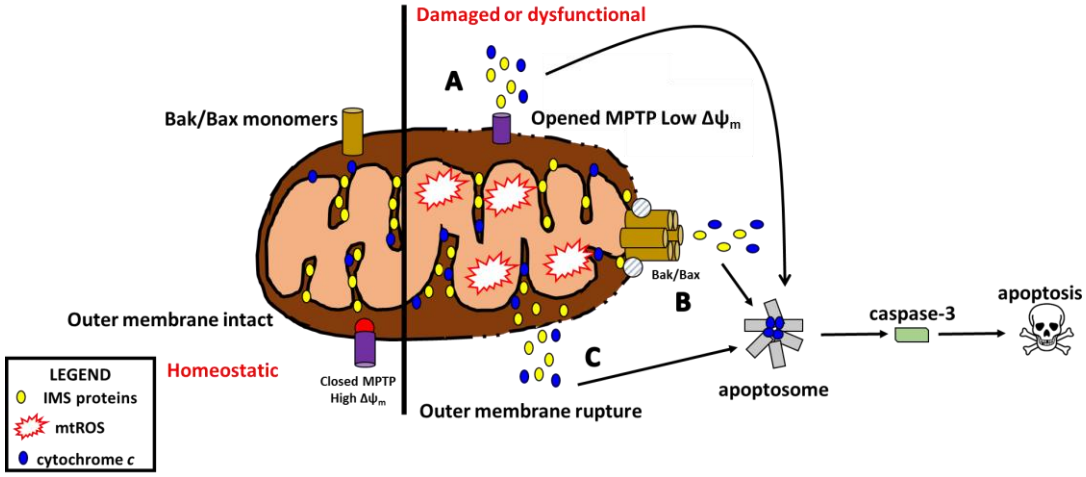

Figure 1.3: Mechanisms of mitochondrial outer membrane permeabilization. During homeostasis, mitochondria maintain high membrane potential (Δψm), have an intact outer membrane, and IMS proteins (e.g. cytochrome *c*) are retained. In the presence of an apoptotic signal, Δψm drops significantly, leading to the release of IMS proteins by: (A) sustained opening of the mitochondrial permeability transition pore (MPTP), (B) Bid-mediated oligomerization of Bak and Bax on the outer mitochondrial membrane or (C) rupture of the outer mitochondrial membrane. Once cytochrome c is released into the cytosol, it interacts with Apaf-1 and caspase-9 to form the apoptosome, a multiprotein complex that activates caspase-3 and induces apoptosis (programmed cell death). This schematic was adapted from Bronner et al. EMBO J, 2014. 33(19):2137-9.

potent proinflammatory cytokines, interleukin-1β (IL-1β) and IL-18 [51]. Canonical inflammasomes are multiprotein complexes that consist of an inflammasome sensor, the adaptor protein ASC, and caspase-1. Once formed, the inflammasome triggers caspase-1 induced proteolytic processing of proIL-1β and proIL-18. Microbial infections and some environmental stress conditions can trigger activation of the inflammasome [52, 53]. The NLRP3 inflammasome sensor is unusual because its activation is associated with diverse stress conditions, such as excessive mtROS, lysosomal damage, ER stress, or mitochondrial damage [54, 55], although whether these stresses employ a common ligand to activate NLRP3 is a question that is actively debated.

ROS produced by mitochondria can activate the NLRP3 inflammasome, a process that occurs at MAMs [55], possibly concomitant with the cytosolic release of mtDNA [46, 47]. Mitochondria are thought to be important for NLRP3 inflammasome activation in response to various noninfectious agents, including uric acid and silica [56]. MtROS production induced by specifically inhibiting Complexes I and III (protein complexes of the ETC) leads to NLRP3 inflammasome activation [57]. Increased ROS levels increase the association of NLRP3 with thioredoxin-interacting protein (TXNIP) [58]. Typically, TXNIP is constitutively bound to the oxidoreductase thioredoxin 1 (TRX1). Upon an increase in mtROS concentration, this complex dissociates and TXNIP binds to and activates NLRP3 once it translocates to the mitochondria [59, 60]. These observations suggest that mitochondrial-associated TXNIP might aid in the release of mitochondrial contents, thus increasing the chances for inflammasome activation. Permeabilization of the

outer mitochondrial membrane not only leads to the release of cytochrome *c,* but also mtDNA into the cytosol. During mitochondrial stress, ROS levels rapidly increase, leading to oxidation of proteins and mtDNA. Studies have shown that oxidized mtDNA directly binds to NLRP3 leading to inflammasome formation and activation [61, 62]. Additionally, macrophages lacking mtDNA were severely deficient in IL-1β production when treated with LPS and ATP, potent inflammasome stimuli [62]. Studies have suggested that mtDNA may also trigger activation of the AIM2 inflammasome. AIM2 is a large cytosolic protein that senses and binds to dsDNA [63, 64]. Upon binding, a conformational change is induced promoting oligomerization of the AIM2 inflammasome. Transfection of mtDNA into macrophages leads to AIM2 activation and IL-1β production [62], and the introduction of DNase I into the cytosol prevented IL-1β production in macrophages. These data show that mitochondrial contents can serve as important mediators of inflammation. In addition to providing inflammasome-activating ligands, mitochondria can also act as a platform where inflammasome complexes can oligomerize. In untreated macrophages, NLRP3 resides in the cytosol in an inactive state. Danger signals induce NLRP3 oligomerization and recruitment to mitochondria by interaction with the mitochondria-associated adaptor protein MAVS [65]. Mitochondria-associated NLRP3 then promotes recruitment of the cytosolic adaptor protein ASC and caspase-1, leading to cleavage of pro-IL-1β to its active, secreted form [66].

Although many pathophysiological conditions and chemically unrelated stimuli (e.g., ROS, toxins, uric acid, etc.) activate the NLRP3 inflammasome, few

studies have highlighted a direct interaction between NLRP3 and these molecular entities. Therefore, it is unclear how these different stimuli all lead to same outcome, NLRP3 activation. A recent study uncovered that many NLRP3 activators (e.g., bacterial pore-forming toxins, nigericin, ATP, and particulate matter) cause mitochondrial perturbation and increased ROS production, but neither were required for NLRP3 activation [67]. Instead, it was suggested that the common activity induced by all NLRP3 agonists is K^+ efflux. Notably, reduction of intracellular K^+ concentration was sufficient to activate NLRP3. These results were the first to demonstrate that K+ efflux may be a common mechanism that drives NLRP3 activation during diverse stress conditions. These findings contrast with previous work that demonstrates a role for mitochondria in inflammasome activation in response to LPS + ATP treatment. These observations would suggest that at least two pathways for NLRP3 inflammasome activation (mitochondria-dependent and mitochondria-independent) might exist, perhaps acting in a cell and/or stimulus-specific manner.

Mitophagy maintains the integrity of the mitochondrial network

When dysfunction occurs within mitochondria, dysfunctional or damaged mitochondria can be removed without comprising the entire mitochondrial network. Low ATP production, enhanced ROS generation, or calcium imbalance serve as signs of dysfunctional or damaged mitochondria, thus leading to induction of a mitochondrial specific form of autophagy called mitophagy (Fig. 1.4). Healthy mitochondria can divide into functional progeny that can reintegrate into the mitochondrial network by fusion. In contrast, dysfunctional mitochondria are

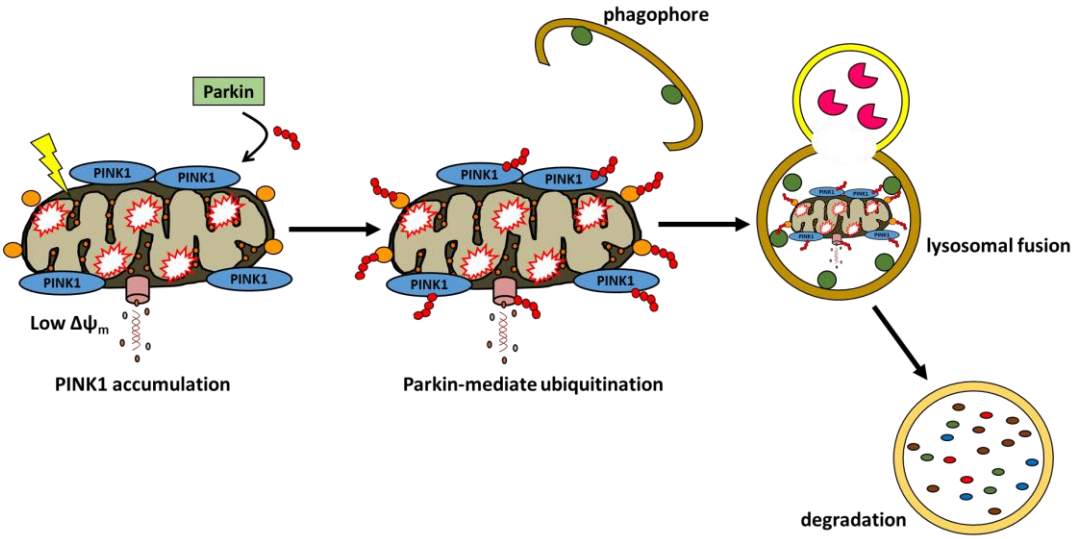

Figure 1.4: Mitophagy, the labelling and removal of damaged mitochondria. When mitochondria are damaged and lose membrane potential, the kinase PTEN-induced putative kinase protein 1 (PINK1) accumulates and recruits the E3 ubiquitin ligase Parkin to the damaged mitochondrion. Parkin ubiquitylates mitochondrial proteins (e.g. VDAC, MFN1 and 2) and causes mitochondria to fragment and be captured by the phagophore that then fuse with lysosomes. This schematic was adapted from Popovic et al. Nat Med, 2014. 20(11):1242-53.

specifically separated from the network and destined for mitophagic degradation [40]. Intact mitochondria are constantly importing the kinase PINK1 into the matrix where it is cleaved by the protease PARL [38]. PINK1 accumulation on the outer mitochondrial membrane serves as a flag for mitochondrial dysfunction [68]. If the $\Delta\psi_m$ decreases, PINK1 accumulates on the outer membrane leading to the recruitment of the ubiquitin ligase Parkin, which ubiquitinates mitochondrial outer membrane proteins such as MFN1 and MFN2 (mitofusin 1 and 2, regulators of mitochondrial fusion). By favoring proteasomal degradation of MFN1 and MFN2, Parkin suppresses mitochondrial fusion and promotes fragmentation of the network [69]. Mitochondrial fragmentation allows for the capture of damaged/dysfunctional mitochondria by autophagosomes. A recent study revealed that the ER stress sensor PERK can regulate Parkin-mediated mitophagy. Parkin expression increased during ER stress in a manner dependent on the PERK/ATF4 branch of the UPR [70]. Upon induction, ATF4 bound to a CREB/ATF site within the Parkin promoter triggering *parkin* transcription. Although Parkin protects cells from ER stress-induced cell death via the removal of damaged mitochondria, it does not reduce the level of ER stress within the cell. These observations support the notion that crosstalk between the ER and mitochondria is critical to maintaining cell survival under stress.

Maintaining integrity of mitochondria is crucial for cell viability because mitochondria are critical regulators of cell death and are responsible for a variety of metabolic functions. Mitochondrial dysfunction is a key feature of neurodegeneration. Mutations in mitochondrial DNA and oxidative stress both

contribute to aging, which is the greatest risk factor for neurodegenerative diseases such as Alzheimer's and Parkinson's disease. In Alzheimer's disease, mitochondrial ROS generation and inhibition of energy metabolism increase amyloid-β peptide levels, the primary component of senile plaques [39, 42, 71]. For Parkinson's disease, defects in mitochondrial associated pathways and proteins contribute to the progression of the disease. Decreased activity or mutations in genes for Complex I (a major contributor member of the ETC) can cause Parkinson's disease [41]. Additionally, mutations in the mitophagy regulator Parkin increases cell death and progression of Parkinson's disease [72, 73]. These observations indicate that maintaining integrity of the mitochondrial network is not only important on a cellular basis but on an organismal basis as well.

Conclusions

Recent findings highlight the contribution of the mitochondria and ER to regulation of inflammation and disease progression. The pathways and players of the mitochondria and ER overlap and are complementary. Furthermore, mitochondria are tethered to the ER, providing the conditions for constant communication between the two organelles [74-76]. ER-mitochondrial crosstalk is important for initiating cell death during certain stress contexts; therefore, it is reasonable to propose that this crosstalk may contribute to initiation of inflammatory responses. Elucidating the context and mechanisms by which ER-mitochondrial crosstalk controls inflammation may aid in identifying targets that modulate many inflammatory and neurodegenerative diseases.

To investigate if ER-mitochondrial crosstalk is essential in mediating inflammation, I utilized the Gram-negative bacterium, *Brucella abortus* RB51, an attenuated cattle vaccine strain. Typically, virulent *Brucella* strains (e.g. S2308, 16M) acquire ER membrane when generating the *Brucella* containing vacuole, an intracellular environment that is conducive for microbial replication [77–79]. Attenuated strains like RB51, are unable to create the BCV; however, these strains can still traffic to the ER [80, 81] (Fig. 1.5). Attenuation is due to multiple mutations in the RB51 genome, including a mutation that prevents addition of the O antigen during *Brucella* lipopolysaccharide (LPS) biosynthesis [82]. Attenuated *Brucella* species have been shown to trigger ER and mitochondrial stress during infection as well as eliciting proinflammatory responses [83–87]. Therefore, RB51 served as a tool for elucidating the role of ER and mitochondrial stress in inflammation regulation. The following chapters will demonstrate that ER stress can modulate inflammation and cell death via two stress sensors. Chapter 2 highlights the consequences of uninhibited inflammation - cell death. Damaged mitochondria release apoptotic molecules thus triggering an unique type of cell death that is reminiscent of both apoptosis (silent) and pyroptosis (inflammatory). In chapter 3, I discuss how IRE1 drives mitochondrial damage, leading to the release of mitochondrial danger signals required for NLRP3 inflammasome activation. Chapter 4 reveals that PERK suppresses NLRP3 inflammasome activation through Parkin-dependent mitophagy, and that induction of mitophagy leads to the removal of dysfunctional mitochondria, thus preventing the release of mitochondrial derived danger signals. Overall, these findings highlight

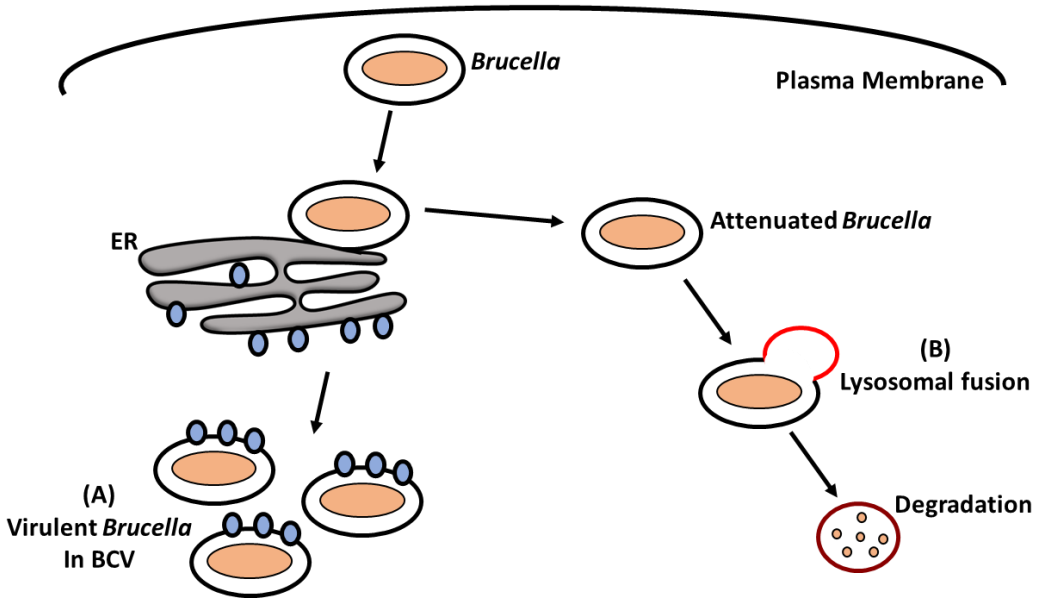

Figure 1.5: *Brucella* interacts with the ER. After entry, virulent intracellular *Brucella* resides within a vacuole (BCV) that interacts with early endosomes. These early BCVs avoid further interactions with the endocytic pathway and are in close contact with, the ER within the first hours after infection (A). Vacuoles containing a attenuated strains fail to sustain interactions with the ER (B) and ultimately fuse with lysosomes. This schematic was adapted from Celli et al. J Exp Med, 2003. 198(4): p. 545-56.

mechanisms by which context-dependent ER stress signals are relayed to mitochondria to promote or suppress inflammation, supporting the idea that the ER acts as a critical hub for integrating cellular stress and innate immune signaling.

References

1. Walter, P. and D. Ron, The unfolded protein response: from stress pathway to homeostatic regulation. Science, 2011. 334(6059): p. 1081-6.

2. Nakajima, S., et al., Selective abrogation of BiP/GRP78 blunts activation of NF-kappaB through the ATF6 branch of the UPR: involvement of C/EBPbeta and mTOR-dependent dephosphorylation of Akt. Mol Cell Biol, 2011. 31(8): p. 1710-8.

3. Li, M., et al., ATF6 as a transcription activator of the endoplasmic reticulum stress element: thapsigargin stress-induced changes and synergistic interactions with NF-Y and YY1. Mol Cell Biol, 2000. 20(14): p. 5096-106.

4. Shen, J., et al., ER stress regulation of ATF6 localization by dissociation of BiP/GRP78 binding and unmasking of Golgi localization signals. Dev Cell, 2002. 3(1): p. 99-111.

5. Yoshida, H., et al., XBP1 mRNA is induced by ATF6 and spliced by IRE1 in response to ER stress to produce a highly active transcription factor. Cell, 2001. 107(7): p. 881-91.

6. Smith, M.H., H.L. Ploegh, and J.S. Weissman, Road to ruin: targeting proteins for degradation in the endoplasmic reticulum. Science, 2011. 334(6059): p. 1086-90.

7. Qian, S.B., J.R. Bennink, and J.W. Yewdell, Quantitating defective ribosome products. Methods Mol Biol, 2005. 301: p. 271-81.

8. Maurel, M., et al., Getting RIDD of RNA: IRE1 in cell fate regulation. Trends Biochem Sci, 2014. 39(5): p. 245-54.

9. Harding, H.P., Y. Zhang, and D. Ron, Protein translation and folding are coupled by an endoplasmic-reticulum-resident kinase. Nature, 1999. 397(6716): p. 271-4.

10. Harding, H.P., et al., An integrated stress response regulates amino acid metabolism and resistance to oxidative stress. Mol Cell, 2003. 11(3): p. 619-33.

11. Vela, L., et al., Direct interaction of Bax and Bak proteins with Bcl-2 homology domain 3 (BH3)-only proteins in living cells revealed by fluorescence complementation. J Biol Chem, 2013. 288(7): p. 4935-46.

12. Huang, L., H. Xie, and H. Liu, Endoplasmic reticulum stress, diabetes mellitus, and tissue injury. Curr Protein Pept Sci, 2014. 15(8): p. 812-8.

13. Martinon, F., et al., TLR activation of the transcription factor XBP1 regulates innate immune responses in macrophages. Nat Immunol, 2010. 11(5): p. 411-8.

14. Zhang, C., et al., ATF4 is directly recruited by TLR4 signaling and positively regulates TLR4-trigged cytokine production in human monocytes. Cell Mol Immunol, 2013. 10(1): p. 84-94.

15. Yamazaki, H., et al., Activation of the Akt-NF-kappaB pathway by subtilase cytotoxin through the ATF6 branch of the unfolded protein response. J Immunol, 2009. 183(2): p. 1480-7.

16. Ozcan, U., et al., Endoplasmic reticulum stress links obesity, insulin action, and type 2 diabetes. Science, 2004. 306(5695): p. 457-61.

17. McGuckin, M.A., et al., Intestinal secretory cell ER stress and inflammation. Biochem Soc Trans, 2011. 39(4): p. 1081-5.

18. Kaser, A., et al., XBP1 links ER stress to intestinal inflammation and confers genetic risk for human inflammatory bowel disease. Cell, 2008. 134(5): p. 743-56.

19. Lee, I.T. and C.M. Yang, Role of NADPH oxidase/ROS in pro-inflammatory mediators-induced airway and pulmonary diseases. Biochem Pharmacol, 2012. 84(5): p. 581-90.

20. Kim, I., W. Xu, and J.C. Reed, Cell death and endoplasmic reticulum stress: disease relevance and therapeutic opportunities. Nat Rev Drug Discov, 2008. 7(12): p. 1013-30.

21. Levine, B., N. Mizushima, and H.W. Virgin, Autophagy in immunity and inflammation. Nature, 2011. 469(7330): p. 323-35.

22. Marquez, R.T. and L. Xu, Bcl-2:Beclin 1 complex: multiple, mechanisms regulating autophagy/apoptosis toggle switch. Am J Cancer Res, 2012. 2(2): p. 214-21.

23. Kouroku, Y., et al., ER stress (PERK/eIF2alpha phosphorylation) mediates the polyglutamine-induced LC3 conversion, an essential step for autophagy formation. Cell Death Differ, 2007. 14(2): p. 230-9.

24. Rouschop, K.M., et al., The unfolded protein response protects human tumor cells during hypoxia through regulation of the autophagy genes MAP1LC3B and ATG5. J Clin Invest, 2010. 120(1): p. 127-41.

25. Yamamoto, K., H. Ichijo, and S.J. Korsmeyer, BCL-2 is phosphorylated and inactivated by an ASK1/Jun N-terminal protein kinase pathway normally activated at G(2)/M. Mol Cell Biol, 1999. 19(12): p. 8469-78.

26. Lei, K. and R.J. Davis, JNK phosphorylation of Bim-related members of the Bcl2 family induces Bax-dependent apoptosis. Proc Natl Acad Sci U S A, 2003. 100(5): p. 2432-7.

27. Gozuacik, D., et al., DAP-kinase is a mediator of endoplasmic reticulum stress-induced caspase activation and autophagic cell death. Cell Death Differ, 2008. 15(12): p. 1875-86.

28. Mikhailov, V., et al., Association of Bax and Bak homo-oligomers in mitochondria. Bax requirement for Bak reorganization and cytochrome c release. J Biol Chem, 2003. 278(7): p. 5367-76.

29. Hammadi, M., et al., Modulation of ER stress and apoptosis by endoplasmic reticulum calcium leak via translocon during unfolded protein response: involvement of GRP78. FASEB J, 2013. 27(4): p. 1600-9.

30. Marciniak, S.J., et al., CHOP induces death by promoting protein synthesis and oxidation in the stressed endoplasmic reticulum. Genes Dev, 2004. 18(24): p. 3066-77.

31. Chu, C.T., et al., Cardiolipin externalization to the outer mitochondrial membrane acts as an elimination signal for mitophagy in neuronal cells. Nat Cell Biol, 2013. 15(10): p. 1197-205.

32. Csordas, G., et al., Structural and functional features and significance of the physical linkage between ER and mitochondria. J Cell Biol, 2006. 174(7): p. 915-21.

33. Grimm, S., The ER-mitochondria interface: the social network of cell death. Biochim Biophys Acta, 2012. 1823(2): p. 327-34.

34. Gincel, D., H. Zaid, and V. Shoshan-Barmatz, Calcium binding and translocation by the voltage-dependent anion channel: a possible regulatory mechanism in mitochondrial function. Biochem J, 2001. 358(Pt 1): p. 147-55.

35. Vance, J.E., MAM (mitochondria-associated membranes) in mammalian cells: lipids and beyond. Biochim Biophys Acta, 2014. 1841(4): p. 595-609.

36. Yi, M., D. Weaver, and G. Hajnoczky, Control of mitochondrial motility and distribution by the calcium signal: a homeostatic circuit. J Cell Biol, 2004. 167(4): p. 661-72.

37. Harr, M.W. and C.W. Distelhorst, Apoptosis and autophagy: decoding calcium signals that mediate life or death. Cold Spring Harb Perspect Biol, 2010. 2(10): p. a005579.

38. Youle, R.J. and D.P. Narendra, Mechanisms of mitophagy. Nat Rev Mol Cell Biol, 2011. 12(1): p. 9-14.

39. Pratico, D., et al., Increased lipid peroxidation precedes amyloid plaque formation in an animal model of Alzheimer amyloidosis. J Neurosci, 2001. 21(12): p. 4183-7.

40. Batlevi, Y. and A.R. La Spada, Mitochondrial autophagy in neural function, neurodegenerative disease, neuron cell death, and aging. Neurobiol Dis, 2011. 43(1): p. 46-51.

41. Schapira, A.H., et al., Mitochondrial complex I deficiency in Parkinson's disease. Lancet, 1989. 1(8649): p. 1269.

42. Khandelwal, P.J., et al., Parkin mediates beclin-dependent autophagic clearance of defective mitochondria and ubiquitinated Abeta in AD models. Hum Mol Genet, 2011. 20(11): p. 2091-102.

43. Ly, J.D., D.R. Grubb, and A. Lawen, The mitochondrial membrane potential (deltapsi(m)) in apoptosis; an update. Apoptosis, 2003. 8(2): p. 115-28.

44. Smeitink, J., L. van den Heuvel, and S. DiMauro, The genetics and pathology of oxidative phosphorylation. Nat Rev Genet, 2001. 2(5): p. 342-52.

45. Bernardi, P., The mitochondrial permeability transition pore: a mystery solved? Front Physiol, 2013. 4: p. 95.

46. Martinou, J.C. and D.R. Green, Breaking the mitochondrial barrier. Nat Rev Mol Cell Biol, 2001. 2(1): p. 63-7.

47. Tait, S.W. and D.R. Green, Mitochondria and cell death: outer membrane permeabilization and beyond. Nat Rev Mol Cell Biol, 2010. 11(9): p. 621-32.

48. Acehan, D., et al., Three-dimensional structure of the apoptosome: implications for assembly, procaspase-9 binding, and activation. Mol Cell, 2002. 9(2): p. 423-32.

49. Riedl, S.J. and G.S. Salvesen, The apoptosome: signalling platform of cell death. Nat Rev Mol Cell Biol, 2007. 8(5): p. 405-13.

50. Horvath, G.L., et al., Intracellular sensing of microbes and danger signals by the inflammasomes. Immunol Rev, 2011. 243(1): p. 119-35.

51. Martinon, F., K. Burns, and J. Tschopp, The inflammasome: a molecular platform triggering activation of inflammatory caspases and processing of proIL-beta. Mol Cell, 2002. 10(2): p. 417-26.

52. Kim, J.J. and E.K. Jo, NLRP3 inflammasome and host protection against bacterial infection. J Korean Med Sci, 2013. 28(10): p. 1415-23.

53. Leemans, J.C., S.L. Cassel, and F.S. Sutterwala, Sensing damage by the NLRP3 inflammasome. Immunol Rev, 2011. 243(1): p. 152-62.

54. Menu, P., et al., ER stress activates the NLRP3 inflammasome via an UPR-independent pathway. Cell Death Dis, 2012. 3: p. e261.

55. Zhou, R., et al., A role for mitochondria in NLRP3 inflammasome activation. Nature, 2011. 469(7329): p. 221-5.

56. Hornung, V., et al., Silica crystals and aluminum salts activate the NALP3 inflammasome through phagosomal destabilization. Nat Immunol, 2008. 9(8): p. 847-56.

57. Betarbet, R., et al., Chronic systemic pesticide exposure reproduces features of Parkinson's disease. Nat Neurosci, 2000. 3(12): p. 1301-6.

58. Zhou, R., et al., Thioredoxin-interacting protein links oxidative stress to inflammasome activation. Nat Immunol, 2010. 11(2): p. 136-40.

59. Saxena, G., J. Chen, and A. Shalev, Intracellular shuttling and mitochondrial function of thioredoxin-interacting protein. J Biol Chem, 2010. 285(6): p. 3997-4005.

60. Zhou, J. and W.J. Chng, Roles of thioredoxin binding protein (TXNIP) in oxidative stress, apoptosis and cancer. Mitochondrion, 2013. 13(3): p. 163-9.

61. Shimada, K., et al., Oxidized mitochondrial DNA activates the NLRP3 inflammasome during apoptosis. Immunity, 2012. 36(3): p. 401-14.

62. Nakahira, K., et al., Autophagy proteins regulate innate immune responses by inhibiting the release of mitochondrial DNA mediated by the NALP3 inflammasome. Nat Immunol, 2011. 12(3): p. 222-30.

63. Burckstummer, T., et al., An orthogonal proteomic-genomic screen identifies AIM2 as a cytoplasmic DNA sensor for the inflammasome. Nat Immunol, 2009. 10(3): p. 266-72.

64. Hornung, V. and E. Latz, Intracellular DNA recognition. Nat Rev Immunol, 2010. 10(2): p. 123-30.

65. Poeck, H., et al., Recognition of RNA virus by RIG-I results in activation of CARD9 and inflammasome signaling for interleukin 1 beta production. Nat Immunol, 2010. 11(1): p. 63-9.

66. Subramanian, N., et al., The adaptor MAVS promotes NLRP3 mitochondrial localization and inflammasome activation. Cell, 2013. 153(2): p. 348-61.

67. Munoz-Planillo, R., et al., K(+) efflux is the common trigger of NLRP3 inflammasome activation by bacterial toxins and particulate matter. Immunity, 2013. 38(6): p. 1142-53.

68. Narendra, D.P., et al., PINK1 is selectively stabilized on impaired mitochondria to activate Parkin. PLoS Biol, 2010. 8(1): p. e1000298.

69. Tanaka, A., et al., Proteasome and p97 mediate mitophagy and degradation of mitofusins induced by Parkin. J Cell Biol, 2010. 191(7): p. 1367-80.

70. Bouman, L., et al., Parkin is transcriptionally regulated by ATF4: evidence for an interconnection between mitochondrial stress and ER stress. Cell Death Differ, 2011. 18(5): p. 769-82.

71. Nunomura, A., et al., Oxidative damage is the earliest event in Alzheimer disease. J Neuropathol Exp Neurol, 2001. 60(8): p. 759-67.

72. Fornai, F., et al., Parkinson-like syndrome induced by continuous MPTP infusion: convergent roles of the ubiquitin-proteasome system and alpha-synuclein. Proc Natl Acad Sci U S A, 2005. 102(9): p. 3413-8.

73. Palacino, J.J., et al., Mitochondrial dysfunction and oxidative damage in parkin-deficient mice. J Biol Chem, 2004. 279(18): p. 18614-22.

74. English, A.R. and G.K. Voeltz, Endoplasmic reticulum structure and interconnections with other organelles. Cold Spring Harb Perspect Biol, 2013. 5(4): p. a013227.

75. Friedman, J.R., et al., ER sliding dynamics and ER-mitochondrial contacts occur on acetylated microtubules. J Cell Biol, 2010. 190(3): p. 363-75.

76. Rowland, A.A. and G.K. Voeltz, Endoplasmic reticulum-mitochondria contacts: function of the junction. Nat Rev Mol Cell Biol, 2012. 13(10): p. 607-25.

77. Starr, T., et al., Brucella intracellular replication requires trafficking thorough the late endosomal/lysosomal compartment. Traffic, 2008. 9(5): p. 678-94.

78. Celli, J., et al., Brucella evades macrophage killing via VirB-dependent sustained interactions with the endoplasmic reticulum. J Exp Med, 2003. 198(4): p. 545-56.

79. Starr, T., et al., Selective subversion of autophagy complexes facilitates completion of the Brucella intracellular cycle. Cell Host Microbe, 2012. 11(1): p. 33-45.

80. Arellano-Reynoso, B., Intracellular trafficking study of a RB51 B. abortus vaccinal strain isolated from cow milk. Vet Microbiol, 2004. 98(3-4): p. 307-12.

81. Arenas, G.N., et al., Intracellular trafficking of Brucella abortus in J774 macrophages. Infect Immun, 2000. 68(7): p. 4255-63.

82. Vemulapalli, R., et al., Complementation of Brucella abortus RB51 with a functional wboA gene results in O-antigen synthesis and enhanced vaccine efficacy but no change in rough phenotype and attenuation. Infect Immun, 2000. 68(7): p. 3927-32.

83. Smith, J.A., et al. Brucella induces an unfolded protein response via TcpB that supports intracellular replication in macrophages. PLoS Pathog, 2013. 9(12):e1003785.

84. de Jong, M.F., et al. Sensing of bacterial type IV secretion via the unfolded protein response. MBio, 2013. 4(1):e00418-12.

85. Qin, Q.M., et al. RNAi screen of endoplasmic reticulum-associated host factors reveals a role for IRE1alpha in supporting Brucella replication. PLoS Pathog, 2008. 4(7):e1000110.

86. Chen, F., et al., Proinflammatory Caspase-2-Mediated Macrophage Cell Death Induced by a Rough Attenuated Brucella suis Strain. Infect Immun, 2011. 79(6): p. 2460-9.

87. Chen, F. and Y. He, Caspase-2 mediated apoptotic and necrotic murine macrophage cell death induced by rough Brucella abortus. PLoS One, 2009. 4(8): p. e6830

88. Bronner, D.N., M.X. O'Riordan, and Y. He, Caspase-2 mediates a Brucella abortus RB51-induced hybrid cell death having features of apoptosis and pyroptosis. Front Cell Infect Microbiol, 2013. 3: p. 83.

Chapter 2

Caspase-2 mediates a *Brucella abortus* RB51-induced hybrid cell death having features of apoptosis and pyroptosis

(Published: Bronner DN et al (2013) Front Cell Infect Microbiol. doi: 10.3389/fcimb.2013.00083)

Abstract

Programmed cell death (PCD) can play a crucial role in tuning the immune response to microbial infection. Although PCD can occur in different forms, all are mediated by a family of proteases called caspases. Caspase-2 is the most conserved caspase; however its function in cell death is ill-defined. Previously we demonstrated that live attenuated cattle vaccine strain *Brucella abortus* RB51 induces caspase-2-mediated PCD of infected macrophages. However, the mechanism of caspase-2-mediated cell death pathway remained unclear. In this study, we found that caspase-2 mediated proinflammatory cell death of RB51-infected macrophages and regulated many genes in different PCD pathways. We show that the activation of proapoptotic caspases-3 and -8 was dependent upon caspase-2. Caspase-2 regulated mitochondrial cytochrome *c* release and TNFα production, both of which are known to activate caspase-3 and caspase-8, respectively. In addition to TNFα, RB51-induced caspase-1 and IL-1β production

was also driven by caspase-2-mediated mitochondrial dysfunction. Interestingly, pore formation, a phenomenon commonly associated with caspase-1-mediated pyroptosis, occurred; however it did not contribute to RB51-induced proinflammatory cell death. Our data suggest that caspase-2 acts as an initiator caspase that mediates a novel RB51-induced hybrid cell death that simulates but differs from typical apoptosis and pyroptosis. The initiator role of the caspase-2-mediated cell death was also conserved in cellular stress-induced cell death of macrophages treated with etoposide, naphthalene, or anti-Fas. Caspase-2 also regulated caspase-3 and -8 activation, as well as cell death in macrophages treated with each of the three reagents. Taken together, our data has demonstrated that caspase-2 can play an important role in mediating a proinflammatory response and a hybrid cell death that demonstrates features of both apoptosis and pyroptosis.

Introduction

Programmed cell death (PCD) is a crucial process initiated by the host in response to cellular stress and microbial infections. PCD can occur in a variety of ways [1]. Apoptosis, pyroptosis, and necroptosis are three pathways of PCD that can occur during microbial infections with substantially different outcomes. Apoptosis is a silent programmed cell death due to a lack of cytokine secretion [2]. Although the plasma membrane remains intact, apoptotic bodies can bleb off and be phagocytosed by other phagocytic cells in the surrounding area. Pyroptosis or "*death by fire*," is inflammatory programmed cell death mediated by caspase-1 [3]. Caspase-1 processes proinflammatory cytokines (IL-1β and IL-18), and secretion

of these cytokines requires pore formation in the plasma membrane, which leads to cell swelling and eventually lysis. Necroptosis is a newly identified type of PCD that includes a proinflammatory response as well as loss of plasma membrane integrity [4]. In contrast to apoptosis and pyroptosis, serine/threonine kinases, RIP1 and RIP3, mediate necroptosis. In addition, necroptosis leads to the release of intracellular contents; mostly damage associated molecular patterns (DAMPs).

Many microbes can induce cell death during infection and dissemination [5]. Avirulent *Mycobacterium* induces apoptosis in macrophages [6]. Neighboring uninfected macrophages, upon phagocytosis, killed *Mycobacterium* in apoptotic bodies released by *Mycobacterium*-infected macrophages. In addition, apoptotic blebs from bacterially infected cells induce a T_H17 response. In contrast, *Shigella* and *Salmonella*-induced pyroptosis leads to the release and exposure of bacteria to reactive oxygen species (ROS) and neutrophils [7-9]. In addition to bacterial pathogens, parasitic and viral pathogens such as *Trypanosoma cruzi* and Vaccinia virus also have the ability to induce apoptosis and necroptosis respectively [10, 11]. The outcomes of necroptosis are an increase in cytokine secretion and leukocyte infiltration as well as ROS production. As illustrated from previous studies, PCD can play an important role in controlling microbial infections. Meanwhile, many pathogens can inhibit these PCD pathways in various approaches. For example, virulent wild type *Brucella* strains typically inhibit PCD of infected macrophages [12-14]. Elucidating the PCD mechanism induced or inhibited by such pathogens is critical to uncovering mechanisms of pathogenesis, as well as protective immunity.

The main executors of the PCD process are caspases, which are divided into two groups: initiators and effectors. Initiator caspases activate effector caspases via cleavage whereas effector caspases initiate cell death by cleaving various downstream apoptotic proteins. *C. elegans* has a single caspase, Ced-3, that mediates all cell death. Of 13 caspases existing in mammalian systems, caspase-2 has the highest sequence homology with Ced-3 [15, 16]. Caspase-2 plays important biological roles from oocyte development to aging control, and in intermediary development stages including DNA damage repair, tumor prevention, and infection control [17-20]. Caspase-2 can play different roles due to its unique domain structure, which resembles an initiator and effector caspase. It contains a caspase activation and recruitment domain (CARD) which is required for auto-activation and binding to other molecules. Caspase-2 also contains a cleavage site [21] which resembles that of the effector caspase-3 [22]. These factors make the classification of caspase-2 difficult. Caspase-2-deficient mice develop without an overt phenotype although only mild apoptotic defects in oocyte and neuron developments were exhibited, suggesting that the function of caspase-2 is largely redundant for cellular homeostasis during development [23]. Caspase-2 has been shown to be instrumental in bacterial infections. Caspase-2 played a role in both caspase-1-dependent and -independent apoptosis of macrophages infected with *Salmonella* [24]. The various and often controversial roles of caspase-2 in different organisms and experimental conditions have been documented and discussed [25, 26]. The role of caspase-2 in regulating cell death and the exact mechanism remain unclear.

We previously demonstrated that rough attenuated *Brucella abortus* strain RB51 induces caspase-2-mediated apoptotic and necrotic cell death [13]. As a licensed cattle vaccine strain, RB51 is able to induce IFNγ and $CD8^+$ T cell mediated cytotoxicity in mice [27]. Unlike its virulent counterparts, RB51 does not replicate in macrophages and induces robust caspase-2-mediated apoptotic and necrotic cell death [13]. In addition, RB51 induces cell death in dendritic cells [14]. However, the caspase-2-mediated RB51-induced cell death pathway is largely unknown. Previously, we showed that caspase-2 activation as well as decrease of the mitochondrial membrane potential occurred in dying macrophages infected with RB51 [13]. These characteristics would suggest that apoptosis via the mitochondria-driven intrinsic pathway was the cell death mechanism. We also showed that rough attenuated *B. suis* strain VTRS1 induces caspase-2-mediated proinflammatory cell death [12]. It is likely that RB51 also induces proinflammatory response that differs inherently from non-proinflammatory apoptosis. How RB51 induces cell death remains unclear.

Here we investigated which PCD mechanism was responsible for RB51-induced cell death in macrophages. We found that RB51-infected macrophages exhibited mitochondrial dysfunction, activation of the caspase cascade (caspase-3 and caspase-8), IL-1β and TNFα secretion, and pore formation in the plasma membrane – all of which were dependent upon caspase-2. In addition to infection, we found that caspase-2 also mediated cell death as well as caspase-3 and -8 activation in macrophages treated with etoposide, naphthalene, and anti-Fas.

These results illustrate that RB51-induced caspase-2-mediated macrophage cell death is unique in that it exhibits characteristics of both apoptosis and pyroptosis.

Results

Caspase-2 mediates RB51-induced cell death via the extrinsic apoptosis pathway

Our previous experiments using a chemical inhibitor and siRNA demonstrated that caspase-2 mediates RB51-induced macrophage cell death [13]. To confirm the caspase-2 mediated cell death, wild type (WT) and caspase-2 deficient (*casp2*$^{-/-}$) bone-marrow derived macrophages (BMDMs) were infected with RB51, and cell death was assessed by Annexin V/propidium iodide (PI) staining and lactate dehydrogenase (LDH) release. Cell death was abolished in *casp2*$^{-/-}$ BMDM (Fig. A1A-B) which confirms that caspase-2 is required for RB51 induced cell death. We assessed if there was any difference in RB51 intracellular behavior by measuring CFU throughout infection. We found that *casp2*$^{-/-}$ BMDM were able to kill RB51 just as efficiently as WT BMDM (Fig. A1C). Therefore, any differences in initiating cell death were not due to lack of infectivity or bacterial killing in *casp2*$^{-/-}$ BMDMs.

Since caspase-2 is required for RB51 induced cell death, we assessed which PCD pathway caspase-2 was mediating RB51-induced cell death. Inhibition of caspase-3 and/or caspase-8 activity led to a decrease in cell death; however, it was not as significant as caspase-2 deficiency (Table 2.1). Inhibition of caspase-3 or -8 in RB51-infected macrophages resulted in 57.3 ± 2.1% and 65.7 ± 3.7% cell death, respectively (P-value <0.001) (Table 2.1). Inhibition of both caspase-3 and

Condition	% Cell Death (±SD)
Untreated	0.7 ±0.9%
WT BMDMs	84.7±1.7%
Casp2KO BMDMs	12.7±2.5%
Z-DEVD-FMK (Casp3 inhibitor)	57.3±2.1%
Z-IETD-FMK (Casp8 inhibitor)	65.7±3.7%
Z-DEVD-FMK + Z-IETD-FMK	36.3±2.5%

Table 2.1: Cell death measurements in casp2 deficient and caspase-3 and -8 inhibited macrophages. Percent ± SD of n≥3 independent experiments. Cells were counted in randomly selected fields of 100 cells. All conditions except untreated where in the presence of RB51 (MOI 200).

-8 led to only 36.3 ± 2.5% cell death, suggesting the two types of inhibitions are synergistic. These data suggest that RB51-induced cell death may involve the apoptotic pathways associated with caspase-3 and caspase-8.

Classically, caspase-3 and caspase-8 are linked to intrinsic (intracellular signal driven) and extrinsic (death receptor driven) apoptotic pathways respectively [2]. Both pathways are linked to caspase-2 by mediating mitochondrial cytochrome *c* release and caspase-8 activation [28, 29]. To assess if caspase-2 regulated these pathways during RB51 infection, we investigated caspase-3 and caspase-8 activation in WT and *casp2*$^{-/-}$ BMDMs by measuring cleavage. The cleavage of both caspase-3 and caspase-8 was abolished in RB51-infected *casp2*$^{-/-}$ BMDMs (Fig. 2.1A). Inhibition of caspase-3 and -8 did not affect caspase-2 activation (Fig. A2A-B). Previous studies illustrated that both the intrinsic and extrinsic cell death pathways can propagate signaling by inducing mitochondrial dysfunction, which eventually leads to cell death. Therefore, we investigated if caspase-2 mediated mitochondrial dysfunction in RB51-infected macrophages. Previously we observed that in RB51-infected macrophages, mitochondrial membrane potential decreased over time, suggesting that mitochondrial cytochrome *c* release (a marker of mitochondrial dysfunction) occurs. We found that in WT BMDMs, cytochrome *c* release increased throughout infection, however in *casp2*$^{-/-}$ BMDMs cytochrome *c* release was abolished (Fig. 2.1A).

To assess if mitochondrial dysfunction contributed to RB51-induced cell death, the cytochrome *c* release was blocked with cyclosporin A (CsA) in RB51-infected RAW264.7 (murine) macrophages. CsA prevents opening of the

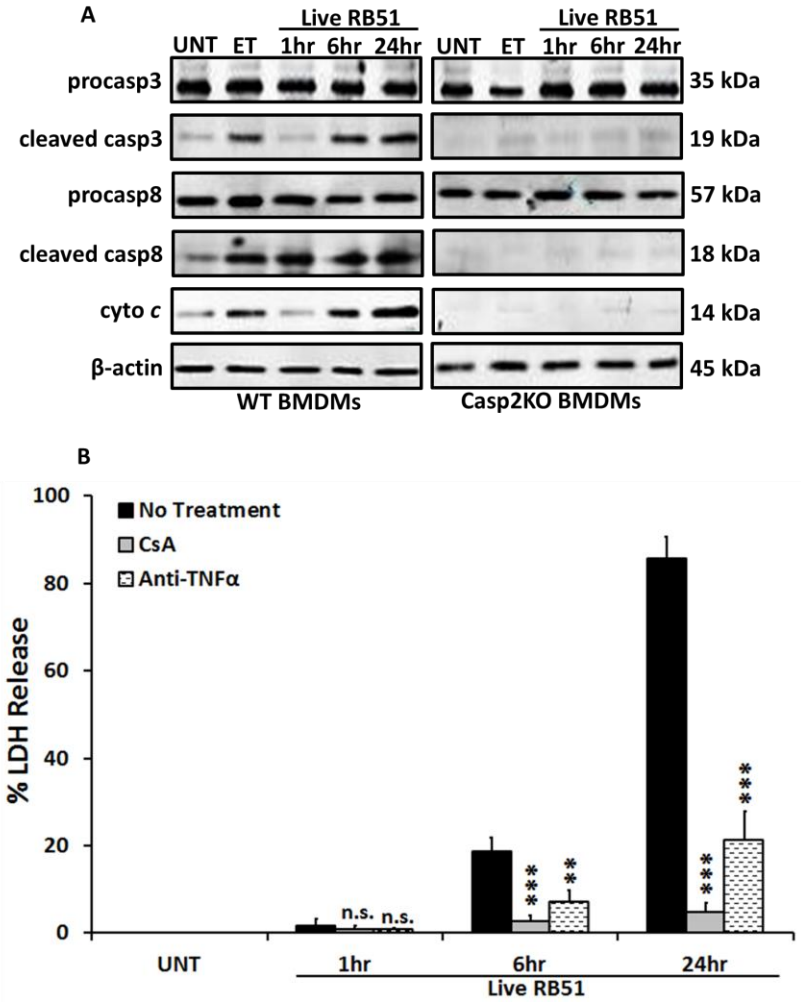

Figure 2.1: Caspase-2 drives both the intrinsic and extrinsic cell death pathways. (A) caspase-3 and -8 cleavage (activation) as well as cytochrome *c* (cyto *c*) release in RB51-infected WT and *casp2*$^{-/-}$ BMDMs. β-actin serves as a loading control. UT and ET represent untreated and etoposide (25 μM, 6hr treatment) respectively. Immunoblots are representatives of n≥3 independent experiments. (B) LDH release in RB51-infected RAW264.7 macrophages in the presence of cyclosporin A (CsA; inhibitor of mitochondrial permeability transition pore, 10 μM) and Anti-TNFα (10 μg/mL). Error bars represent mean ± SD of n≥3 independent experiments. **p < 0.001 and ***p < 0.0001, Student's *t*-test. n.s. = not significant. Immunoblots are representatives of n≥3 independent experiments.

mitochondrial permeability transition pore (MPTP), a pore responsible for the release of mitochondrial contents such as cytochrome *c* [30]. In the presence of CsA, cell death was significantly reduced ($p<0.0001$) in RB51-infected macrophages (Fig. 2.1B). Seeing that mitochondrial dysfunction occurs and both caspase-3 and caspase-8 are activated, we explored if RB51-induced cell death was acting through the extrinsic pathway. Extrinsic or death receptor mediated cell death can be activated by Fas ligand (FasL) and TNFα. Since live attenuated *B. suis* strain VTRS1 induces a proinflammatory response [12], we investigated if TNFα played a role in mediating RB51-induced cell death. We treated RAW264.7 macrophages with anti-TNFα and assessed cell death via LDH release. Anti-TNFα treatment led to a decrease in LDH release when compared to untreated RB51-infected RAW264.7 macrophages (Fig. 2.1B, 85.5±5.1% vs. 21.4±6.5% respectively). These observations suggest that caspase-2 drives the extrinsic cell death pathway in RB51-infected macrophages.

Caspase-2 regulates caspase-1 activation and IL-1β production in RB51-infected macrophages

Studies have illustrated that a proinflammatory response can be the trigger or product of cell death [2, 3]. Since TNFα played a role in RB51-induced cell death, we assessed if caspase-2 mediated TNFα production. Over time, TNFα levels increased in RB51-infected WT BMDMs. However, in *casp2*$^{-/-}$ BMDMs, TNFα was reduced to untreated levels (Fig. 2.2A). In addition, CsA treatment led to a decrease in TNFα production.

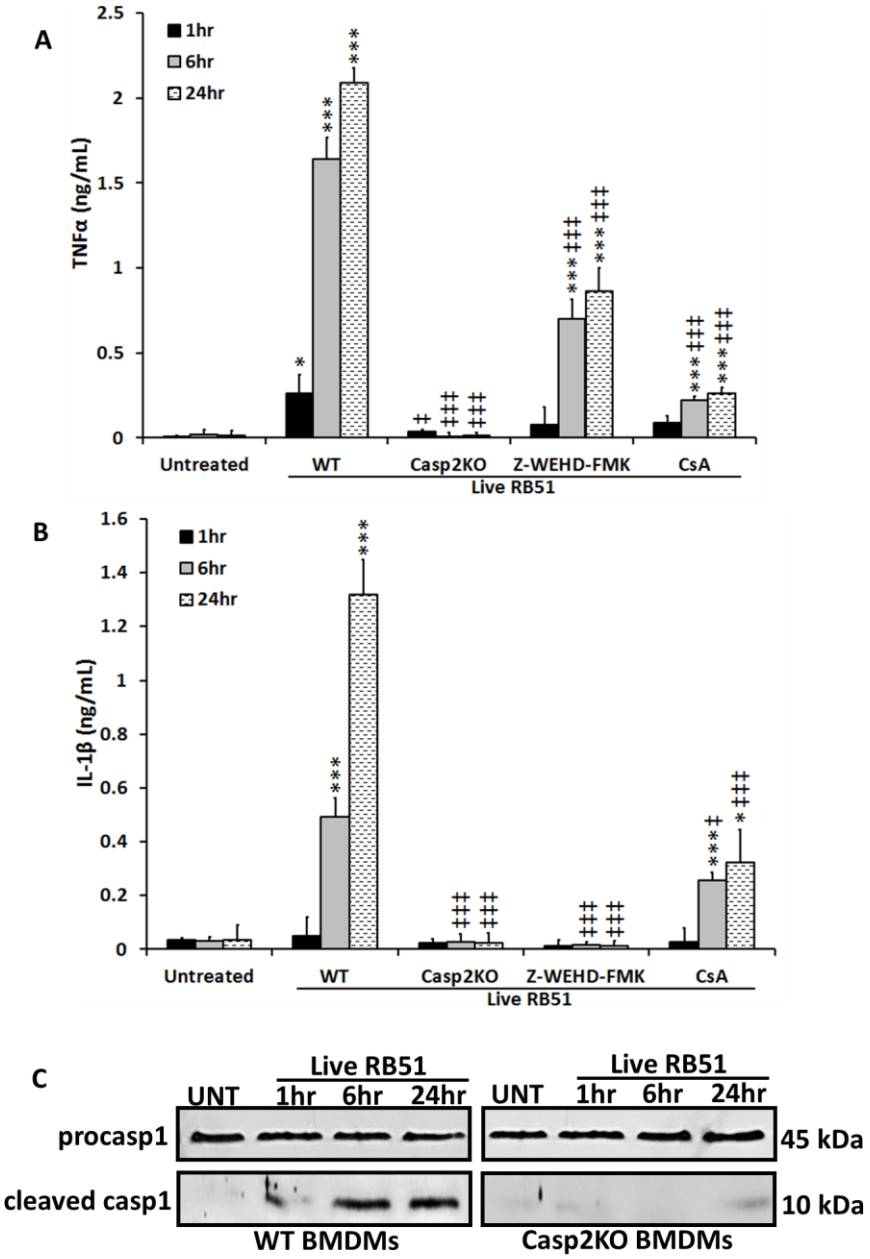

Figure 2.2: Caspase-2 drives proinflammatory responses in RB51-infected macrophages. (A) TNFα and (B) IL-1β levels in WT, *casp2*$^{-/-}$, CsA (cyclosporin A, inhibitor of mitochondrial permeability transition pore, 10 μM) and Z-WEHD-FMK (caspase-1 inhibitor, 20 μM) treated BMDMs. Error bars represent mean ± SD of n≥3 independent experiments. ‡,*p < 0.01 and ‡‡‡, ***p < 0.0001, Student's *t*-test. (*,***) and (‡, ‡‡‡) represent comparison to untreated and WT + RB51 respectively. (C) caspase-1 cleavage (activation) in RB51-infected WT and *casp2*$^{-/-}$ BMDMs. UT represents untreated (negative control). Immunoblots are representatives of n≥3 independent experiments.

Another cytokine associated with proinflammatory cell death is IL-1β. During pyroptosis, caspase-1 processes IL-1β and aids in its secretion. Interestingly, caspase-2 contains a CARD domain and has been shown to mediate caspase-1 activation during *Salmonella* infections [24]. Similar to TNFα, IL-1β levels increased above untreated levels starting at 6 h.p.i. however, in *casp2*$^{-/-}$ and caspase-1 inhibited BMDMs, IL-1β production was abolished (Fig. 2.2B). In the presence of CsA, IL-1β levels were significantly reduced in RB51-infected macrophages. A decrease in IL-1β levels in *casp2*$^{-/-}$ BMDMs suggested that either caspase-2 regulates caspase-1 activation or caspase-2 is directly responsible for the processing of IL-1β. To evaluate these two possibilities, caspase-1 cleavage in RB51-infected WT and *casp2*$^{-/-}$ BMDMs was measured. RB51 induced caspase-1 cleavage in WT BMDMs starting at 6 h.p.i.; however, cleaved caspase-1 was absent in *casp2*$^{-/-}$ BMDMs (Fig. 2.2C). These data suggest that caspase-2, via mitochondrial dysfunction, mediates caspase-1 activation and IL-1β production in RB51-infected macrophages.

Pore formation is not required for RB51-induced cell death

Caspase-1 activation and IL-1β production are key indicators of pyroptosis. During pyroptosis, pores form in the plasma membrane, leading to a change in ionic gradient and water influx. The consequence of the pores is cell swelling, due to water influx, and eventually cell lysis. *Salmonella enterica* serovar Typhimurium SL1344 is a pathogen known for inducing pyroptosis in macrophages [31]. We hypothesized that RB51 induced pore formation in macrophages. To test this, RB51-infected RAW264.7 macrophages were stained with two membrane

impermeant dyes, ethidium bromide (EtBr, 394 Da) and the larger sized ethidium homodimer-2 (EthD2, 1293 Da). Uptake of EtBr and EthD2 would represent discrete pore formation and loss of plasma membrane integrity respectively. Gliotoxin (apoptosis inducer) treated RAW264.7 macrophages excluded both impermeant dyes (Fig. 2.3A), indicative of an intact plasma membrane. In RB51-infected WT BMDMs, uptake of EtBr began at 1 h.p.i. and increased throughout infection (Fig. 2.3A). Uptake of EthD2 was significantly less than EtBr and did not occur until 6 h.p.i. in RB51-infected macrophages (Fig. 2.3A). Since pore formation has been shown to be dependent upon caspase-1, it was not surprising to see that uptake of both EtBr and EthD2 were abolished in RB51-infected *casp2*$^{-/-}$ and caspase-1 inhibited WT BMDMs (Fig. 2.4A and Fig. A3).

We further assessed if pore formation in RB51-infected macrophages contributed to RB51-induced cell death. RB51-infected macrophages were treated with glycine, a cytoprotective agent. Glycine prevents cell death by stabilizing the ion gradient [32]. Glycine treatment decreased SL1344-induced macrophage cell death however, no effect was seen with RB51 (Fig. 2.3B). These findings demonstrate that although pore formation occurs in RB51-infected macrophages, it is not the cause of the RB51-induced macrophage cell death.

Caspase-2 mediates cell death in other contexts

Since caspase-2 can regulate cell death in the context of a *Brucella* infection, we investigated if caspase-2 also plays a critical role in the presence of different cell death chemical inducers – etoposide, naphthalene, anti-Fas, and gliotoxin. Etoposide and naphthalene are DNA damaging agents that trigger

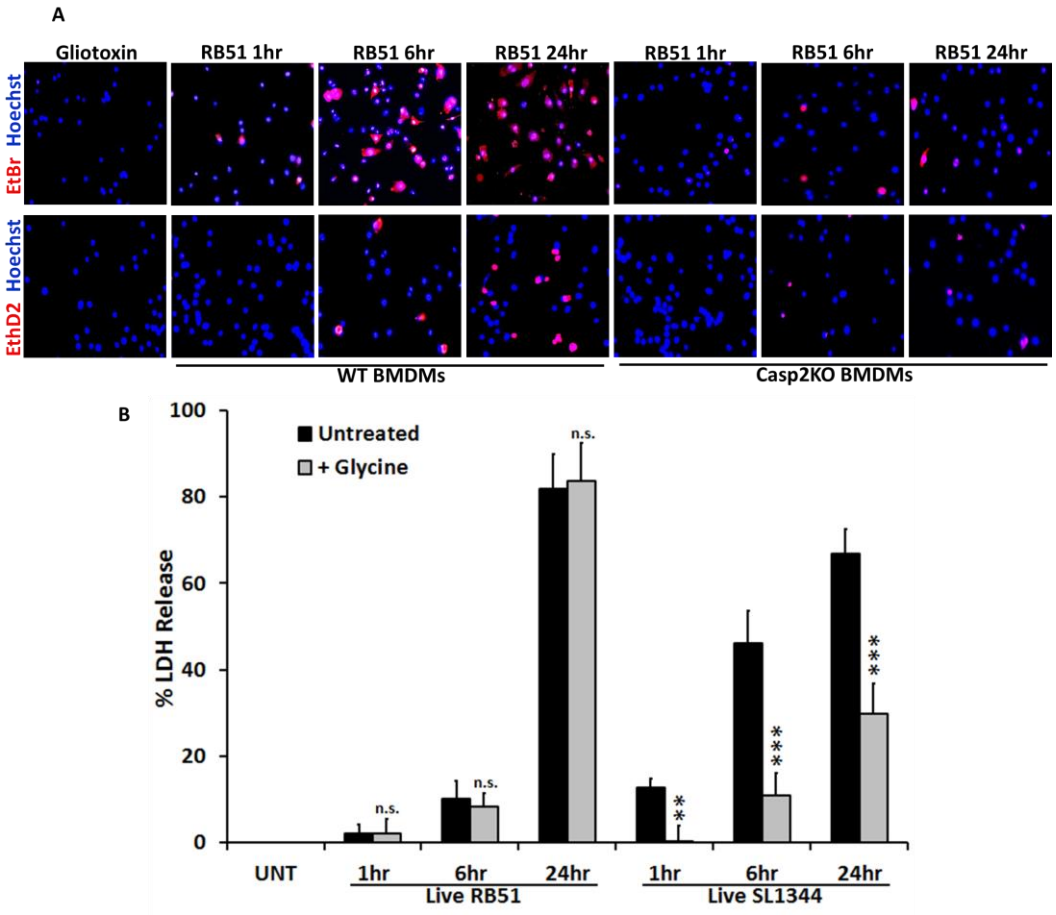

Figure 2.3: Pore formation does not contribute to RB51-induced cell death. (A) WT and *casp2*$^{-/-}$ BMDMs treated with Gliotoxin (10 µM, 6 hr treatment) or infected with RB51 were stained with the membrane permeable dye Hoechst 33342 (blue) and the membrane impermeant dyes (red), EtBr (MW 394) or EthD2 (MW 1293). Adherent cells were visualized by fluorescence microscopy (100x). Images are representatives of n≥3 independent experiments. (B) LDH release in RB51 and SL1344-infected RAW264.7 macrophages in the absence or presence of glycine (5mM). Error bars represent mean ± SD of n≥3 independent experiments. **p < 0.001 and ***p < 0.0001, Student's *t*-test. n.s. = not significant.

mitochondrial ROS production, inducing cell death via the intrinsic pathway [33-36]. Treatment with anti-Fas antibody mimics activation of death receptor signaling by Fas ligand through the extrinsic pathway. [37]. Gliotoxin mediates Bak activation leading to cytochrome *c* release from the mitochondria and cell death [38]. To assess the role of caspase-2 in the presence of these chemical inducers, we first assessed caspase-2 activation. In macrophages treated with etoposide, naphthalene, and anti-Fas, caspase-2 was activated. However, gliotoxin did not induce caspase-2 activation (Fig. 2.4A). Next, we investigated if caspase-2 mediated cell death in the presence of these inducers via Annexin V/PI staining. All four chemicals induced cell death after 6 hr of treatment. The caspase-2 deficiency led to a significant decrease in cell death in etoposide, naphthalene, and anti-Fas treated but not gliotoxin treated macrophages (Fig. 2.4B).

Knowing the mechanism by which these chemical inducers mediate cell death, we assessed whether caspase-3 and -8 activation occurred and whether caspase-2 mediated their activation as seen in RB51-infected macrophages. Caspase-3 was activated in etoposide, naphthalene, anti-Fas, and gliotoxin treated WT BMDMs (Fig. 2.4C). Caspase-3 activation was abolished in *casp2*$^{-/-}$ BMDMs treated with etoposide, naphthalene, and anti-Fas but not gliotoxin. Caspase-8 activation was observed in etoposide, naphthalene, and anti-Fas treatment yet absent during gliotoxin treatment (Fig. 2.4C). Similar to caspase-3, caspase-8 activation was abolished in etoposide, naphthalene, anti-Fas treated *casp2*$^{-/-}$ BMDMs. These data indicate that caspase-2 can exhibit a crucial role in mediating cell death initiated by other stimuli besides microbial infection.

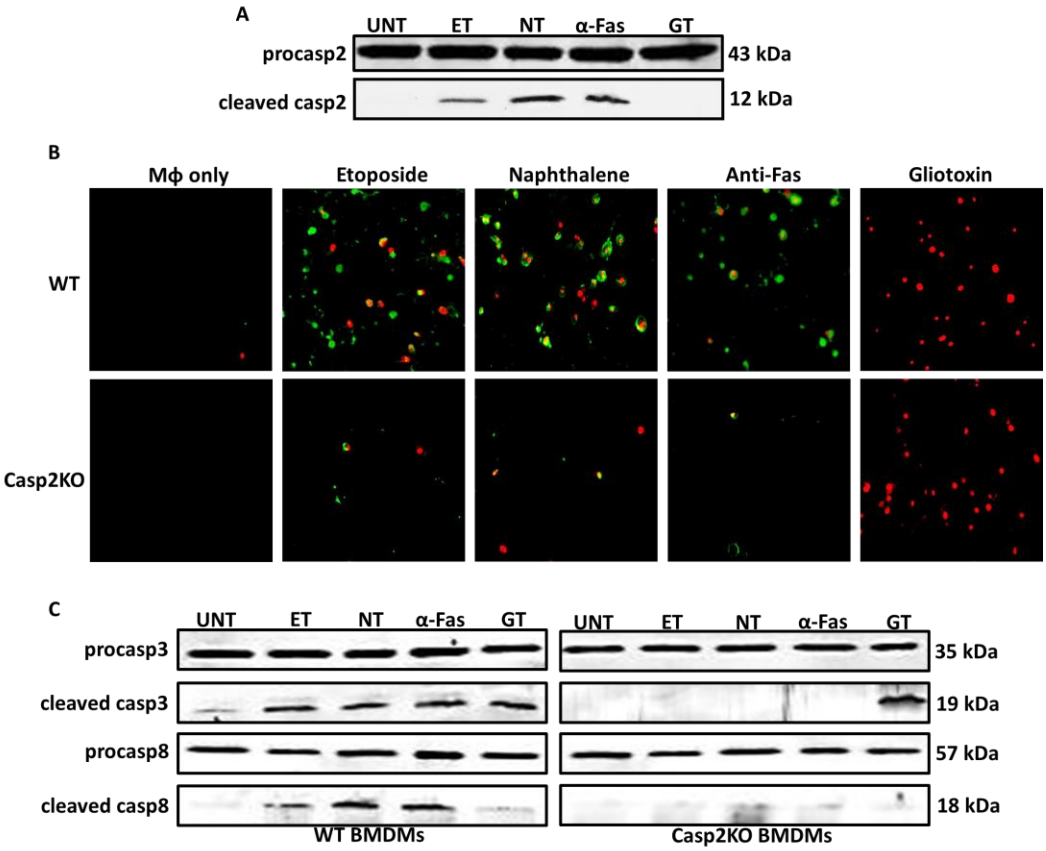

Figure 2.4: Caspase-2 can also mediate caspase-3 and -8 activation in other contexts. (A) Caspase-2 cleavage (activation) in RB51-infected RAW264.7 macrophages. UT, ET, NT, α-Fas, and GT represent untreated, etoposide (25 µM, 6hr treatment), Naphthalene (100 µM, 6hr treatment), Anti-Fas (1 µg/mL, 6h4 treatment), and Gliotoxin (10 µM, 6hr treatment) respectively. (B) ET, NT, α-Fas, GT treated WT and *casp2*$^{-/-}$ BMDMs were stained with Annexin V/propidium iodide (PI). Adherent cells were visualized by fluorescence microscopy (100x). Cells were counted in randomly selected fields of 100 cells. Images are representatives of n≥3 independent experiments. (C) Caspase-3 and -8 cleavage (activation) in ET, NT, α-Fas, GT treated WT and *casp2*$^{-/-}$ BMDMs. Immunoblots are representatives of n≥3 independent experiments.

Conclusions

Here we report that RB51-induced cell death is driven by the caspase-2/mitochondrial axis. Our results demonstrated that RB51-infected macrophages induce the caspase-2 activation, and the activated caspase-2 mediates caspase-1, -3 and -8 activations, and TNFα and IL-1β secretions. Mitochondrial release of cytochrome *c* was associated with caspase-3 activation and contributed to RB51-induced cell death. Although pores formed in the plasma membrane upon infection, they did not contribute to cell death. In addition to cell death, we showed that the RB51-induced proinflammatory response was mediated by caspase-2 and mitochondrial dysfunction. In addition to microbial infections, caspase-2 also demonstrated a contributing role in mediating cell death with different cell death inducers.

Rough *Brucella* species are known to induce cell death as well as a robust immune response. Here we show that proinflammatory cytokine TNFα plays a role in RB51-induced macrophage cell death; however, in the case of CA180, another *B. abortus* rough strain, this is not the case [39]. Although both RB51 and CA180 belong to the same genus and share a rough LPS phenotype, there are striking differences in their LPS. Both RB51 and CA180 lack an O-antigen on their LPS however, CA180 has a truncated core polysaccharide due to a mutation in the phosphomannomutase gene [40]. Phosphomannomutase is needed to the elongation of the polysaccharide core. The polysaccharide core has been shown to elicit cytokine production, any changes (e.g. shortening) can decrease cytokine

production [41, 42]. Therefore, unlike RB51, CA180 may not elicit strong TNFα production, which may explain the differences in TNFα dependent cell death.

Although caspase-2 has been linked to many different cellular processes, caspase-2 is still considered primarily a proapoptotic caspase. Here we show that caspase-2 can mediate IL-1β production, as well as caspase-1 activation. In addition to *Brucella* infection, caspase-2 has also been shown to regulate caspase-1 activation in *Salmonella* infected macrophages. We speculate that caspase-2 might regulate caspase-1 by interacting with the inflammasome complexes responsible for caspase-1 activation or by inducing an inflammasome trigger (*e.g.* ER stress, mitochondrial DNA release, or ROS production). Caspase-1 interacts with different inflammasome proteins and accessory proteins via its CARD domain. Inflammatory caspases (caspase-1, -4, -5, -11) interact with inflammasome and accessory proteins via their CARD domain. Caspase-2 also contains a CARD domain. Further investigation into whether caspase-2 can interact with different inflammasome components is needed. Another possible mechanism for caspase-2 regulation of caspase-1 activation is through mitochondrial dysfunction. As seen with CsA treatment, there was a sharp decrease in IL-1β production suggesting that the mitochondria can aid in inflammasome activation during RB51 infection. Recent studies have linked NLRP3 and AIM2 activation to mitochondrial dysfunction [43-45]. It is possible that caspase-2-induced mitochondrial dysfunction leads to release of mitochondrial danger associated molecular patterns (DAMPs). Mitochondrial DAMPs (e.g. mtDNA or cardiolipin exposure) can lead to NLRP3 and AIM2 inflammasome activation [44]. Caspase-2 has been

linked to mediating mitochondrial dysfunction – caspase-2 cleaves Bid leading to mitochondrial outer membrane pore formation and eventually release of mitochondrial content (*e.g.* cytochrome *c*). Whether caspase-2-mediated release of mitochondrial DAMPs is the mechanism by which the inflammasome and caspase-1 activation occurs remains to be elucidated.

The caspase-2-mediated cell death pathway seen in RB51-infected macrophages differs from classical apoptosis, pyroptosis, and necroptosis (Table 2). RB51-induced cell death is not mediated by caspase-1. Our data suggest that RIP1 and RIP3 (mediators of necroptosis) are not active because both caspase-2 and -8 activated by RB51 infection can cleave RIP1 and RIP3 – the cleavage of these two prevents necroptosis from occurring [46, 47]. In addition, RB51-infected macrophages secrete proinflammatory cytokines starting at 6 h.p.i., a characteristic absent in apoptosis. Caspase-1 is active and contributes to IL-1β production. However, unlike the phenomenon seen in pyroptosis, neither caspase-1 nor the pore in the plasma membrane contributes to cell death. Our data suggest that RB51-induced caspase-2-mediated cell death does not fall into any of the three classical programmed cell death pathways. Owing to the common feature of caspase-mediated proinflammatory cell death between caspase-1-mediated pyroptosis and caspase-2-mediated cell death, previously we tentatively labeled the caspase-2-mediated proinflammatory cell death as “caspase-2-mediated pyroptosis” [12]. Considering that current study also clearly shows that caspase-2 also mediates apoptosis-like features (e.g., caspase-3 and -8 activation and loss of mitochondrial membrane potential) (Table 2.2), caspase-2 appears to mediate

	Apoptosis	Pyroptosis	Necroptosis	*Casp2* -mediated cell death
Plasma membrane pore formation	-	+	-	+
Loss in plasma membrane integrity	-	+ (swelling = lysis)	+	+ (6 & 24 h.p.i.)
Loss of mitochondrial membrane potential	+	-	+	+
Cytochrome *c* release	+	-	+	+
Proinflammatory	-	+	+	+
Caspase-1 mediated	-	+	-	-
Caspase-2 mediated	+/-	-	-	+
Caspase-3 activation	+	-	-	+
Caspase-8 activation	+/- (extrinsic)	-	-	+
ROS production	+	-	+	+
Release of DAMPs	-	+	+	+
RIP1/3-mediated	-	-	+	?

Table 2.2: Comparison of caspase-2-mediated cell death to classical apoptosis and pyroptosis. +: occurs, -: does not occur, +/-: may occur but not required, ? = unknown.

a hybrid cell death that includes partial features of both apoptosis and pyroptosis. Although distinct, caspase-2-mediated cell death and necroptosis appear to share some similarities as well (Table 4.2).

Our studies on the relationship between caspase-2 and cell death induced by different cell death inducers further illustrate the critical role and the mechanism of caspase-2 in triggering PCD. Both etoposide and naphthalene are DNA damage inducers, a stimulus known for activating caspase-2. Interestingly, both etoposide and naphthalene induced caspase-8 activation. Previous studies have illustrated a connection between DNA damage, caspase-8, and caspase-2. Both caspase-2 and caspase-8 can be activated by p53 [48, 49]; this suggests that upon etoposide and naphthalene treatment, p53 activates caspase-2 leading to caspase-8 activation. Anti-Fas works through the extrinsic pathway and leads to cell death via caspase-8 dependent activation of caspase-3. Seeing that caspase-2 aided in caspase-8 activation (outside of DNA damage) clearly suggests that caspase-2 can act as an initiator caspase to mediate activation of other caspases. Whether caspase-2 mediates caspase-8 activation directly or indirectly remains unclear. Gliotoxin induced cell death via the intrinsic pathway. Only caspase-3 was activated in gliotoxin-treated macrophages. Cytochrome *c* can aid in caspase-2 activation however [50], in the context of gliotoxin intoxication this was not the case because caspase-2 activation did not occur. Gliotoxin acts on Bak and its downstream target t-Bid (a known target cleaved by caspase-2, [28]); therefore, it is possible that gliotoxin short-circuits the classical intrinsic pathway and does not require signaling components upstream of the mitochondria. In the case of

etoposide and naphthalene, the data suggest that caspase-2 regulates caspase-3 activation via the mitochondria. Caspase-3 is activated via the apoptosome, a multiprotein complex dependent upon cytochrome *c* release. Caspase-2 was previously reported to act upstream of caspase-8 during ceramide-induced mitochondrial apoptosis in T cells [29]. It appears that the caspase-2 regulation of caspase-3 and -8 can occur in different cell types with different treatments, so this type of regulation is neither cell specific nor context specific. These observations suggest that caspase-2 can play a critical role in initiating programmed cell death.

The caspase-2-mediated cell death pathway is likely critical to microbial pathogenesis and host immunity. In the context of RB51, cell death and the proinflammatory response may have synergistic effects on host immune responses. Cell death may result in the exposure of RB51 to a more hostile extracellular environment (as seen in pyroptosis and necroptosis). In addition, neighboring macrophages and dendritic cells may recognize processed RB51 antigens leading to cross priming of $CD8^+$ T cells (important for RB51-induced protective immunity). We recently showed that RB51 induced cell death in bone marrow derived dendritic cells and aided in maturation as well as priming of T cells – all of which were dependent upon caspase-2 [14]. These observations demonstrate the importance for caspase-2, as well as cell death, in initiating the immune response. Utilizing this programmed cell death pathway may ensure that the host triggers a potent immune response. Prevention of this pathway may aid in enhancing survival of virulent *Brucella* in macrophages. Our previous work

suggested prevention – virulent strain *B. abortus* S2308 did not induce caspase-2 activation nor cytochrome *c* release in infected macrophages [13].

Caspase-2 is also implicated in other processes (cancer regulation and metabolism) and may take on a regulatory role in these processes as well. We have made an original observation that caspase-2 plays a non-redundant role in triggering the proinflammatory cell death of RB51-infected macrophages and in macrophages treated with various drugs. After the evolution of complex caspase-cascade cell death signaling pathways in advanced animals, it is suggestive that the protein functions of the highly conserved caspase-2 have been preserved during evolution and serve as safeguards to regulate various cell death pathways. It is likely that intracellular pathogens with similar lifestyles to *Brucella* (*e.g., Salmonella*, *Mycobacterium*, *Listeria*, and *Legionella*) may utilize caspase-2 during infection. Further understanding of caspase-2-mediated pyroptosis can aid in supplying a blueprint for effective brucellosis vaccines (both animals & humans) as well as effective therapeutics against cancers and other diseases.

Materials and Methods

Mice

The caspase-2 knockout (Casp2KO) mice were originally generated by Junying Yuan and kindly provided by Dr. Brian Herman of the University of Texas Health Science Center at San Antonio with Dr. Yuan's consent [23]. The deletion inactivates both the long and short form of caspase-2. The mice were backcrossed with C57BL/6 once in the Unit for Laboratory Animal Medicine at the University of

Michigan Medical School, and then used as founders. Casp2KO and wild type C57BL/6 (Jackson) mice with similar ages were applied in the experiments. The University Committee on Use and Care of Animals (UCUCA) at the University of Michigan approved the protocol (#09695) to use mice for studies described here.

Bacterial strains and reagents

RAW264.7 macrophages and bone marrow derived macrophages (BMDMs) were infected with *Brucella abortus* strain RB51 (from Dr. G. Schurig, Virginia Polytechnic Institute and State University) and *Salmonella typhimurium* SL1344 (from Mary O'Riordan, University of Michigan). The following inhibitors and inducers were used: cyclosporin A (Sigma-Aldrich), etoposide (Sigma-Aldrich), naphthalene (Sigma-Aldrich), Anti-Fas (BioVision), gliotoxin (-Aldrich), glycine (Sigma-Aldrich), Z-WEHD-FMK (Caspase-1 inhibitor, R&D Systems), Z-DEVD-FMK (Caspase-3 inhibitor, R&D Systems), Z-IETD-FMK (Caspase-8 inhibitor, R&D Systems), and anti-TNFα (mouse specific, BioVision).

The following antibodies were used: anti-cytochrome *c* (cat#:4272S, Cell Signaling), anti-caspase-3 (cat#: 9662S, Cell Signaling), anti-caspase-8 (cat#: 4927S, Cell Signaling), anti-caspase-2 (cat#: 3027-100, BioVision), anti-caspase-1 (cat#: sc-514, Santa Cruz), and anti-actin (cat#: MS1295P1, Thermo Scientific).

Cell culture and infection

BMDMs were isolated from WT and *casp2*$^{-/-}$ mice on a C57BL/6 background. Isolated BMDMs were differentiated in DMEM (GIBCO) supplemented with 20% heat-inactivated FBS (GIBCO), 1% L-glutamine (200 mM), 1% sodium pyruvate

(100 mM), 0.1% β-mercaptoethanol (55 mM) , and 30% L-929 fibroblast conditioned medium. BMDMs were cultured in non-TC treated plates, fed fresh media on day 3, and harvested on day 6. BMDMs were maintained at 37°C under 5% CO_2.

Four million RAW264.7 macrophages and BMDMs were seeded in 6 well plates 18 hr prior to infection. The following day, where indicated cells were pretreated with cyclosporin A (10 μM), Z-WEHD-FMK (20 μM), Z-DEVD-FMK (20 μM), Z-IETD-FMK (20 μM) and Anti-TNFα (10 μg/mL) for 1 hr prior to infection. Untreated and pretreated cells were infected with RB51 (MOI 200) or SL1344 (MOI 25) for 30 min, after which the inoculum was removed and cells were washed with PBS. Medium containing 50 μg/ml of gentamicin was added to kill extracellular bacteria. To synchronize infection, cells were spun at 1200 rpm for 3 min after adding inoculum. Cells were treated with etoposide (25 μM), naphthalene (100 μM), anti-Fas (1 μg/mL), and gliotoxin (10 μM) for 6 hr. At the indicated times, cells were lysed in buffer containing 1% NP-40 on ice for 15 min and spun at 13,000 rpm for 15 min to pellet the insoluble fraction. Soluble fractions were used for immunoblot assays.

Immunoblot Assay

Cytosolic extracts collected at various time points (1, 6, and 24h pi) were separated by SDS-PAGE, transferred to PVDF membranes (Millipore), blocked with 5% milk in TBS-Tween20 (TBS-T), and incubated overnight at 4°C with primary antibodies stated above. Membranes were washed with TBS-T and incubated with secondary HRP conjugated to either goat anti-rabbit IgG (cat#: 12-348, Millipore) or goat anti-

mouse IgG (cat#: 1034-05, Southern Biotech) at room temperature for 1 hr. Bands were visualized using the ECL Western Blotting Substrate Kit (Pierce). Immunoblots in the figures are representative of n≥3 independent experiments.

Cytokine Detection

Culture supernatants were collected at different time points (1, 6, and 24h pi) from macrophages infected as described above. IL-1β and TNFα levels were determined by sandwich enzyme-linked immunosorbent assay (ELISA) according to manufacturer's instructions (BioLegend). A minimum of three technical replicates per experiment and three experimental replicates were analyzed for each condition.

Cell Death Assay

RAW264.7 macrophages were seeded in 6 well plates at a concentration 9.6 X 10^4 per well and infected with RB51 as stated above. Cells were stained with Annexin V and propidium iodide (PI) using the Annexin V-FLUOS staining kit (Roche Diagnostics Corporation). Cells were washed with PBS and incubated with the fluorescent dyes for 15 min in the dark at room temperature. Fluorescence was observed with a Nikon TK-2000-S microscope and photographed with a RT Slide Spot digital camera and QCapture Pro software. Uninfected macrophages served as negative controls.

Ethidium bromide (EtBr) and Ethidium homodimer-2 (EthD2) staining

Macrophages were grown in 6-well plates and infected as described above. At different time points post infection, cells were washed with PBS (GIBCO) and

stained with Hoechst 33342 (5 μg/mL) and either EtBr or EthD2 (25 μg/mL) according to the manufacturer's instructions. Cell were analyzed with a Nikon TK-2000-s microscope and photographed with a RT slide spot digital camera and QCapture Pro Software.

Lactate dehydrogenase (LDH) Release Assay

Macrophages were seeded in 96-well plates and infected with RB51 or SL1344 as stated above. Supernatants were analyzed for the presence of LDH enzyme using the CytoTox-ONE™ Homogeneous Membrane Integrity Assay (Promega) as directed by the manufacturer's instructions. Percentage of LDH release was calculated as 100 X [(Experimental LDH Release - Culture Medium Background)/(Maximum LDH Release – Culture Medium Background)].

Statistical Analysis

All p values were generated between identified samples using unpaired two-tailed Student's *t*-tests and represent analysis of ≥3 replicates per condition. ‡,*$p<0.01$ ‡‡,**$p<0.001$ and ‡‡‡,***$p<0.0001$.

Acknowledgments

XL prepared bone marrow derived macrophages for this study. We thank Drs. Michele S. Swanson, Victor J. DiRita, and George W. Jourdian for their discussions. We acknowledge financial support by the Rackham Spring/Summer Research grant (to YH), Rackham Merit Fellowship (to DNB), startup and research bridging funds to YH from the Unit for Laboratory Animal Medicine and the

Endowment for Basic Science (EBS) in the University of Michigan Medical School, and NIH R21AI101777 (MOR).

Author Contributions

DNB and YH designed the experiments. DNB performed the experiments. DNB, MOR and YH analyzed the data. YH and MOR contributed reagents and materials. DNB and YH wrote the paper. All authors edited and approved the manuscript.

Author Information

The research was conducted in the absence of any commercial or financial relationships that could be construed as a potential conflict of interest. Correspondence and requests for materials should be addressed to Y.H. (yongqunh@med.umich.edu).

References

1. Galluzzi, L., et al., Molecular definitions of cell death subroutines: recommendations of the Nomenclature Committee on Cell Death 2012. Cell Death Differ, 2012. 19(1): p. 107-20.

2. Elmore, S., Apoptosis: a review of programmed cell death. Toxicol Pathol, 2007. 35(4): p. 495-516.

3. Bergsbaken, T., S.L. Fink, and B.T. Cookson, Pyroptosis: host cell death and inflammation. Nat Rev Microbiol, 2009. 7(2): p. 99-109.

4. Vandenabeele, P., et al., Molecular mechanisms of necroptosis: an ordered cellular explosion. Nat Rev Mol Cell Biol, 2010. 11(10): p. 700-14.

5. Gao, L. and Y. Abu Kwaik, Hijacking of apoptotic pathways by bacterial pathogens. Microbes Infect, 2000. 2(14): p. 1705-19.

6. Fratazzi, C., et al., Macrophage apoptosis in mycobacterial infections. J Leukoc Biol, 1999. 66(5): p. 763-4.

7. Miao, E.A., et al., Caspase-1-induced pyroptosis is an innate immune effector mechanism against intracellular bacteria. Nat Immunol, 2010. 11(12): p. 1136-42.

8. Brennan, M.A. and B.T. Cookson, Salmonella induces macrophage death by caspase-1-dependent necrosis. Mol Microbiol, 2000. 38(1): p. 31-40.

9. Hilbi, H., et al., Shigella-induced apoptosis is dependent on caspase-1 which binds to IpaB. J Biol Chem, 1998. 273(49): p. 32895-900.

10. Cho, Y.S., et al., Phosphorylation-driven assembly of the RIP1-RIP3 complex regulates programmed necrosis and virus-induced inflammation. Cell, 2009. 137(6): p. 1112-23.

11. Duaso, J., et al., Trypanosoma cruzi induces apoptosis in ex vivo infected human chorionic villi. Placenta, 2011. 32(5): p. 356-61.

12. Chen, F., et al., Proinflammatory Caspase-2-Mediated Macrophage Cell Death Induced by a Rough Attenuated Brucella suis Strain. Infect Immun, 2011. 79(6): p. 2460-9.

13. Chen, F. and Y. He, Caspase-2 mediated apoptotic and necrotic murine macrophage cell death induced by rough Brucella abortus. PLoS One, 2009. 4(8): p. e6830.

14. Li, X. and Y. He, Caspase-2-dependent dendritic cell death, maturation, and priming of T cells in response to Brucella abortus infection. PLoS One, 2012. 7(8): p. e43512.

15. Hengartner, M.O., Cell Death. 1997.

16. Geng, X., et al., Caenorhabditis elegans caspase homolog CSP-2 inhibits CED-3 autoactivation and apoptosis in germ cells. Cell Death Differ, 2009. 16(10): p. 1385-94.

17. Guo, Y., et al., Caspase-2 induces apoptosis by releasing proapoptotic proteins from mitochondria. J Biol Chem, 2002. 277(16): p. 13430-7.

18. Ho, L.H., et al., A tumor suppressor function for caspase-2. Proc Natl Acad Sci U S A, 2009. 106(13): p. 5336-41.

19. Shi, M., et al., DNA-PKcs-PIDDosome: a nuclear caspase-2-activating complex with role in G2/M checkpoint maintenance. Cell, 2009. 136(3): p. 508-20.

20. Bouchier-Hayes, L. and D.R. Green, Caspase-2: the orphan caspase. Cell Death Differ, 2012. 19(1): p. 51-7.

21. Hofmann, K., P. Bucher, and J. Tschopp, The CARD domain: a new apoptotic signalling motif. Trends Biochem Sci, 1997. 22(5): p. 155-6.

22. Talanian, R.V., et al., Substrate specificities of caspase family proteases. J Biol Chem, 1997. 272(15): p. 9677-82.

23. Bergeron, L., et al., Defects in regulation of apoptosis in caspase-2-deficient mice. Genes Dev, 1998. 12(9): p. 1304-14.

24. Jesenberger, V., et al., Salmonella-induced caspase-2 activation in macrophages: a novel mechanism in pathogen-mediated apoptosis. J Exp Med, 2000. 192(7): p. 1035-46.

25. Troy, C.M. and E.M. Ribe, Caspase-2: vestigial remnant or master regulator? Sci Signal, 2008. 1(38): p. pe42.

26. Kitevska, T., D.M. Spencer, and C.J. Hawkins, Caspase-2: controversial killer or checkpoint controller? Apoptosis, 2009. 14(7): p. 829-48.

27. He, Y., et al., Induction of specific cytotoxic lymphocytes in mice vaccinated with Brucella abortus RB51. Infect Immun, 2001. 69(9): p. 5502-8.

28. Upton, J.P., et al., Caspase-2 cleavage of BID is a critical apoptotic signal downstream of endoplasmic reticulum stress. Mol Cell Biol, 2008. 28(12): p. 3943-

29. Lin, C.F., et al., Sequential caspase-2 and caspase-8 activation upstream of mitochondria during ceramide and etoposide-induced apoptosis. J Biol Chem, 2004. 279(39): p. 40755-61.

30. Handschumacher, R.E., et al., Cyclophilin: a specific cytosolic binding protein for cyclosporin A. Science, 1984. 226(4674): p. 544-7.

31. Fink, S.L. and B.T. Cookson, Caspase-1-dependent pore formation during pyroptosis leads to osmotic lysis of infected host macrophages. Cell Microbiol, 2006. 8(11): p. 1812-25.

32. Frank, A., U. Rauen, and H. de Groot, Protection by glycine against hypoxic injury of rat hepatocytes: inhibition of ion fluxes through nonspecific leaks. J Hepatol, 2000. 32(1): p. 58-66.

33. Pham, N.A. and D.W. Hedley, Respiratory chain-generated oxidative stress following treatment of leukemic blasts with DNA-damaging agents. Exp Cell Res, 2001. 264(2): p. 345-52.

34. Gorman, A., A. McGowan, and T.G. Cotter, Role of peroxide and superoxide anion during tumour cell apoptosis. FEBS Lett, 1997. 404(1): p. 27-33.

35. Bagchi, M., et al., Naphthalene-induced oxidative stress and DNA damage in cultured macrophage J774A.1 cells. Free Radic Biol Med, 1998. 25(2): p. 137-43.

36. Bagchi, M., et al., Protective effect of melatonin on naphthalene-induced oxidative stress and DNA damage in cultured macrophage J774A.1 cells. Mol Cell Biochem, 2001. 221(1-2): p. 49-55.

37. Aggarwal, S. and S. Gupta, Increased activity of caspase 3 and caspase 8 in anti-Fas-induced apoptosis in lymphocytes from ageing humans. Clin Exp Immunol, 1999. 117(2): p. 285-90.

38. Pardo, J., et al., The mitochondrial protein Bak is pivotal for gliotoxin-induced apoptosis and a critical host factor of Aspergillus fumigatus virulence in mice. J Cell Biol, 2006. 174(4): p. 509-19.

39. Pei, J., et al., Brucella abortus rough mutants induce macrophage oncosis that requires bacterial protein synthesis and direct interaction with the macrophage. Infect Immun, 2006. 74(5): p. 2667-75.

40. Allen, C.A., L.G. Adams, and T.A. Ficht, Transposon-derived Brucella abortus rough mutants are attenuated and exhibit reduced intracellular survival. Infect Immun, 1998. 66(3): p. 1008-16.

41. Berntzen, G., et al., The tumor necrosis factor-inducing potency of lipopolysaccharide and uronic acid polymers is increased when they are covalently linked to particles. Clin Diagn Lab Immunol, 1998. 5(3): p. 355-61.

42. Otterlei, M., et al., Similar mechanisms of action of defined polysaccharides and lipopolysaccharides: characterization of binding and tumor necrosis factor alpha induction. Infect Immun, 1993. 61(5): p. 1917-25.

43. Misawa, T., et al., Microtubule-driven spatial arrangement of mitochondria promotes activation of the NLRP3 inflammasome. Nat Immunol, 2013. 14(5): p. 454-60.

44. Nakahira, K., et al., Autophagy proteins regulate innate immune responses by inhibiting the release of mitochondrial DNA mediated by the NALP3 inflammasome. Nat Immunol, 2011. 12(3): p. 222-30.

45. Subramanian, N., et al., The adaptor MAVS promotes NLRP3 mitochondrial localization and inflammasome activation. Cell, 2013. 153(2): p. 348-61.

46. Lamkanfi, M., et al., A novel caspase-2 complex containing TRAF2 and RIP1. J Biol Chem, 2005. 280(8): p. 6923-32.

47. Lin, Y., et al., Cleavage of the death domain kinase RIP by caspase-8 prompts TNF-induced apoptosis. Genes Dev, 1999. 13(19): p. 2514-26.

48. Liu, J., et al., Essential role of caspase-8 in p53/p73-dependent apoptosis induced by etoposide in head and neck carcinoma cells. Mol Cancer, 2011. 10: p. 95.

49. Seth, R., et al., p53-dependent caspase-2 activation in mitochondrial release of apoptosis-inducing factor and its role in renal

50. Slee, E.A., et al., Ordering the cytochrome c-initiated caspase cascade: hierarchical activation of caspases-2, -3, -6, -7, -8, and -10 in a caspase-9-dependent manner. J Cell Biol, 1999. 144(2): p. 281-92.

Chapter 3

ER stress activates the inflammasome via NLRP3-caspse-2 driven mitochondrial damage

Abstract

Endoplasmic reticulum (ER) stress is observed in many human diseases, often associated with inflammation. ER stress can trigger inflammation through NLRP3, which may stimulate inflammasome formation by association with damaged mitochondria. How ER stress triggers mitochondrial dysfunction and inflammasome activation is ill defined. Here we use an infection model to show that the IRE1α ER stress sensor regulates mitochondrial dysfunction through an NLRP3-mediated feed-forward loop, independently of ASC. IRE1α activation increased mitochondrial reactive oxygen species, promoting NLRP3 association with mitochondria. NLRP3 was required for ER stress-induced cleavage of caspase-2 and Bid, and subsequent release of mitochondrial contents. Caspase-2 and Bid were necessary for activation of the canonical inflammasome by infection-associated or sterile ER stress. These data identify an NLRP3-caspase-2 dependent mechanism that relays ER stress to the mitochondria to promote inflammation, integrating cellular stress and innate immunity.

Introduction

Cellular stress provokes release of molecular danger signals that stimulate inflammatory signaling [1, 2], but the mechanisms linking stress with release of danger associated molecular patterns (DAMPs) are not fully defined. Such mechanisms are highly relevant to human health as molecular stress and inflammation increase with age and are associated with many acute and chronic diseases [3-6]. Mitochondria can act as platforms to nucleate signaling by large molecular complexes, like the NLRP3 inflammasome, and drive inflammation through release of mitochondrial DAMPs in response to diverse stressors [7]. How such different stressors as infection, glucose deprivation, oxidative stress, or disruption of calcium homeostasis trigger these inflammatory events is not fully understood. The endoplasmic reticulum (ER) is a large endomembrane compartment that is highly sensitive to perturbation and is central to the function of many organelle networks, suggesting that ER may act as a relay station between stressors and the mitochondria, linking stress and inflammatory signaling.

Three ER-resident unfolded protein sensors ATF6, IRE1 (IRE1), and PERK control the ER stress response, an adaptive program that defines the fate of the stressed cell [8]. Toll-like receptors (TLR), which primarily recognize microbial ligands like lipopolysaccharide (LPS), selectively stimulate ER stress sensors [9], and LPS-primed macrophages react to ER stress by activating the NLRP3 inflammasome [10]. Microbial infection represents a useful model for investigating ER stress and inflammation because infection is often associated with ER stress, and animals deficient in components of the IRE1 signaling pathway are more

susceptible to bacterial infection than controls [9, 11-13]. *Brucella abortus* strain RB51 is an attenuated bacterial vaccine strain that infects macrophages, causes ER stress, and provokes a robust immune response without the complex effects of intracellular replication [14]. We therefore used RB51 as a probe to elucidate ER stress-dependent immune signaling. Virulent *B. abortus* mediates inflammasome activation through NLRP3 [15], a sensor responsive to diverse cellular stresses, suggesting that *B. abortus* strains could be appropriate for studying the interplay between ER stress and NLRP3-dependent immune signaling [4]. NLRP3-deficient animals exhibit increased susceptibility and decreased survival during infection by some microbial pathogens [16]. Notably, NLRP3 in a resting state is associated with ER, but upon stimulation moves to ER-mitochondrial junctions [17]. These data led us to hypothesize that ER stress sensors could modulate NLRP3-dependent crosstalk between ER and mitochondria leading to inflammasome activation.

Results

RB51-induced inflammasome activation requires IRE1 and TXNIP

TLR ligands (e.g., LPS) activate IRE1, but not ATF6 or PERK, activating transcription of proinflammatory cytokines [9]. To determine if IRE1 was stimulated during RB51 infection, we investigated splicing of *xbp1* transcript, a direct target of the endonuclease domain of activated IRE1 [8]. Tunicamycin (TM), an inhibitor of protein glycosylation [8, 18], served as a positive control for ER stress assays. Robust splicing of *xbp1* was seen in tunicamycin-treated bone marrow derived macrophages (BMDM) as well RB51-infected BMDM at 8h post-infection (pi) (Fig.

3.1A). ER stress signaling can lead to cell death in some contexts, so we measured release of the large cytosolic lactate dehydrogenase complex as a measure of cell death and found that the majority of infected cells remained viable by 8h post infection (Fig A4A). Thus, infection by RB51 stimulated IRE1 activation, as previously observed for other microbial ligands [9].

Recent studies revealed that ER stress induced by metabolic perturbation could mediate inflammasome activation [19]. In addition, RB51 stimulates robust IL-1β production at both low and high multiplicity of infection (Fig. A4B). We therefore tested whether ER stress was also required for RB51-induced IL-1β production. We infected BMDM with RB51 in the presence of 4μ8C, an inhibitor of the IRE1 endonuclease [20]. Treatment with 4μ8C led to a decrease in caspase-1 cleavage, but not in bacterial uptake. (Fig. 3.1B and Fig. A5). Treatment with tauroursodeoxycholic acid (TUDCA), a molecular chaperone that alleviates ER stress, or 4μ8C, led to a significant decrease in IL-1β production in RB51-infected BMDM, but not BMDM treated with LPS+ATP (L+A), our positive control condition for inflammasome activation assays (Fig. 3.1C). IRE1 inhibition had no effect on L+A-induced caspase-1 cleavage and IL-1β production. These data suggest that unlike RB51, L+A does not rely on IRE1 to induce IL-1β production. Knockdown of IRE1 (IRE1KD, Fig. A6A and B) similarly resulted in decreased IL-1β production and caspase-1 cleavage.

To determine whether IRE1 plays a role in modulating inflammation *in vivo*, we treated C57BL/6 mice with either 5% DMSO (vehicle control) or 4μ8C and infected the animals intraperitoneally with 10^8 CFU of RB51. Consistent with our

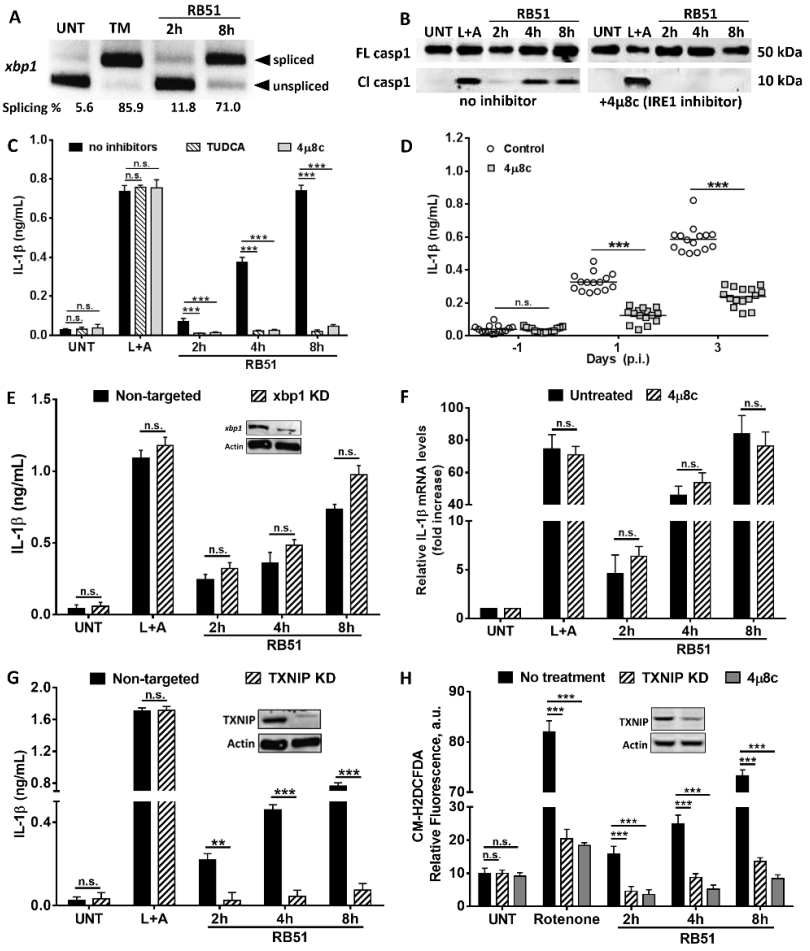

Figure 3.1: IRE1 via TXNIP modulates RB51-induced inflammasome activation. (A) *xbp1* splicing, in RB51-infected BMDM. qRT-PCR samples were treated with PstI to distinguish between spliced (184 bp) and unspliced variants (119 bp following PstI digestion). (B) Caspase-1 cleavage in RB51-infected BMDM in absence or presence of 4μ8c. (C) IL-1β ELISA analysis of supernatants from RB51-infected BMDM treated with or without TUDCA (chemical chaperone, 300 μM) and 4μ8c (IRE1 inhibitor, 50 μM). Error bars represent mean ± SD of n≥3 independent experiments. *** represent p-value <0.0001, n.s. = not significant. (D) Serum IL-1β levels in mice treated with 5% DMSO (control, n = 15) or 4μ8c (n = 15) and infected with RB51 (i.p., CFU 1 x 10^8). (E) qPCR analysis of IL-1β transcript levels RB51-infected BMDM in absence or presence of 4μ8c. IL-1β ELISA analysis of supernatants from RB51-infected BMDM transfected with (F) non-target and *xbp1* siRNA or (G) non-target and TXNIP siRNA. (H) CM-H2DCFGA was used to measure ROS levels during RB51 infection in presence of 4μ8c or TXNIP siRNA. UNT, TM, and L+A represent untreated, tunicamycin (10 μg/mL, positive control for ER stress activation) and LPS+ATP (200 ng/mL and 1mM respectively; positive control for inflammasome activation).

in vitro findings, 4μ8C-treated mice showed significantly decreased serum IL-1β, as well as increased bacterial burden in the spleen (Fig. 3.1D and Fig. A7). These data point to IRE1 as an important regulator of ER stress-induced inflammasome activation during infection.

Previous studies have identified multiple targets for the IRE1 endonuclease, including *xbp1* and miR-17, a negative regulator of thioredoxin-interacting protein (TXNIP) translation. The XBP1 transcription factor selectively enhances transcription of pro-inflammatory cytokine genes. IRE1-dependent miR-17 degradation increases TXNIP protein, which shuttles to the mitochondria and binds thioredoxin-2, raising levels of mitochondrial ROS. To assess if *xbp1* or TXNIP control IRE1-driven IL-1β production, we transfected BMDM with *xbp1* or *txnip* specific siRNA and measured IL-1β levels. Transient knockdown of XBP1 had no effect on RB51-induced IL-1β production, and *IL1b* as well as NLRP3 transcription was unchanged with 4μ8C treatment (Fig. 3.1E-F and Fig. A8). Transient knockdown of TXNIP led to a significant decrease in IL-1β and ROS levels in RB51-infected BMDM. These data suggest that following RB51 infection IRE1 is not involved in IL-1β priming, but acts through TXNIP to induce IL-1βproduction.

ER stress-induced mitochondrial dysfunction aids in inflammasome activation

ER stress drives mitochondria to release mtDAMPs, which can activate the inflammasome [17, 21, 22]. Concomitant with the mtDAMPs release, mitochondrial ROS (mtROS) can increase sharply. Previous studies have shown that TXNIP increases overall levels of ROS in mitochondria [23]. Moreover, we observed an increase in ROS levels over time in RB51-infected BMDM, a phenotype dependent

upon IRE1 and TXNIP (Fig. 3.1H). To determine if mtROS was involved in IRE1-induced IL-1β production, we infected BMDM derived from transgenic mice that express a catalase targeted to mitochondria (mCAT), thus preventing ROS accumulation in the mitochondrial network [24]. Both ROS and IL-1β levels significantly decreased in infected mCAT BMDM when compared to infected WT BMDM (Fig. 3.2A and B). The absence of ROS had no effect on L+A-induced IL-1β production, consistent with previous work that demonstrated mitochondrial function is not essential for activation of the NLRP3 inflammasome [25]. Studies have reported that mtROS mediates release of mitochondrial contents into the cytosol. Since we observed an increase in ROS levels upon RB51 infection, we hypothesized that infected BMDM would release mitochondrial contents into the cytosol. We therefore infected BMDM with RB51 and measured cytochrome *c* and mtDNA release in comparison to tunicamycin treatment, which is known to induce ER stress and mitochondrial dysfunction. TM-treated and RB51-infected macrophages released cytochrome *c* and mtDNA into the cytosol, a process blocked by IRE1 inhibition or knockdown (Fig.3.2C and Fig. A9A and B). Since the presence of transfected mtDNA in the cytosol can stimulate IL-1β production [21, 26], we investigated whether release of mitochondrial components during RB51 infection contributed to IL-1β production by treating BMDM with cyclosporin A (CsA), which prevents opening of the mitochondrial permeability transition pore [27]. We infected BMDM with RB51 or L+A in the presence or absence of CsA, and measured IL-1β production by ELISA. CsA treatment significantly decreased IL-1β levels in RB51-infected macrophages, even though bacterial uptake was

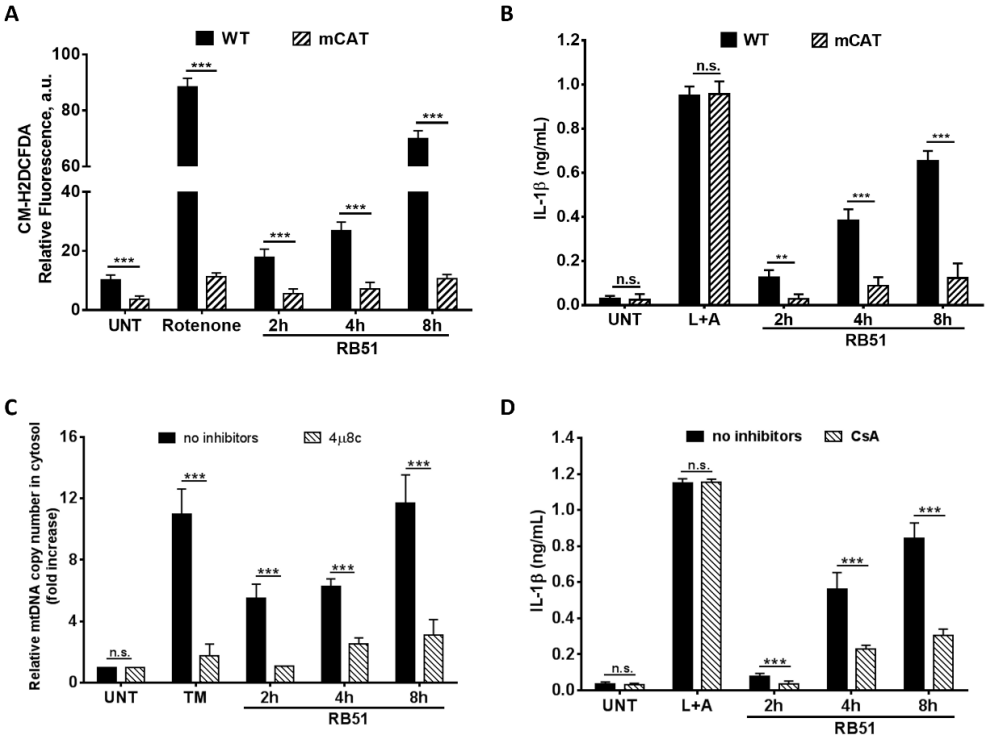

Figure 3.2: ER stress-induced mitochondrial dysfunction drives IL-1β production. (A) CM-H2DCFGA was used to measure ROS levels in WT and mitochondrial-specific catalase (mCAT) BMDM infected with RB51. Rotenone serves as a positive control for ROS induction. (B) IL-1β levels in RB51-infected WT and mCAT BMDM. (C) qPCR analysis of mitochondrial DNA (mtDNA) release into cytosol during RB51 BMDM infection. (D) IL-1β levels in RB51-infected BMDM with or without cyclosporin A (CsA, 10 μM). Error bars in (A - D) represent mean ±SD of n≥3 independent experiments. *** represent p-value <0.0001, n.s. = not significant. UNT, TM, and L+A represent untreated and tunicamycin (10 μg/mL, positive control for ER stress activation), and LPS+ATP (200 ng/mL and 1mM respectively; positive control for inflammasome activation).

unaffected (Fig. A10). CsA treatment did not affect IL-1β production in L+A treated BMDM, suggesting that our L+A treatment protocol, which results in little mtDNA release, induces IL-1β production independently of mitochondrial damage (Fig. 3.2D). These data indicate that RB51 infection damages mitochondria via a IRE1-dependent mechanism.

NLRP3 mediates IRE1-induced mitochondrial stress in an ASC-independent manner

We reasoned that NLRP3 would be the most likely sensor to respond to the infection-induced ER stress signal [10, 19, 28]. Upon activation, NLRP3 can translocate from the ER to the mitochondria [17]. NLRP3 is also reported to trigger mitochondrial dysfunction and IL-1β production in the presence of oxidized mtDNA [21, 26]. In macrophages infected with virulent *B. abortus*, both NLRP3 and the cytosolic DNA sensor AIM2 were required for IL-1β production [15]. Moreover, the AIM2 inflammasome was shown to regulate IL-1β production when stimulated by mtDNA transfected into the cell [21]. Since RB51 induced mtDNA release, we first assessed if AIM2 was required for RB51-induced IL-1β production by measuring IL-1β levels in supernatants of RB51-infected WT and *Aim2*$^{-/-}$ BMDM. We found that AIM2 did not contribute to IL-1β production induced by RB51 infection or by LPS+ATP, which depends on NLRP3 (Fig. A11).

To determine if NLRP3 was involved in controlling the release of mitochondrial contents during RB51 infection, we first assessed if NLRP3 was recruited to mitochondria. In RB51-infected WT BMDM, NLRP3 was recruited to the mitochondrial fraction at 4h p.i., a time point that corresponds with cytochrome

c and mtDNA release (Fig. 3.3A and B). NLRP3 recruitment to the mitochondria was abolished in mCAT and TXNIP KD BMDM. NLRP3-deficient macrophages did not release mtDNA nor cytochrome *c* into the cytosol upon RB51 infection or treatment with the ER stress inducer tunicamycin (Fig. 3.3C and Fig. A12A). In addition, NLRP3 deficiency abolished RB51-induced IL-1β production and caspase-1 cleavage, but did not affect overall caspase-1 levels (Fig. 3.3D and Fig. A12B). Since NLRP3 appeared to be a key component of RB51-induced inflammasome activation, we investigated whether ASC or caspase-1, other key components of the canonical inflammasome, were also crucial to inducing mitochondrial damage. *Asc*$^{-/-}$ and YVAD-CHO (caspase-1 inhibitor)-treated BMDM were not required for mtDNA and cytochrome *c* release into the cytosol upon infection (Fig. 3.3C and Fig. A12C). However, ASC and caspase-1 were necessary for IL-1β production during RB51 infection (Fig. 3.3D). The inability to produce IL-1β in YVAD-CHO-treated macrophages was not due to a decrease in bacterial uptake (Fig. A13). Together, these results show that during RB51-induced inflammasome activation, NLRP3 has a critical role upstream of the mitochondria, independent of ASC and caspase-1, in mediating release of mitochondrial contents.

NLRP3 drives mitochondrial dysfunction through caspase-2

During ER stress, we considered that NLRP3 might facilitate mitochondrial dysfunction through the cysteine protease caspase-2. Caspase-2 can cause mitochondrial dysfunction leading to cytochrome *c* release [29]. Moreover, caspase-2 is activated by ER stress or RB51 infection [30-32], and regulates

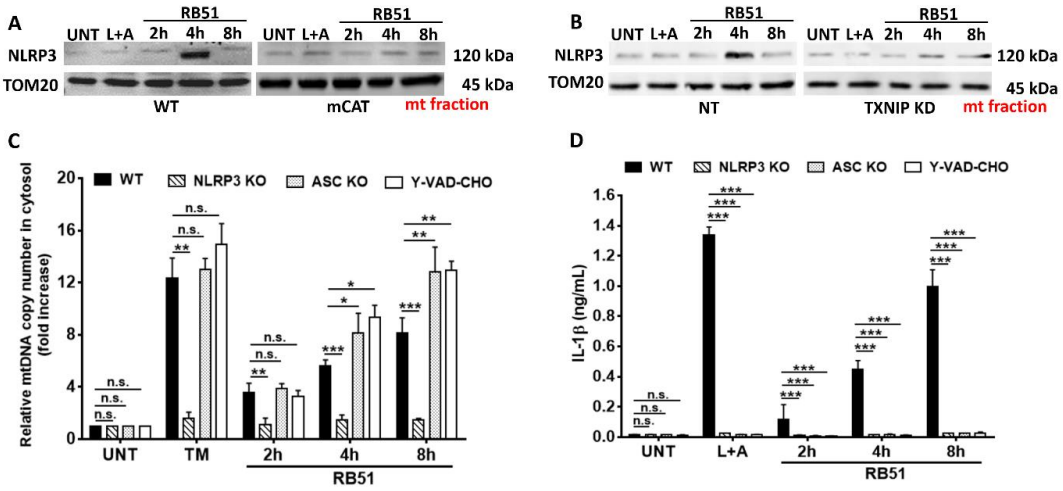

Figure 3.3: NLRP3 is required for RB51-induced release of mitochondrial contents. Immunoblot of NLRP3 at the mitochondrial fraction of (A) WT and mCAT BMDM and (B) non-target (NT) and TXNIP KD BMDM. (C) Quantitative PCR of mtDNA in cytosolic extracts from RB51-infected WT and *nlrp3*$^{-/-}$, *asc*$^{-/-}$, and Z-YVAD-CHO (caspase-1 inhibitor, 2 μM) treated BMDM. (D) IL-1β levels in RB51-infected WT and *nlrp3*$^{-/-}$, *asc*$^{-/-}$, and Z-YVAD-CHO (caspase-1 inhibitor, 2 μM) inhibited BMDM. Error bars represent mean ± SD of n≥3 independent experiments. *, **, and *** represent p-values of <0.05, <0.001, and <0.0001 respectively. n.s. = not significant. UNT, TM, and LPS+ATP represent untreated, tunicamycin (positive control for ER stress induction, 10 μg/mL), and LPS+ATP (positive control for inflammasome activation, 200 ng/mL and 1mM) respectively. Immunoblots in (A) and (B) are representative of n≥3 independent experiments that were performed and imaged in parallel with identical parameters using a LiCor Odyssey imaging system.

caspase-1 activation [33, 34]. We reasoned that, under conditions of ER stress, NLRP3 might be inducing activation of caspase-2 leading to release of mtDNA and cytochrome *c* into the cytosol. We probed lysates of control, 4μ8C-treated, as well as IRE1KD infected macrophages, for the full-length or cleaved active form of caspase-2 (Fig. 3.4A and Fig. A14A). IRE1 was required for caspase-2 cleavage during RB51 infection, but not for caspase-2 cleavage triggered by the positive control genotoxic agent, etoposide (ET), [29]. These data suggest that unlike ET, RB51-induced caspase-2 activation is dependent upon IRE1.

To determine whether NLRP3 acted upstream or downstream of caspase-2, C57BL/6 and *Nlrp3*$^{-/-}$ BMDM were infected with RB51, and lysates probed for cleaved caspase-2 (Fig. 3.4B). Caspase-2 cleavage was nearly absent in infected *nlrp3*$^{-/-}$ macrophages. In contrast, caspase-2 cleavage appeared independent of ASC, as well as caspase-1, essential components for activation of the canonical inflammasome (Fig. A14B). In addition, caspase-2 is recruited to mitochondria in an IRE1 and NLRP3-dependent matter (Fig. 3.4C and D). We next assessed mitochondrial dysfunction in caspase-2 deficient BMDM and found that infected *casp2*$^{-/-}$ BMDM released significantly less mtDNA and cytochrome *c* into the cytosol (Fig. 3.4E and Fig. A14C). Moreover, caspase-2 deficiency abolished IL-1β production and caspase-1 activation without affecting bacterial uptake (Fig. 3.4F, Fig. A14D and E). Although these caspase-2 deficient BMDM were infected to similar levels as WT, it is possible that these BMDM were deficient in transcription of *IL1b*. We performed quantitative RT-PCR analysis to measure *IL1b* transcript levels in WT and *casp2*$^{-/-}$ BMDM. In the absence of caspase-2, infected

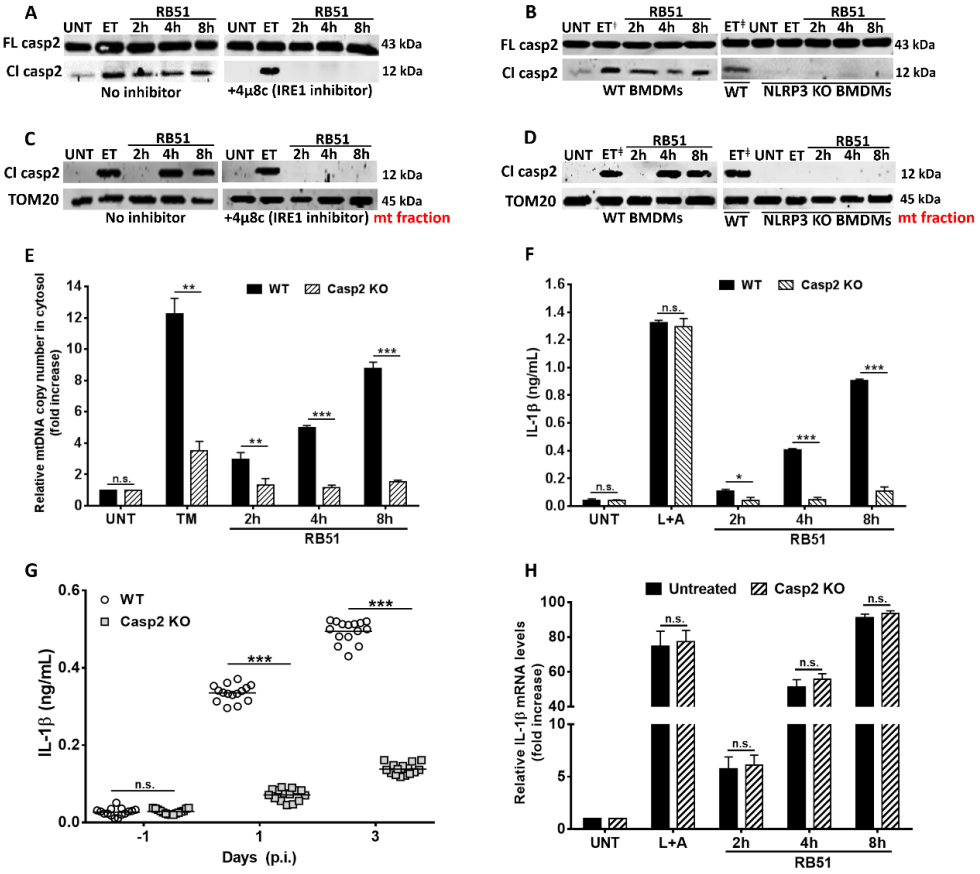

Figure 3.4: NLRP3 and caspase-2 are required for ER stress-induced inflammasome activation. Immunoblot analysis of caspase-2 in (A) with or without 4μ8c (IRE1 inhibitor, 50 μM) and (B) RB51-infected WT and *nlrp3*$^{-/-}$ BMDM. Immunoblot analysis of caspase-2 in the mitochondrial fraction (C) with or without 4μ8c (IRE1 inhibitor, 50 μM) and (D) RB51-infected WT and *nlrp3*$^{-/-}$ BMDM – ET‡ identifies duplicate lanes of the same sample. (E) qPCR analysis of mtDNA in cytosolic fractions of infected WT and *casp2*$^{-/-}$ BMDM. IL-1β levels in (F) WT and *casp2*$^{-/-}$ RB51-infected (i.p., CFU 1 x 10^{8}) BMDM and (G) WT (n = 15) and *casp2*$^{-/-}$ mice (n = 15). Data in (G) were pooled from 2 independent experiments. (H) qPCR analysis of IL-1β transcript levels in WT and *casp2*$^{-/-}$ RB51-infected BMDM. Error bars represent mean ± SD of n≥3 independent experiments. *, **, and *** represent p-values of <0.05, <0.001, and <0.0001 respectively. n.s. = not significant. UNT, ET, TM, and L+A represent untreated, etoposide (positive control for caspase-2 activation and Bid truncation, 25 μM), tunicamycin (positive control for ER stress induction, 10 μg/mL), and LPS+ATP (positive control for inflammasome activation, 200 ng/mL and 1mM respectively). Immunoblots in (A-D) are representative of n≥3 independent experiments that were performed and imaged in parallel with identical parameters using a LiCor Odyssey imaging system. Full length caspase-2 and TOM20 (mitochondrial specific outer membrane protein) serve as loading controls.

BMDM still produced similar levels of *IL1b* to WT BMDM (Fig. 3.4G) suggesting that the defect in IL-1β production is not in priming but in activating the inflammasome. Similar to our *in vitro* data, *casp2*$^{-/-}$ mice exhibited low serum IL-1β levels and higher bacterial burden in the spleen (Fig. 3.4H). These data suggest that NLRP3 can mediate RB51-induced mitochondrial damage and inflammasome activation by a caspase-2-dependent mechanism.

NLRP3 and caspase-2 induce mitochondrial damage via Bid truncation

We next aimed to elucidate the mechanism by which NLRP3 and caspase-2 could regulate mitochondrial dysfunction. NLRP3 and caspase-2 could lead to activation of Bid, which damages mitochondria by licensing pore formation of Bax and Bak, pro-apoptotic factors of the Bcl-2 family [35]. Caspase-2 can truncate Bid (tBid), leading to activation [35]. To determine if Bid was involved in RB51-induced mitochondrial damage, we infected 4μ8C-treated or IRE1KD macrophages with RB51 and probed for the presence of tBid. Etoposide served as a positive control condition for Bid truncation. Total Bid levels remained constant under all conditions, but Bid truncation was diminished in 4μ8C-treated and IRE1KD macrophages (Fig. 3.5A and Fig. A15A), implicating Bid in RB51-induced mitochondrial dysfunction. ET induces mitochondrial dysfunction but does not induce ER stress [36, 37]. Therefore, it was not surprising to see that IRE1 inhibition had no effect on Bid truncation in ET-treated BMDM. To determine the role of NLRP3 and caspase-2 in this process, C57BL/6, N*lrp3*$^{-/-}$, and *Casp2*$^{-/-}$ BMDM were infected with RB51 to assay Bid truncation, which was markedly decreased in the absence of NLRP3 and caspase-2 (Fig. 3.5B and Fig. A15B).

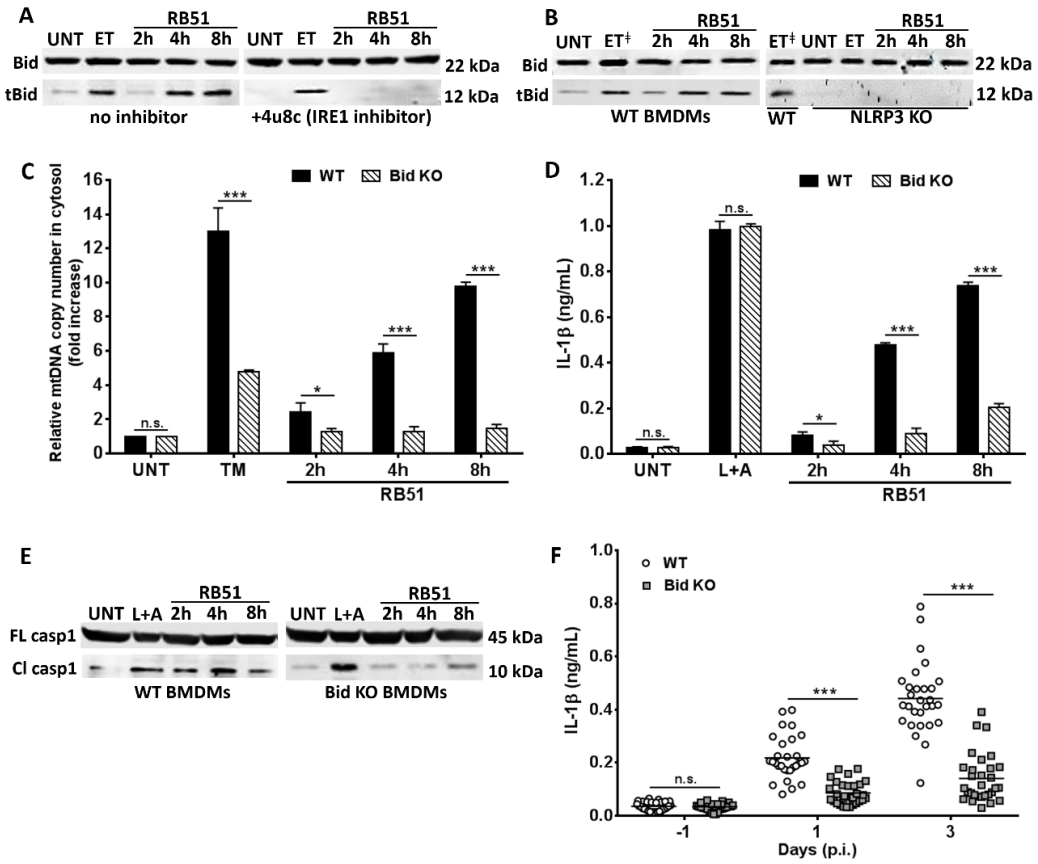

Figure 3.5: NLRP3 controls mitochondrial dysfunction by a Bid dependent mechanism. Bid truncation in RB51-infected (A) with or without 4μ8c (IRE1 inhibitor, 50 μM) and (B) WT and *nlrp3*$^{-/-}$ BMDM – ET‡ identifies duplicate lanes of the same sample. (C) Quantitation of mtDNA in cytosolic extracts from RB51-infected WT and *bid*$^{-/-}$ BMDM. (D) ELISA of IL-1β levels in supernatants from RB51-infected WT and *bid*$^{-/-}$ BMDM. (E) Immunoblot analysis of caspase-1 in WT and *bid*$^{-/-}$ BMDM infected with RB51. (f) Serum IL-1β levels in WT (n = 29) and *bid*$^{-/-}$ (n = 30) mice RB51-infected (i.p. CFU 1 x 10^8) mice. The data in (F) were pooled from 2 independent experiments. Error bars represent mean ± SD of n≥3 independent experiments. * and *** represent p-values of <0.05 and <0.0001 respectively. n.s. = not significant. UNT, ET, TM, and L+A represent untreated, etoposide (positive control for Bid truncation, 25 μM), tunicamycin (positive control for ER stress induction, 10 μg/mL), and LPS+ATP (positive control for inflammasome activation, 200 ng/mL and 1mM) respectively. Immunoblots in (A), (B), and (E) are representative of n≥3 independent experiments that were performed and imaged in parallel with identical parameters using a LiCor Odyssey imaging system. Full length (FL) caspase-1 and Bid serve as loading controls.

Infected *Bid*$^{-/-}$ BMDM released significantly less mtDNA into the cytosol than wildtype controls, confirming that Bid is required for mitochondrial damage, even though Bid-deficiency did not affect bacterial uptake (Fig. 3.5C and Fig. A15C). *Bid*$^{-/-}$ BMDM infected with RB51 also exhibited diminished secretion of IL-1β and caspase-1 cleavage (Fig. 3.5D and E). Consistent with our *in vitro* results, RB51-infected *Bid*$^{-/-}$ mice showed a significant decrease in serum IL-1β, as well as an increase in bacterial burden in the spleen, compared to wildtype controls (Fig. 3.5F and Fig. A16). Thus, during RB51 infection, NLRP3 and caspase-2 trigger mitochondrial damage through Bid, leading to inflammasome activation.

NLRP3 and caspase-2 are required for inflammasome activation in response to UPR-inducing chemicals

Our data thus far identified the IRE1-NLRP3-caspase2-Bid axis as a mechanism for relaying infection-induced ER stress signals to the mitochondria, leading to inflammasome activation. We considered the possibility that this pathway might be important for infection-induced inflammasome activation, but not in the general ER stress response. We therefore tested whether IRE1, NLRP3, caspase-2 and Bid were required for inflammasome activation in response to thapsigargin (TG), tunicamycin (TM), and brefeldin A (BFA), three chemical inducers of ER stress that act by distinct mechanisms. The sesquiterpene lactone, thapsigargin, is a selective inhibitor of Ca^{2+} uptake from the cytosol by ER Ca^{2+} ATPases [38], which results in net loss of ER luminal Ca^{2+} and ER stress. Tunicamycin, a nucleoside antibiotic, inhibits N-glycosylation of proteins in the Golgi apparatus resulting in ER stress [39]. Brefeldin A, a fungal lactone antibiotic,

induces disassembly as well as collapse of the Golgi into the ER leading to a backup of Golgi protein in the ER and ER stress [40]. Treatment of WT BMDM with TG, TM, or BFA resulted in weak IL-1β production, but robust caspase-1 cleavage, suggesting that minimal priming was occurring during TG, TM, and BFA treatment in contrast to L+A treatment (Fig. 3.6A and B). Priming to stimulate *IL1b* transcription, and inflammasome activation are the two signals required for robust IL-1β secretion [41]. We assessed proIL-1β production by immunoblot and found that unlike LPS, TM and BFA induced weak proIL-1β production whereas TG did not trigger any detectable proIL-1β production (Fig. A17A). These data suggest that ER stress can serve as the second signal for inducing inflammasome activation, but is a weak inducer of the first signal (priming) that regulates transcription of *IL1b*. When we assessed inflammasome activation, we found that similar to our infection model, caspase-1 cleavage was abrogated in 4μ8C-treated BMDM in the presence of TG and TM (Fig.3.6B). Although BFA did trigger IRE1 activation (Fig. A17B), IRE1 was not required for BFA-induced inflammasome activation, as previously reported by Tschopp and colleagues [10], perhaps due to the more extensive perturbations induced by BFA, compared to TG or TM. In TM and TG-treated BMDM deficient in NLRP3, caspase-2, and Bid, caspase-1 cleavage was virtually absent (Fig. 3.6C-E). Although caspase-2 and Bid were critical for sterile ER stress-induced inflammasome activation, neither was required for inflammasome activation by L+A (Fig. 3.6D and E). Taken together, our data support the IRE1-NLRP3-caspase2-Bid axis as a key mechanism by which general ER stress drives mitochondrial damage and inflammasome activation.

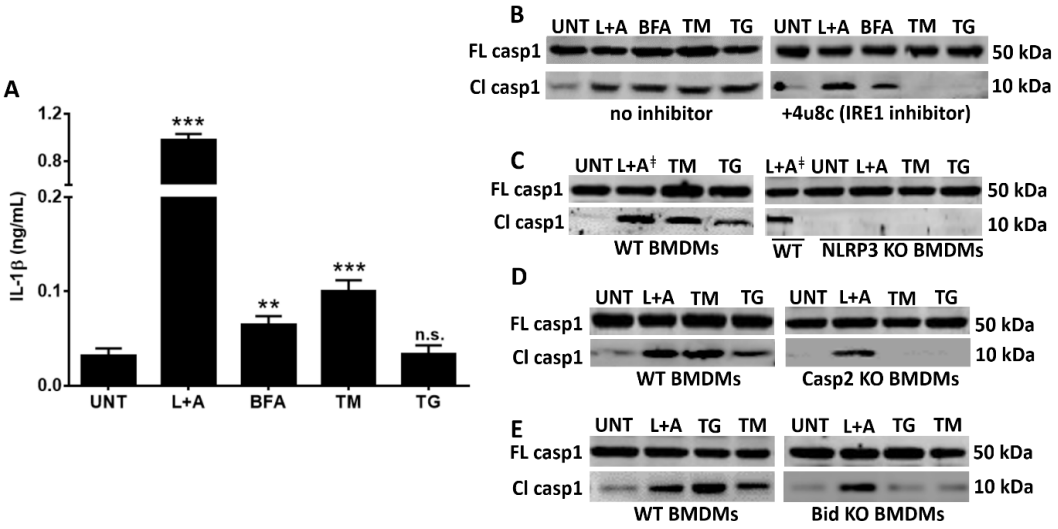

Figure 3.6: NLRP3 and caspase-2 are required for caspase-1 activation during ER stress. (A) ELISA analysis of IL-1β levels in supernatants from BMDM treated with L+A (LPS+ATP, 200 ng/mL and 1mM respectively; positive control for inflammasome activation), or the ER stressors BFA (brefeldin A, 20 µM), TM (tunicamycin, 10 µg/mL), and TG (thapsigargin, 10 µM). Error bars represent mean ± SD of n≥3 independent experiments. ** and *** represent p-values of <0.001 and <0.0001 respectively. n.s. = not significant. Immunoblot analysis of caspase-1 in (B) BMDM in the absence or presence of 4µ8c (IRE1 inhibitor, 50 µM), (C) WT and *nlrp3*$^{-/-}$ BMDM – L+A‡ identifies duplicate lanes of the same sample, (D) WT and *casp2*$^{-/-}$ BMDM, and (E) WT and *bid*$^{-/-}$ BMDM. Immunoblots in (B-E) are representative of n≥3 independent experiments that were performed and imaged in parallel with identical parameters using a LiCor Odyssey imaging system. Full length (FL) caspase-1 serves as a loading control.

Conclusions

ER stress is increasingly implicated in human disease, including infection, Alzheimer's Disease and diabetes [42]. More recent studies, have demonstrated a connection between ER stress and the inflammasome, although the mechanisms that control signaling have not been fully elucidated [10, 19, 28]. Our results reveal that activation of the IRE1 ER stress sensor leads to NLRP3-mediated crosstalk between ER and mitochondria, resulting in release of mitochondrial contents through activation of the caspase-2/Bid axis (Fig. 3.7A). Notably, the requirement of NLRP3 in ER stress-induced mitochondrial damage was independent of ASC and caspase-1, suggesting that this is not a function of the canonical inflammasome. Our data place NLRP3 upstream of caspase-2 in the ER-mitochondrial signaling pathway, and provide a mechanism by which NLRP3 can facilitate mitochondrial damage to activate the inflammasome. Whether NLRP3 or additional inflammasome regulators act as downstream sensors of mitochondrial damage in ER stress conditions remains to be determined, although AIM2 was not required.

The role of mitochondria in activating inflammasomes has been somewhat controversial. Previously, K^+ efflux was proposed as a common mechanism by which diverse stresses that increase membrane permeability, e.g., bacterial toxins or LPS+ATP, activate the NLRP3 inflammasome without requiring mitochondrial damage [25, 43]. However, other studies have reported that mitochondrial damage was critical for inflammasome activation by LPS+ATP or by cytosolic DNA [26, 44, 45]. In the conditions we used, NLRP3-dependent inflammasome

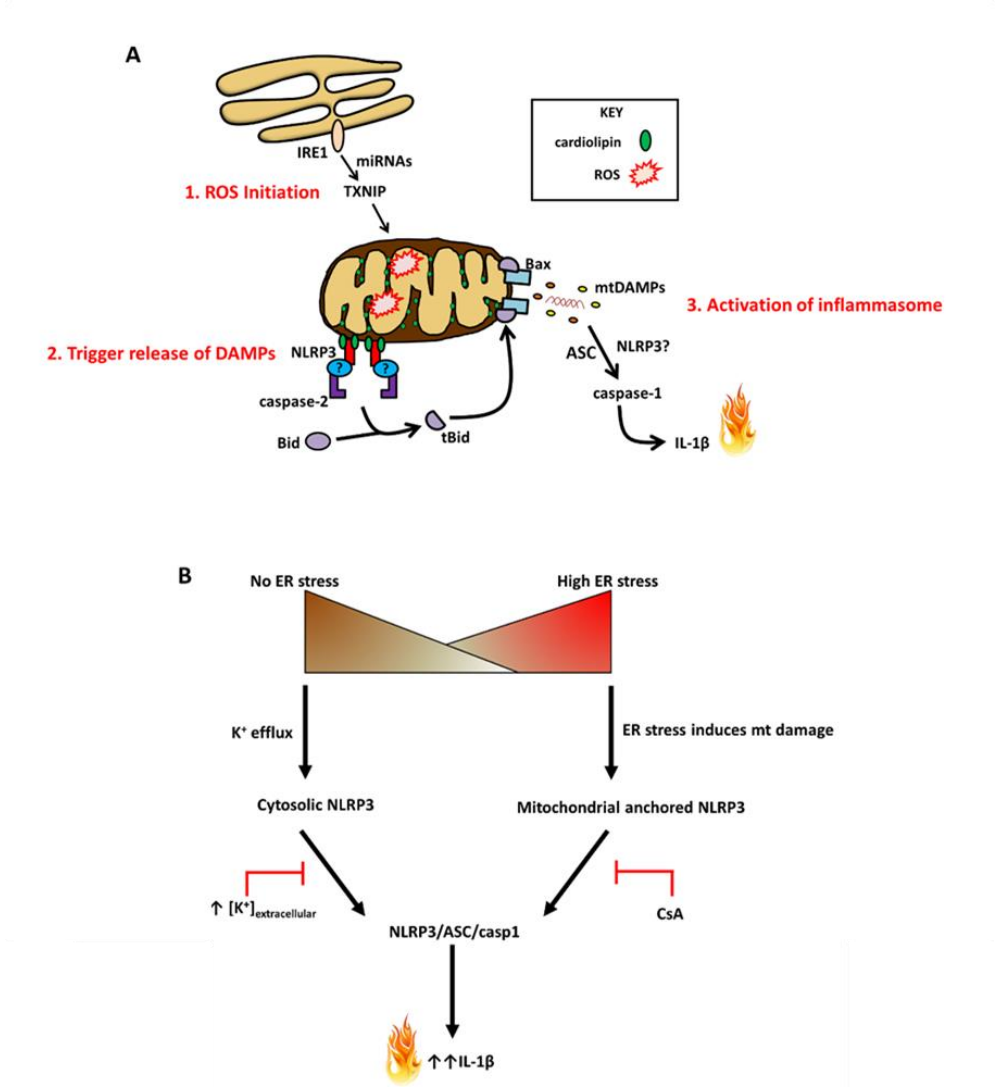

Figure 3.7: Working model of IRE1-induced inflammasome activation. Upon IRE1 activation, TXNIP translocates to the mitochondria and increases ROS levels. The increase in ROS levels, recruits NLRP3 and caspase-2 to the mitochondria and triggers Bid truncation. The processing of Bid is required for mtDNA and cytochrome *c* release, indicative of mitochondrial damage. Release of mtDAMPs aids in activation of the NLRP3-ASC-caspase-1 inflammasome. Blockade of ROS, caspase-2, Bid, or mtDAMPs release will lead to decreased NLRP3-dependent inflammasome activation and IL-1β production. (B) Oligomerization of NLRP3 oligomerization (cytosolic vs. mitochondrial anchored) depends upon the magnitude of ER stress. Regardless of location, NLRP3 aids in IL-1β processing.

activation by LPS+ATP was essentially independent of IRE1, caspase-2, Bid, or mitochondrial content release. However, ER stress-induced inflammasome activation both provoked and required mitochondrial damage. To reconcile our results with previously published reports, we propose that NLRP3-dependent oligomerization, necessary for inflammasome activation, may exhibit distinct signaling requirements depending on the types or magnitude of stress (Fig. 3.7B). For example, a stress that initiates strong K^+ efflux, such as pore formation by bacterial toxins or pannexin-1, might not require mitochondrial damage and would not be blocked by cyclosporin A. Stress that triggers weaker K^+ efflux might be more dependent on mitochondrial danger signals. Notably, protocol-specific conditions may be critical in defining the reliance of inflammasome activation on K^+ efflux vs. mitochondrial damage [21, 26, 46]. In fact, we found that differing times and concentrations of LPS+ATP treatments resulted in substantially different levels of mtDNA release (Fig. A18), perhaps providing an explanation for why conflicting results have been reported. Therefore, the molecular context of cellular stress will likely be critical in defining the key principles that govern inflammasome activation.

Microbial infection imposes complex stress conditions upon infected cells that are not fully defined for most microbes, but may include K^+ efflux, nutrient deprivation, cytoskeletal perturbations and ROS. Microbes or microbial ligands activate IRE1 through TLR signaling [9], and *in vivo* data clearly show that XBP1, a component of the IRE1 signaling pathway, and NLRP3 can mediate resistance to microbial infection [9, 16]. These observations are consistent with the idea that

activation of ER stress machinery influences the outcome of infection by tuning inflammatory responses. Importantly, a recent study demonstrated that IRE1 was required for optimal secretion of pro-inflammatory cytokines, including IL-1β, in a mouse model of inflammatory arthritis [47]. Cellular stress in the form of ER perturbation and mitochondrial dysfunction may provide critical contextual danger signals that together with microbial ligands provoke robust immunity. Because ER stress and mitochondrial dysfunction are also associated with Type 2 diabetes, obesity, Crohn's disease and cancer [48, 49], it will be of interest to determine whether the NLRP3-caspase-2 regulatory axis is more broadly involved in sterile inflammatory diseases.

NLRP3 has emerged as a critical regulator of the inflammasome in response to ER stress and IRE1 activation. How IRE1 leads to NLRP3-dependent stimulation of caspase-2 is still unclear. NLRP3 binds to the signaling adaptor, TXNIP, whose levels are controlled by activated IRE1 [19, 28, 50], suggesting that interaction as a possible interface that may lead to recruitment and cleavage of caspase-2. Alternatively, NLRP3 may interact with an accessory protein similar to ASC that recruits caspase-2 through its CARD domain. IRE1 itself was reported to modulate caspase-2 total protein levels by controlling degradation of regulatory microRNAs in BFA, TG, or TM-treated murine embryonic fibroblasts [32]. However, a recent report indicated that overall caspase-2 levels did not change in response to ER stress induced in human leukemia- and lymphoma-derived cell lines [51], which is in agreement with our data in macrophages showing that caspase-2 cleavage is the key event induced by ER stressors. Our results emphasize the

requirement for caspase-2 and mitochondrial damage in triggering caspase-1 activation specifically in conditions for ER stress since mitochondrial damage is not absolutely required for other triggers of the NLRP3 inflammasome [25]. Determining specific mechanisms by which ER stress tunes the inflammatory response will lay the groundwork for better design of therapeutic approaches for diseases of inflammation and immunity.

Materials and Methods

Mice

Humane animal care at the University of Michigan is provided by the Unit for Lab Animal Medicine, which is accredited by the American Association for Accreditation of Laboratory Animal Care and the Department of Health and Human Services. This study was carried out in strict accordance with the recommendations in the Guide for the Care and Use of Laboratory Animals of the National Institutes of Health. The protocol was approved by the Committee on the Care and Use of Animals (UCUCA) of the University of Michigan.

Bid WT (n = 29), *bid*$^{-/-}$[52] (n = 30), DMSO treated (n = 15),4μ8c treated (n = 15), casp2 WT (n = 15) and *casp2*$^{-/-}$ (n = 15) C57BL/6 mice (8 -12 weeks) were injected intraperitoneally (i.p.) with *Brucella abortus* RB51 vaccine strain (1 x 10^8 CFU) in 200 μl of phosphate-buffered saline (PBS). Mice were matched by sex and age. Mice were treated with DMSO (5% in PBS) and 4μ8c (25mg/kg) daily in 200 μl of PBS. Blood was collected by saphenous vein on day -1, 1, and 3 days post infection (p.i.). Serum was extracted from blood by centrifugation for 3 min at

10,000 rpm and used for assessing IL-1β production by ELISA. At day 3 p.i., spleens were removed from euthanized mice, homogenized in 1 ml 0.2% NP-40, and serial dilutions plated onto *Brucella* agar plates to enumerate CFU.

Cell culture and infection

BMDM were isolated from WT, *casp2*$^{-/-}$, *asc*$^{-/-}$, *nlrp3*$^{-/-}$, *bid*$^{-/-}$ and *aim2*$^{-/-}$ mice. *Casp2*$^{-/-}$ with corresponding WT were purchased from Jackson Laboratories (stock #007899) [53]. *Nlrp3*$^{-/-}$ [54] and *asc-/-* [55] were maintained by the Nuñez laboratory. B*id*$^{-/-}$ [52] and corresponding WT mice were maintained by the Yin laboratory. *Aim2*$^{-/-}$ [56] and corresponding WT mice were maintained by the Fitzgerald laboratory.

Isolated BMDM were differentiated in DMEM (GIBCO) supplemented with 20% heat-inactivated FBS (Invitrogen), 1% L-glutamine (2 mM), 1% sodium pyruvate (1 mM), 0.1% β-mercaptoethanol (55 µM), and 30% L-929 conditioned medium. BMDM were cultured in non-TC treated plates at 37°C in 5% CO_2, fed fresh media on day 3, and harvested on day 6. Four million RAW264.7 macrophages or BMDM were seeded in 6 well plates 18 hr prior to infection. The LPS+ATP samples were pretreated with LPS (200 ng/mL) overnight. The following day, where indicated, cells were pretreated with cyclosporin A (10 µM), TUDCA (300 µM), 4µ8c (50 µM), and Y-VAD-CHO (2 µM) for 1 hr prior to infection. Untreated and pretreated cells were infected with RB51 (MOI 200) for 30 min, after which the inoculum was removed and cells were washed with PBS. Medium containing 50 µg/ml of gentamicin was added to kill extracellular bacteria. To synchronize infection, cells were spun at 1200 rpm for 3 min after adding inoculum. Cells were treated with

etoposide (25 μM), thapsigargin (10 μM), tunicamycin (10 μg/mL), brefeldin A (20 μM), or ATP (1mM) for 4 hr. At the indicated times, cells were lysed in buffer containing 1% NP-40 on ice for 15 min and spun at 16,000 x *g* for 15 min to pellet the insoluble fraction. Soluble fractions were used for immunoblot assays. The insoluble fraction was resuspended in mitochondrial suspension buffer (10mM TrisHCl pH 6.7, 0.15 mM $MgCl_2$, 0.25 sucrose, 1 mM PMSF, 1 mM DTT) and centrifuged at 11,000 x *g* for 15 minutes at 4ºC to pellet the isolated mitochondria. Purity of isolated mitochondria was assessed by immunoblotting for calreticulin - ER marker, TOM20- mitochondrial marker, Lamin B1 - nuclear marker, and Actin - cytosolic marker (Fig. A19).

Bacterial strains and reagents

Brucella abortus strain RB51 was obtained from Dr. G. Schurig (Virginia Polytechnic Institute and State University). Reagents were obtained from the following vendors: cyclosporin A (Sigma-Aldrich), thapsigargin (Fisher), tunicamycin (Sigma-Aldrich), etoposide (Sigma-Aldrich), brefeldin A (Sigma-Aldrich), TUDCA (Calbiochem), 4μ8c (Axon), ATP (Sigma-Aldrich), and Y-VAD-CHO (Santa Cruz). Antibodies were obtained from the following vendors: anti-PERK (cat#: 3192S, Cell Signaling), anti-p-PERK (cat#: sc-32577, Santa Cruz), anti-ATF6 (cat#: sc-22799, Santa Cruz), anti-IRE1 (cat#: 3294S, Cell Signaling), anti-NLRP3 (cat.# MAB7578, Fisher), anti-cytochrome *c* (cat#:4272S, Cell Signaling), anti-caspase-2 (cat#: 3027-100, BioVision), anti-caspase-1 (cat#: sc-514, Santa Cruz), anti-Bid (cat#: 2003S, Cell Signaling), anti-Calreticulin (cat.#

2891, Cell Signaling), anti-TOM20 (cat.# sc-11415, Santa Cruz), anti-Actin (cat#: MS1295P1, Thermo Scientific), and anti-Lamin-b1 (cat#: sc-20682, Santa Cruz).

Lentivirus production and knockdown of IRE1

HEK293T cells were grown in DMEM with 10% fetal bovine serum (Invitrogen). Lentivirus particles were produced by transfecting the cells with the TRC shRNA encoding plasmid (pLKO.1) along with the packaging plasmids (pVSV-G, pGAG-PAL) obtained from the University of Michigan Vector Core. The medium was changed after 24 hr, and virus particles collected at 48 hr. Virus-containing medium was concentrated 10-fold by centrifugation (24000 rpm) for 2 hr at 4°C. Concentrated virus was used to transduce RAW264.7 cells seeded in 60-mm dishes. The medium was changed 24 hr post transduction and cells were left to grow for an additional 24 hr. Transduced cells were selected with puromycin (4 µg/mL). The mouse specific IRE1 shRNA plasmid with antisense sequence of (5'-TTTCTCTATCAATTCACGAGC-3') was purchased from Open Biosystems. The non-targeted control shRNA plasmid was purchased from Sigma-Aldrich.

siRNA knockdown of TXNIP and xbp1

Immortalized BMDM were transfected with specific Dharmacon siGENOME TXNIP siRNA (cat# M-040441-01-0005), xbp1 (cat.# M-040825-00-0005) or non-target siRNA (cat.# D-001206-13-20) using DharmaFECT 4 transfection reagent according to the manufacturer's protocol. Knockdown efficiency was assessed via immunoblot using anti-TXNIP (cat.# NBP1-54578, Novus Biologicals) and anti-xbp1 (cat.# ab37152, Abcam) antibodies.

ROS measurements

BMDM were plated in a 96 well plate with black slides and clear bottom. At designated time points, BMDM were washed with PBS and then incubated with CM-H_2DCFDA (Invitrogen) at a final concentration of 2.5 µM in Ringer buffer (155 mM NaCl, 5 mM KCl, 1 mM $MgCl_2$ $6H_2O$, 2 mM NaH_2PO_4 H_2O, 10 mM HEPES, 10 mM glucose). Cell were incubated for 30 min at 37ºC, washed three times with cold PBS, and incubated for an additional 15 min at 37ºC in warm media for recovery. After recovery, cells were washed one more time with PBS. Florescence was measured at excitation/emission 485nm/525nm.

Immunoblot Assay

Cytosolic extracts collected at indicated time points (2, 4, and 8 hr pi) were separated by SDS-PAGE, transferred to nitrocellulose membranes (Millipore), blocked with 5% nonfat dry milk in TBS-0.1% Tween20 (TBS-T), and incubated overnight at 4°C with primary antibodies specified above. Membranes were washed with TBS-T and incubated with secondary IRDye 680LT Goat anti-rabbit or IRDye 680LT Goat anti-mouse (1:20,000) at room temperature for 1 hr. Bands were visualized using the Li-Cor Odyssey Infrared Imaging System. Immunoblots shown in the figures are representative of n≥3 independent experiments. All immunoblots shown within an individual panel were analyzed in parallel with identical parameters using the Li-Cor System.

Cytokine Analysis

Culture supernatants were collected at indicated time points from macrophages infected as described. IL-1β levels were determined by sandwich enzyme-linked immunosorbent assay (ELISA) according to the manufacturer's instructions (BioLegend). A minimum of 3 technical replicates per experiment and 3 experimental replicates were analyzed for each condition.

Xbp1 splicing assay

Total RNA (2 µg) extracted from samples was prepared using the RNeasy Mini Kit (Qiagen) and used for cDNA synthesis. Primers encompassing the spliced sequences in *xbp1* mRNA (forward 5'-GAACCAGGAGTTAAGAACACG-3' and reverse 5'-AGGCAACAGTGTCAGAGTCC-3') were used for PCR amplification with GoTaq polymerase (Invitrogen). The thermal cycling profile consisted of 30 cycles at 94°C for 1 min, 60°C for 1 min, and 72°C for 1 min. PCR products were incubated with PstI (Invitrogen) at 37°C overnight. PstI digested products were separated by electrophoresis through a 2.5% agarose gel.

Mitochondrial DNA (mtDNA) release assay

DNA was isolated from 200 µL of the cytosolic fraction using a DNeasy Blood & Tissue Kit (Qiagen). Quantitative PCR was employed to measure mtDNA using Brilliant II SYBR Green with Low ROX (Agilent Technologies) on a Stratagene MX300 QPCR System. The copy number of mtDNA encoding cytochrome *c* oxidase I was normalized to nuclear DNA encoding 18S ribosomal RNA. The following primers were used: cytochrome c oxidase I (forward 5'-

GCCCCAGATATAGCATTCCC-3' and reverse 5'-GTTCATCCTGTTCCTGCTCC-3') and 18S rRNA (forward 5'-TAGAGGGACAAGTGGCGTTC-3' and reverse 5'-CGCTGAGCCAGTCAGTGT-3').

Lactate dehydrogenase (LDH) Release Assay

Macrophages were seeded in 96-well plates and infected with RB51 as stated above. Supernatants were analyzed for the presence of LDH enzyme using the CytoTox-ONE™ Homogeneous Membrane Integrity Assay (Promega) as directed by the manufacturer's instructions. Percentage of LDH release was calculated as 100 X [(Experimental LDH Release - Culture Medium Background)/(Maximum LDH Release – Culture Medium Background)].

Statistical Analysis

All p values were generated between identified samples using unpaired two-tailed Student's *t*-tests and represent analysis of ≥3 replicates per condition. Asterisks denote the following p values: *$p<0.05$, **$p<0.001$ and ***$p<0.0001$.

Author Contributions:

DNB, YH, and MXDO designed the experiments. DNB, BA, and MXDO performed the experiments. BA, KF, GN, YH, XC, and XMY contributed critical reagents, materials, and discussion. DNB and MXDO analyzed the data and wrote the paper.

Author Information:

The authors have declared that no competing interests exist.

Acknowledgments

We acknowledge members of the O'Riordan lab for many helpful discussions. We thank Drs. D. Monack and V. Carruthers, for critical review of the manuscript. We are grateful to Dr. V. Rathinam, Dr. Yuan He, and Dr. D. Ron for providing critical reagents and experimental guidance. We thank the staff of the UM Unit for Laboratory Animal Medicine that provided assistance with saphenous vein blood collection. The University of Michigan Vector Core provided the TRC shRNA plasmids for IRE1 knockdown. We acknowledge financial support from the University of Michigan Rackham Graduate School (YH and DNB) and Michigan Genetics Training Fellowship (DNB, GM007544). This research was supported by funding from the NIH to MXDO (AI101777), KAF (AI083713), GN (AI063331, AR059688), XMY (AA021751), and funds from the University of Michigan Medical School Unit for Laboratory Animal Medicine and Endowment for Basic Science (YH). The funders had no role in study design, data collection and analysis, decision to publish, or preparation of the manuscript.

References

1. Zhang, Q., et al., DAMPs and autophagy: cellular adaptation to injury and unscheduled cell death. Autophagy, 2013. 9(4): p. 451-8.

2. Kono, H. and K.L. Rock, How dying cells alert the immune system to danger. Nat Rev Immunol, 2008. 8(4): p. 279-89.

3. Brown, M.K. and N. Naidoo, The endoplasmic reticulum stress response in aging and age-related diseases. Front Physiol, 2012. 3: p. 263.

4. Davis, B.K., H. Wen, and J.P. Ting, The inflammasome NLRs in immunity, inflammation, and associated diseases. Annu Rev Immunol, 2011. 29: p. 707-35.

5. Hao, L.Y., X. Liu, and L. Franchi, Inflammasomes in inflammatory bowel disease pathogenesis. Curr Opin Gastroenterol, 2013. 29(4): p. 363-9.

6. Tan, M.S., et al., The NLRP3 Inflammasome in Alzheimer's Disease. Mol Neurobiol, 2013.

7. Subramanian, N., et al., The adaptor MAVS promotes NLRP3 mitochondrial localization and inflammasome activation. Cell, 2013. 153(2): p. 348-61.

8. Hetz, C., The unfolded protein response: controlling cell fate decisions under ER stress and beyond. Nat Rev Mol Cell Biol, 2012. 13(2): p. 89-102.

9. Martinon, F., et al., TLR activation of the transcription factor XBP1 regulates innate immune responses in macrophages. Nature immunology, 2010. 11(5): p. 411-8.

10. Menu, P., et al., ER stress activates the NLRP3 inflammasome via an UPR-independent pathway. Cell Death Dis, 2012. 3: p. e261.

11. Pillich, H., et al., Activation of the unfolded protein response by Listeria monocytogenes. Cell Microbiol, 2012. 14(6): p. 949-64.

12. Seimon, T.A., et al., Induction of ER stress in macrophages of tuberculosis granulomas. PloS one, 2010. 5(9): p. e12772.

13. Bischof, L.J., et al., Activation of the unfolded protein response is required for defenses against bacterial pore-forming toxin in vivo. PLoS Pathog, 2008. 4(10): p. e1000176.

14. Li, X. and Y. He, Caspase-2-dependent dendritic cell death, maturation, and priming of T cells in response to Brucella abortus infection. PLoS One, 2012. 7(8): p. e43512.

15. Gomes, M.T., et al., Critical role of ASC inflammasomes and bacterial type IV secretion system in caspase-1 activation and host innate resistance to Brucella abortus infection. J Immunol, 2013. 190(7): p. 3629-38.

16. von Moltke, J., et al., Recognition of bacteria by inflammasomes. Annu Rev Immunol, 2013. 31: p. 73-106.

17. Zhou, R., et al., A role for mitochondria in NLRP3 inflammasome activation. Nature, 2011. 469(7329): p. 221-5.

18. Zeng, Y. and A.D. Elbein, UDP-N-acetylglucosamine:dolichyl-phosphate N-acetylglucosamine-1-phosphate transferase is amplified in tunicamycin-resistant soybean cells. Eur J Biochem, 1995. 233(2): p. 458-66.

19. Lerner, A.G., et al., IRE1alpha induces thioredoxin-interacting protein to activate the NLRP3 inflammasome and promote programmed cell death under irremediable ER stress. Cell Metab, 2012. 16(2): p. 250-64.

20. Cross, B.C., et al., The molecular basis for selective inhibition of unconventional mRNA splicing by an IRE1-binding small molecule. Proc Natl Acad Sci U S A, 2012. 109(15): p. E869-78.

21. Nakahira, K., et al., Autophagy proteins regulate innate immune responses by inhibiting the release of mitochondrial DNA mediated by the NALP3 inflammasome. Nat Immunol, 2011. 12(3): p. 222-30.

22. Iyer, S.S., et al., Mitochondrial cardiolipin is required for nlrp3 inflammasome activation. Immunity, 2013. 39(2): p. 311-23.

23. Saxena, G., J. Chen, and A. Shalev, Intracellular shuttling and mitochondrial function of thioredoxin-interacting protein. J Biol Chem, 2010. 285(6): p. 3997-4005.

24. Lee, H.Y., et al., Targeted expression of catalase to mitochondria prevents age-associated reductions in mitochondrial function and insulin resistance. Cell Metab, 2010. 12(6): p. 668-74.

25. Munoz-Planillo, R., et al., K(+) efflux is the common trigger of NLRP3 inflammasome activation by bacterial toxins and particulate matter. Immunity, 2013. 38(6): p. 1142-53.

26. Shimada, K., et al., Oxidized mitochondrial DNA activates the NLRP3 inflammasome during apoptosis. Immunity, 2012. 36(3): p. 401-14.

27. Handschumacher, R.E., et al., Cyclophilin: a specific cytosolic binding protein for cyclosporin A. Science, 1984. 226(4674): p. 544-7.

28. Oslowski, C.M., et al., Thioredoxin-interacting protein mediates ER stress-induced beta cell death through initiation of the inflammasome. Cell Metab, 2012. 16(2): p. 265-73.

29. Robertson, J.D., et al., Caspase-2 acts upstream of mitochondria to promote cytochrome c release during etoposide-induced apoptosis. J Biol Chem, 2002. 277(33): p. 29803-9.

30. Chen, F. and Y. He, Caspase-2 mediated apoptotic and necrotic murine macrophage cell death induced by rough Brucella abortus. PLoS One, 2009. 4(8): p. e6830.

31. Upton, J.P., et al., Caspase-2 cleavage of BID is a critical apoptotic signal downstream of endoplasmic reticulum stress. Mol Cell Biol, 2008. 28(12): p. 3943-51.

32. Upton, J.P., et al., IRE1alpha cleaves select microRNAs during ER stress to derepress translation of proapoptotic Caspase-2. Science, 2012. 338(6108): p. 818-22.

33. Jesenberger, V., et al., Salmonella-induced caspase-2 activation in macrophages: a novel mechanism in pathogen-mediated apoptosis. J Exp Med, 2000. 192(7): p. 1035-46.

34. Bronner, D.N., M.X. O'Riordan, and Y. He, Caspase-2 mediates a Brucella abortus RB51-induced hybrid cell death having features of apoptosis and pyroptosis. Front Cell Infect Microbiol, 2013. 3: p. 83.

35. Korsmeyer, S.J., et al., Pro-apoptotic cascade activates BID, which oligomerizes BAK or BAX into pores that result in the release of cytochrome c. Cell Death Differ, 2000. 7(12): p. 1166-73.

36. Hitomi, J., et al., Involvement of caspase-4 in endoplasmic reticulum stress-induced apoptosis and Abeta-induced cell death. J Cell Biol, 2004. 165(3): p. 347-56.

37. Wang, X.Z., et al., Identification of novel stress-induced genes downstream of chop. EMBO J, 1998. 17(13): p. 3619-30.

38. Thastrup, O., et al., Thapsigargin, a tumor promoter, discharges intracellular Ca2+ stores by specific inhibition of the endoplasmic reticulum Ca2(+)-ATPase. Proc Natl Acad Sci U S A, 1990. 87(7): p. 2466-70.

39. Olden, K., R.M. Pratt, and K.M. Yamada, Role of carbohydrates in protein secretion and turnover: effects of tunicamycin on the major cell surface glycoprotein of chick embryo fibroblasts. Cell, 1978. 13(3): p. 461-73.

40. Pahl, H.L. and P.A. Baeuerle, A novel signal transduction pathway from the endoplasmic reticulum to the nucleus is mediated by transcription factor NF-kappa B. EMBO J, 1995. 14(11): p. 2580-8.

41. Schroder, K. and J. Tschopp, The inflammasomes. Cell, 2010. 140(6): p. 821-32.

42. Wang, S. and R.J. Kaufman, The impact of the unfolded protein response on human disease. J Cell Biol, 2012. 197(7): p. 857-67.

43. Allam, R., et al., Mitochondrial apoptosis is dispensable for NLRP3 inflammasome activation but non-apoptotic caspase-8 is required for inflammasome priming. EMBO Rep, 2014.

44. Franchi, L., et al., Cytosolic Double-Stranded RNA Activates the NLRP3 Inflammasome via MAVS-Induced Membrane Permeabilization and K+ Efflux. J Immunol, 2014.

45. Heid, M.E., et al., Mitochondrial Reactive Oxygen Species Induces NLRP3-Dependent Lysosomal Damage and Inflammasome Activation. J Immunol, 2013.

46. Horng, T., Calcium signaling and mitochondrial destabilization in the triggering of the NLRP3 inflammasome. Trends Immunol, 2014. 35(6): p. 253-61.

47. Qiu, Q., et al., Toll-like receptor-mediated IRE1alpha activation as a therapeutic target for inflammatory arthritis. EMBO J, 2013. 32(18): p. 2477-90.

48. Garg, A.D., et al., ER stress-induced inflammation: does it aid or impede disease progression? Trends Mol Med, 2012. 18(10): p. 589-98.

49. Escames, G., et al., Mitochondrial DNA and inflammatory diseases. Hum Genet, 2012. 131(2): p. 161-73.

50. Zhou, R., et al., Thioredoxin-interacting protein links oxidative stress to inflammasome activation. Nat Immunol, 2010. 11(2): p. 136-40.

51. Sandow, J.J., et al., ER stress does not cause upregulation and activation of caspase-2 to initiate apoptosis. Cell Death Differ, 2014. 21(3): p. 475-80.

52. Yin, X.M., et al., Bid-deficient mice are resistant to Fas-induced hepatocellular apoptosis. Nature, 1999. 400(6747): p. 886-91.

53. Bergeron, L., et al., Defects in regulation of apoptosis in caspase-2-deficient mice. Genes Dev, 1998. 12(9): p. 1304-14.

54. Kanneganti, T.D., et al., Bacterial RNA and small antiviral compounds activate caspase-1 through cryopyrin/Nalp3. Nature, 2006. 440(7081): p. 233-6.

55. Ozoren, N., et al., Distinct roles of TLR2 and the adaptor ASC in IL-1beta/IL-18 secretion in response to Listeria monocytogenes. J Immunol, 2006. 176(7): p. 4337-42.

56. Rathinam, V.A., et al., The AIM2 inflammasome is essential for host defense against cytosolic bacteria and DNA viruses. Nat Immunol, 2010. 11(5): p. 395-402.

Chapter 4

PERK suppresses inflammasome activity via Parkin-dependent mitophagy

Abstract

Controlling the extent of inflammatory signaling is critical for effective immune responses to infection, while minimizing host damage. Previously, we found that infection-induced activation of the endoplasmic reticulum stress sensor, IRE1, led to mitochondrial damage and triggered the NLRP3-dependent inflammasome. The mechanisms that downregulate IRE1-induced inflammasome activation are poorly defined. Here we show that PERK, a second ER stress sensor, dampens IRE1-induced IL-1β production *in vitro* and *in vivo*. Microbial activation of the PERK signaling pathway induced transcription of *parkin*, which encodes an E3 ubiquitin ligase that regulates mitophagy. Parkin recruitment to mitochondria promoted fragmentation of the mitochondrial network, as well as a decrease in IL-1β production. Inhibition of PERK or mitochondrial fission increased IL-1β production induced by infection-associated ER stress. These data provide evidence that PERK-dependent mitophagy can play a suppressive role in regulating inflammatory responses to infection.

Introduction

Endoplasmic reticulum (ER) and mitochondrial stress programs can contribute to progression of degenerative and inflammatory diseases [1-4].

Previous work has implicated ER stress in triggering inflammatory responses during infection. Recognition of microbes by Toll-like receptors (TLR) stimulates the ER stress sensor, IRE1, increasing transcription of proinflammatory cytokines IL-6 and TNFα [5]. Previously, we discovered that IRE1 induces IL-1β production by increasing mitochondrial reactive oxygen species (mtROS). The rapid increase in mtROS recruited NLRP3 and caspase-2 to the mitochondria, facilitating damage and release of mitochondrial contents into the cytosol. The newly released mitochondrial danger associated molecular patterns (mtDAMPs) activated the inflammasome, a multiprotein complex that processes the proinflammatory cytokine, IL-1β [6, 7]. Although IRE1 acts as the initiator of this ER stress-induced process, mechanisms for modulating this potential inflammatory signaling pathway are poorly defined. Previous studies identified autophagy as a key mechanism that could suppress inflammation by eliminating signaling molecules that trigger inflammasome activation [7-9]. Damaged mitochondria are removed by mitophagy, a mitochondrial-specific form of autophagy. Our previous studies indicated that infection-induced ER stress causes mitochondrial damage, leading us to hypothesize that mitophagy might be employed to downregulate that inflammatory process.

Here we show that the ER stress sensor PERK can modulate IRE1-induced inflammasome activity. We provide evidence that inflammasome activity is suppressed by PERK-dependent mitophagy. These data reveal a novel regulatory role for PERK during infection and inflammation, and demonstrate that ER stress sensors can fine-tune inflammatory output during infection.

Results

Microbial viability affects IL-1β processing but not priming

Previously, we showed that IRE1 is critical in triggering inflammasome activation and IL-1β production during infection by the live attenuated cattle vaccine *Brucella abortus* strain RB51. Treatment of bone marrow derived macrophages (BMDM) with heat-killed (HK) RB51 resulted in significantly less IL-1β secretion compared to live RB51 (Fig. 4.1A). To determine whether HK RB51 stimulated less cytokine transcription (priming) or less cytokine translation, we measured proIL-1β protein production by immunoblot and found that HK-infected and Live-infected BMDM expressed similar levels of proIL-1β (Fig. 4.1B). Taken together, these observations suggested that the absence of IL-1β might be due to decreased activity of the inflammasome, leading to less processing of proIL-1β. We first tested whether HK could activate IRE1 similarly to live RB51 by measuring splicing of *xbp1* transcript, a direct downstream target of IRE1, in Live and HK-infected BMDM. X*bp1* splicing was comparable in both Live and HK-infected BMDM at 8h post infection (pi) (Fig. A20A). These data indicate that the effect of HK treatment on inflammasome activation was likely occurring downstream of IRE1.

With no difference in IRE1 activation, we investigated whether activation of the other two ER stress sensors, ATF6 and PERK, differed between Live and HK-infected BMDM. ATF6 cleavage, indicative of activation, occurred in both Live and HK-infected BMDM (Fig. A20B). Notably, HK RB51 triggered PERK activation, as assessed by phosphorylation (Fig. 4.2A). To determine if PERK could serve as a

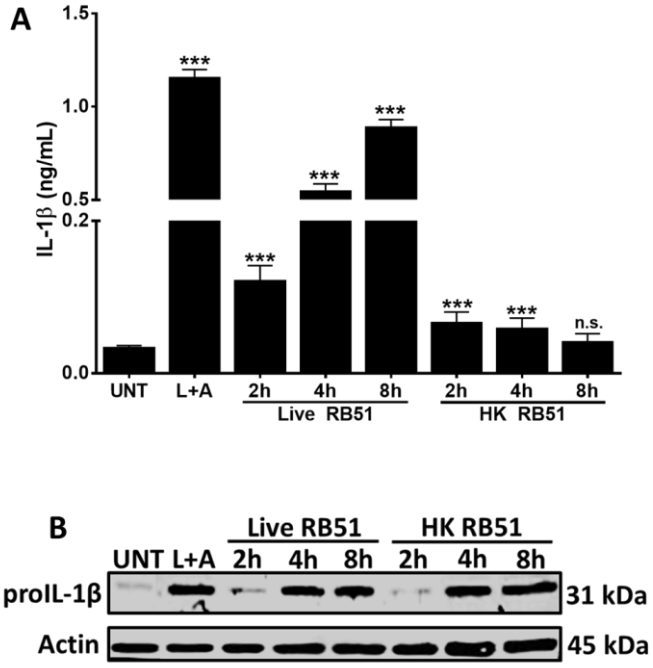

Fig 4.1: IL-1β processing, not priming, depends upon microbial viability. (A) IL-1β ELISA analysis of supernatants from Live and HK RB51-infected BMDM. Error bars represent mean ± SD of n≥3 independent experiments. *** represent p-value <0.0001, n.s. = not significant. (B) Immunoblot of proIL-1β in Live and HK RB51-infected (MOI 20) BMDMs. Immunoblots in (B) are representative of n≥3 independent experiments performed and imaged using a LiCor Odyssey imaging system.

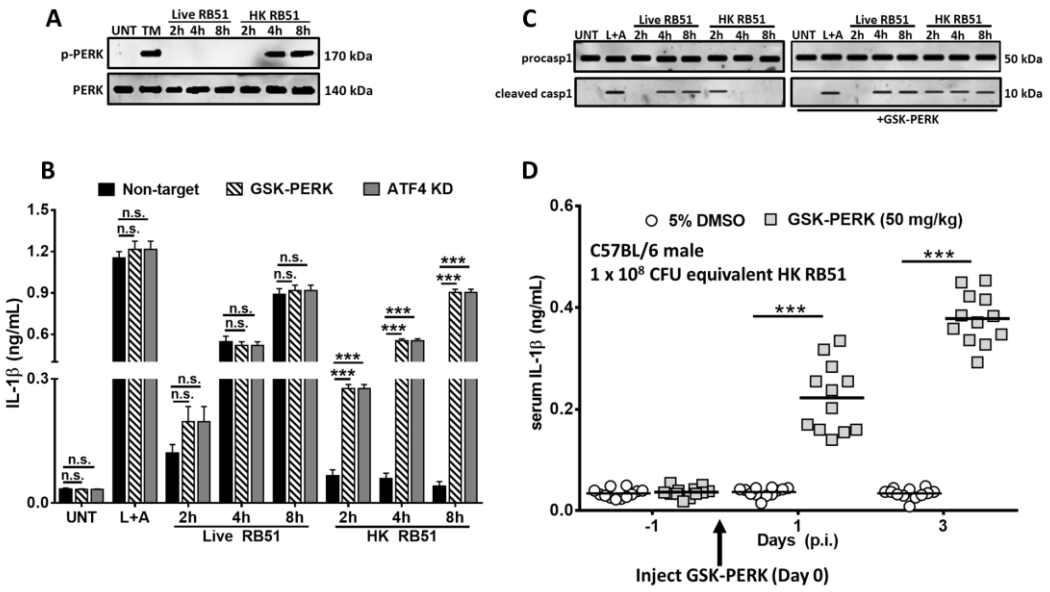

Fig. 4.2: PERK suppresses IRE1-induced inflammasome activation. (A) PERK phosphorylation in Live and HK RB51-infected (MOI 20) BMDM. PERK and TM served as the loading and positive controls respectively. (B) IL-1β ELISA analysis of supernatants from Live and HK RB51-infected BMDM in the presence of GSK-PERK (GSK2606414 specific PERK inhibitor, 5 μM) and ATF4 siRNA. Error bars represent mean ± SD of n≥3 independent experiments. *** represent p-value <0.0001, n.s. = not significant. (C) Caspase-1 cleavage in Live and HK RB51-infected (MOI 20) BMDMs in absence or presence of GSK2606414. (D) Serum IL-1β levels in mice treated with 5% DMSO (control, n = 12) or GSK2606414 (n = 12) and infected with HK RB51 (i.p., CFU equivalent 1 x 10^8). Data in (D) were pooled from 2 independent experiments. Immunoblots in (A) and (C) are representative of n≥3 independent experiments performed and imaged using a LiCor Odyssey imaging system.

switch to negatively regulate IL-1β production, we utilized two approaches: a PERK-specific inhibitor (GSK-PERK2606414 or GSK-PERK, locks PERK in an inactive state) and siRNA knockdown of ATF4, a transcription factor that is preferentially translated when the PERK signaling pathway is activated. L+A (LPS+ATP) served as a positive control for inflammasome activation and triggers IL-1β production independently of ER stress. GSK-PERK treatment as well as ATF4 knockdown (KD) had no effect on L+A and Live-induced IL-1β production and caspase-1 cleavage (activation) in BMDM, conditions where there is no PERK activation (Fig. 4.2B and C). In contrast, GSK-PERK and ATF4 KD led to a significant increase in IL-1β production and sustained caspase-1 cleavage in HK-infected BMDM. Consistent with our *in vitro* findings, GSK-PERK-treated mice injected with HK RB51 showed a significant increase in serum IL-1β compared to control-treated mice (Fig. 4.2D). These data point to PERK as a possible suppressor of IRE1-induced inflammasome activation during infection.

PERK minimizes induction of IRE1-mediated mitochondrial dysfunction

In Live-infected BMDM, mitochondrial damage was essential for inflammasome activation, a process initiated by IRE1. With IRE1 activation, but a lack of IL-1β production in HK-infected BMDM, we hypothesized that PERK might interfere with IRE1-induced mitochondrial damage. The mitochondrial membrane potential ($\Delta\psi_m$) is a key indicator of mitochondrial health or damage [10]. Normal and healthy mitochondria have a high $\Delta\psi_m$, whereas damaged mitochondria have low $\Delta\psi_m$. We measured $\Delta\psi_m$ with JC-1, a mitochondrial probe whose red fluorescence decreases as $\Delta\psi_m$ dissipates [11]. Treatment with carbonyl cyanide

m-chlorophenyl hydrazine (CCCP, a mitochondrial proton gradient uncoupler) or Live RB51 caused the $\Delta\psi_m$ to drop significantly (Fig. 4.3A). In HK-infected BMDM, the $\Delta\psi_m$ decreased at 2h pi but increased after 4h pi – when we observe robust activation of PERK. Only in the presence of the PERK inhibition did $\Delta\psi_m$ levels decrease persistently in HK-infected BMDM. With a sharp decrease in $\Delta\psi_m$, mitochondria release mtDNA into the cytosol and mtROS accumulates. We measured mtDNA cytosolic release by qPCR and found that Live-infected BMDM contained substantial amounts of cytosolic mtDNA (Fig. 4.3B). HK-infected BMDM initially released mtDNA into the cytosol, however after 4h p.i., this release was abrogated, a phenotype seen with caspase-1 activation. Release of mtDNA increased throughout HK infection in GSK-PERK-treated or ATF KD BMDM (Fig. A21A). ROS levels were relatively low in HK-infected and TM-treated BMDM, consistent with low levels of mtDNA release, but increased upon GSK-PERK treatment or ATF4 KD (Fig. 4.3C and Fig. A21B). In contrast, ROS levels were high in Live-infected BMDM and were unaffected by PERK inhibition or ATF4 KD. Together, these results indicate that PERK signaling can interfere with IRE1-driven mitochondrial damage.

PERK induces mitochondrial fragmentation via mitophagy

Autophagy can suppress proinflammatory responses by eliminating damaged organelles and pathogens [7, 8]. Previous studies reported that PERK coordinates the transcription of the gene encoding Beclin-1, an initiator of autophagy [12]. Moreover, PERK signaling may enhance conversion of LC3, a process required for autophagosome formation [13]. These observations led us to

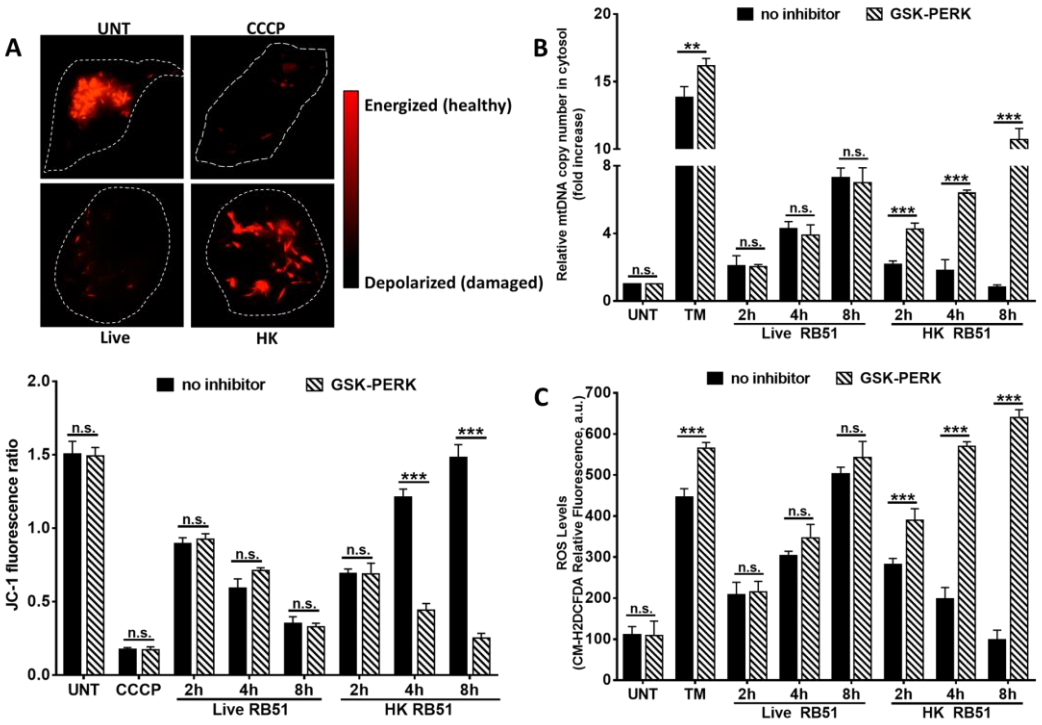

Fig. 4.3: PERK inhibits IRE1-driven mitochondrial damage. (A) Fluorescence images and quantification of JC-1 staining of BMDMs treated with CCCP (mitochondrial uncoupler, 20 μM) or infected with Live and HK RB51 (MOI 20). The ratio of JC-1 red/green fluorescence represents the mitochondrial membrane potential ($\Delta\psi_m$). (B) qPCR analysis of mitochondrial DNA (mtDNA) release into cytosol during Live and HK RB51 BMDM infection in the absence or presence of GSK2606414. (C) CM-H2DCFDA was used to measure ROS levels with or without GSK2606414 in Live and HK-RB51 infected BMDM. Tunicamycin (TM) serves as a positive control for ROS induction.

hypothesize that PERK could be preventing release of mtDAMPs by autophagic removal of damaged mitochondria, thus inhibiting inflammasome activation. We therefore tested if autophagy was involved in controlling IL-1β production in HK-infected macrophages, using *Beclin-1*$^{+/-}$ and *Lc3b*$^{-/-}$ BMDM. Neither Beclin-1 haploinsufficiency nor LC3 deficiency had any effect on L+A-induced and Live-induced IL-1β production in BMDM (Fig. 4.4A). Deficiency in LC3, but not Beclin-1, led to an increase in IL-1β levels in HK-infected BMDM. These data establish that beclin-1-dependent autophagy is not involved in PERK-mediated suppression of IL-1β, but implicate LC3 in this process.

We reasoned that removal of damaged mitochondria via mitophagy could be the mechanism of PERK-mediated suppression of the inflammasome. When mitochondria are damaged, PINK1 accumulates on the outer mitochondrial membrane serving as a tag. PINK accumulation recruits the E3 ubiquitin ligase, Parkin, to the mitochondrial network resulting in ubiquitination of mitochondrial proteins. This triggers fragmentation and eventual capture of damaged mitochondria by LC3^{+} autophagosomes. A recent study reported that PERK can control mitophagy by regulating transcription of *parkin* in an ATF4-dependent manner. Since we observed an increase in IL-1β production in LC3 deficient HK-infected BMDM, we next assessed the induction of mitophagy by probing PINK1 accumulation, as well as LC3 and PARKIN recruitment to the mitochondrial fraction by immunoblot. CCCP is a potent inducer of mitophagy and served as a positive control. PINK1 accumulated in the mitochondrial fraction of Live-infected, HK-infected, and CCCP-treated BMDM, consistent with mitochondrial damage (Fig.

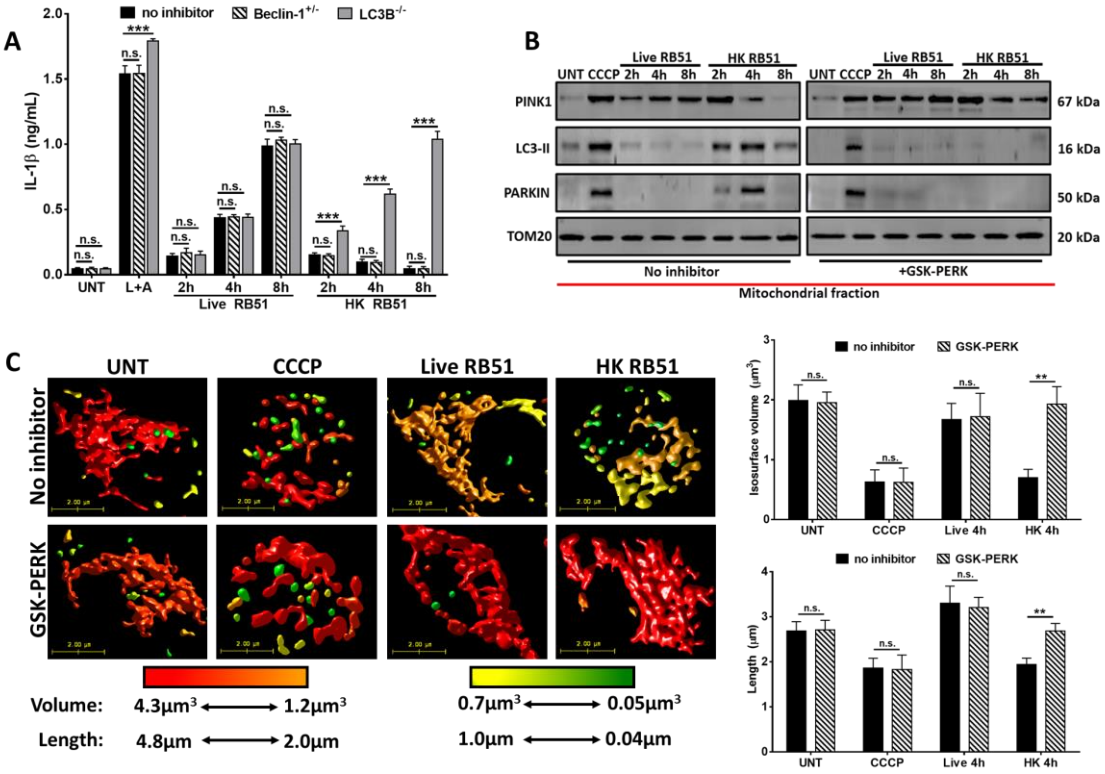

Fig. 4.4: PERK drives removal of damaged mitochondria via mitophagy. (A) IL-1β levels in *Beclin-1*$^{+/-}$ and *LC3B*$^{-/-}$ BMDM infected with Live and HK-RB51. (B) Immunoblot of mitophagy markers PINK1, LC3-II, and PARKIN in the mitochondrial fraction of CCCP and Live/HK-infected BMDM. TOM20 serves as loading control and mitochondrial marker. (C) 3-D reconstruction and quantification of the mitochondrial network labeled with TOM20 (mitochondrial marker, outer membrane protein) with or without GSK2606414 in CCCP and Live/HK-infected BMDM. Colors represent the size of the fragments within the network. Error bars in (A and C) represent mean ±SD of n≥3 independent experiments. ** and *** represent p-values <0.001 and <0.0001 respectively. n.s. = not significant. UNT, CCCP, and L+A represent untreated and Carbonyl cyanide m-chlorophenyl hydrazine (20 µM, positive control for mitophagy induction), and LPS+ATP (200 ng/mL and 1mM respectively; positive control for inflammasome activation).

4.4B). Notably, PINK1 accumulation began to decrease after 4h p.i. only in HK-infected cells, suggesting the possibility that damaged mitochondria were being removed and degraded in HK-infected BMDM. Additionally, we observed PARKIN and LC3 mitochondrial recruitment only in HK-infected BMDM, but not Live-infected BMDM. This result further indicated that mitochondrial damage occurs early in HK infection.

Next, we assessed if PERK contributed to mitophagy induction in HK-infected BMDM. GSK-PERK treatment or ATF4 KD abolished PARKIN and LC3 recruitment in HK-infected BMDM (Fig. 4.4B and Fig. A21C). PINK1 levels increased in HK-infected BMDM treated with GSK-PERK, suggesting that removal of damaged mitochondria was inhibited, consistent with increased inflammasome activity and IL-1β levels.

Upon induction of mitophagy, the mitochondrial network fragments, allowing for damaged mitochondria to be separated from the network to maintain network integrity [14]. To quantify mitochondrial fragmentation, we measured length and volume of the mitochondrial network by confocal immunofluorescence imaging and deconvolution of the TOM20 outer mitochondrial membrane protein. We observed that CCCP treatment and HK infection led to a significantly fragmented phenotype, as well as a decrease in isosurface volume and length of the mitochondrial network (Fig. 4.4C). Although Live infection induced damage, the mitochondrial network did not fragment further, consistent with our observations that mitophagy does not occur in Live-infected BMDM. GSK-PERK treatment or ATF4 KD in HK-infected BMDM yielded a largely intact mitochondrial network, with increased volume and

length (Fig. 4.4C and Fig. A21D). These data demonstrate that PERK signaling can serve as a trigger for mitophagy.

PERK prevents inflammasome activation by Parkin-dependent mitophagy

Fragmentation of the mitochondrial network allows for capture of damaged mitochondria and is dependent upon Parkin, which is transcriptionally regulated by the PERK signaling pathway during ER stress conditions [15]. We observed that HK induced Parkin transcription, whereas in Live-infected BMDM, Parkin transcript levels were similar to UNT levels (Fig. 4.5A). Additionally, HK-induced Parkin transcription was abrogated by PERK inhibition. These observations led us to hypothesize that Parkin-driven mitophagy was the critical mechanism for PERK-mediated inflammasome suppression in HK-infected BMDM. To test this idea, we infected *Parkin*$^{-/-}$ BMDM or BMDM treated with Mdivi-1, a mitochondrial fission inhibitor [16], with HK and measured IL-1β levels. Parkin deficiency resulted in a significant increase in IL-1β production in HK-infected but not Live-infected or LPS+ATP treated BMDM (Fig, 4.5B). Similar to Parkin deficiency, Mdivi-1 treatment also increased IL-1β levels, suggesting that fragmentation was essential in inflammasome suppression in HK-treated BMDM. HK did not induce mitochondrial fragmentation in *Parkin*$^{-/-}$ nor Mdivi-1 treated BMDM (Fig. 4.5C). Although IL-1β levels increased in HK-infected *LC3b*$^{-/-}$ BMDM, the mitochondrial network was still able to fragment, further supporting that the autophagic capture of damaged mitochondria aids in removing mtDAMPs, suppressing inflammasome activation and IL-1β production (Fig. A22). These results demonstrate that PERK suppresses inflammasome activation through PARKIN-mediated mitophagy.

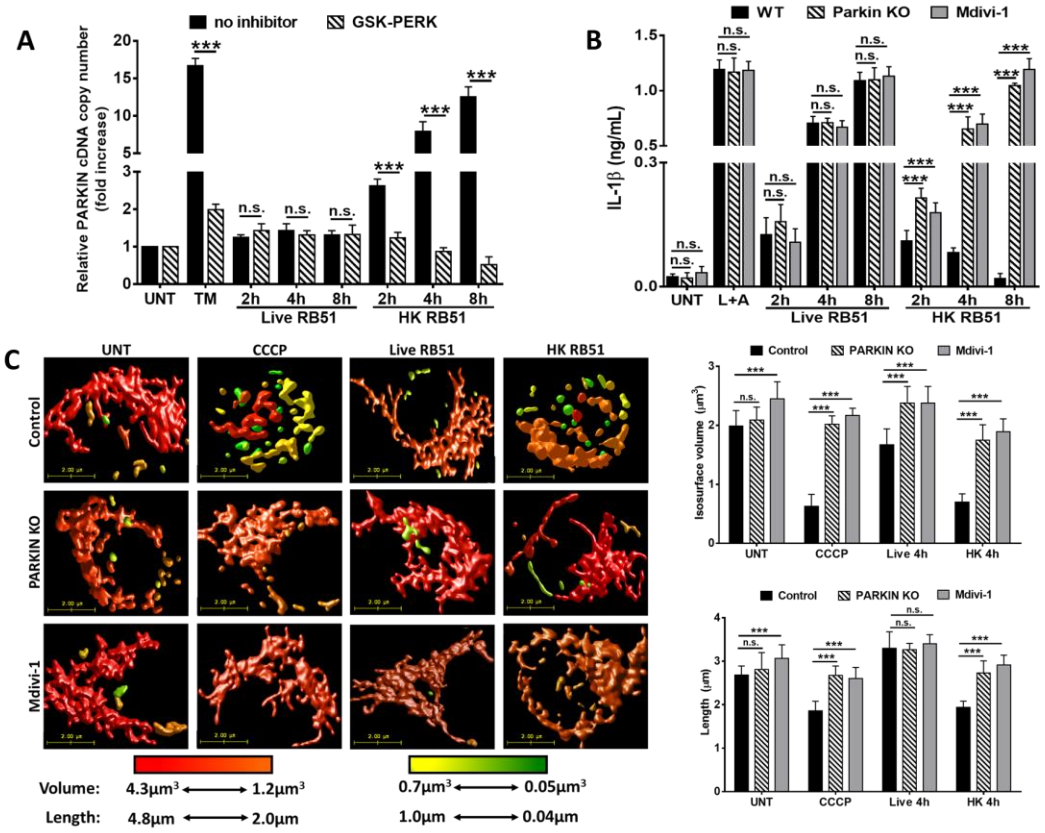

Fig. 4.5: PERK-induced mitophagy is mediated by Parkin. (A) qPCR analysis of PARKIN transcription during Live and HK RB51 BMDM infection in the absence or presence of GSK2606414. Tunicamycin (TM) serves as a positive control for PARKIN induction. (B) IL-1β ELISA analysis of supernatants from Live and HK RB51-infected WT, *Parkin*$^{-/-}$, and Mdivi-1 (mitochondrial fission inhibitor, 20 μM) treated BMDM. Error bars represent mean ± SD of n≥3 independent experiments. *** represents p-values of <0.0001, n.s. = not significant. L+A (LPS+ATP, 200 ng/mL and 1mM respectively) serves as a positive control for inflammasome activation. (C) 3-D reconstruction and quantification of the mitochondrial network labeled with TOM20 (mitochondrial marker, outer membrane protein) of CCCP treated and Live/HK-infected WT, *Parkin*$^{-/-}$, and Mdivi-1 BMDM. Colors represent the size of the fragments within the network. Error bars in (A - C) represent mean ±SD of n≥3 independent experiments. ** and *** represent p-values <0.001 and <0.0001 respectively. n.s. = not significant.

Parkin-dependent mitophagy decreases RSV-induced inflammation in vivo

Mitophagy may be important in controlling NLRP3 inflammasome activation and promoting cell survival during infection. However, HK RB51 is not a useful model to study the role of mitophagy in infection since there are no live bacteria. Viral pathogens can hijack this mitophagic process to aid in viral replication by dampening innate immune responses and preventing apoptosis [17-21]. Respiratory syncytial virus (RSV), a single stranded RNA (- ssRNA) virus, is a major cause of lower respiratory tract infections and pneumonia symptoms in infants and children [22]. Previous studies have found that RSV proteins colocalize with the mitochondrial network [23, 24]. As seen with Live RB51, IRE1 and ROS are important for RSV-induced NLRP3-mediated IL-1β production [25]. Moreover, LC3b deficiency led to elevated IL-1β levels and lung pathology in RSV-infected mice. These observations suggest that mitophagy can aid in decreasing inflammasome activation and IL-1β production during RSV infection.

IRE1 is activated during RSV infection, however it is not known if PERK activation occurs as seen in HK-infected BMDM. We were able to observe phosphorylation of PERK and induction of CHOP, a downstream transcriptional target of PERK, in RSV-infected BMDM (Fig. 4.6A). To assess if mitophagy was occurring, we probed for PINK1 and Parkin/LC3 as markers of mitophagy in RSV-infected BMDM. PINK1 tagging of damaged mitochondria occurred early, and removal of mitochondria began at 4 hr post infection in RSV-infected BMDM (Fig. 4.6B). Similar to HK-infected BMDM, GSK-PERK treatment led to increased PINK1 accumulation but decreased Parkin and LC3 recruitment in RSV-infected BMDM.

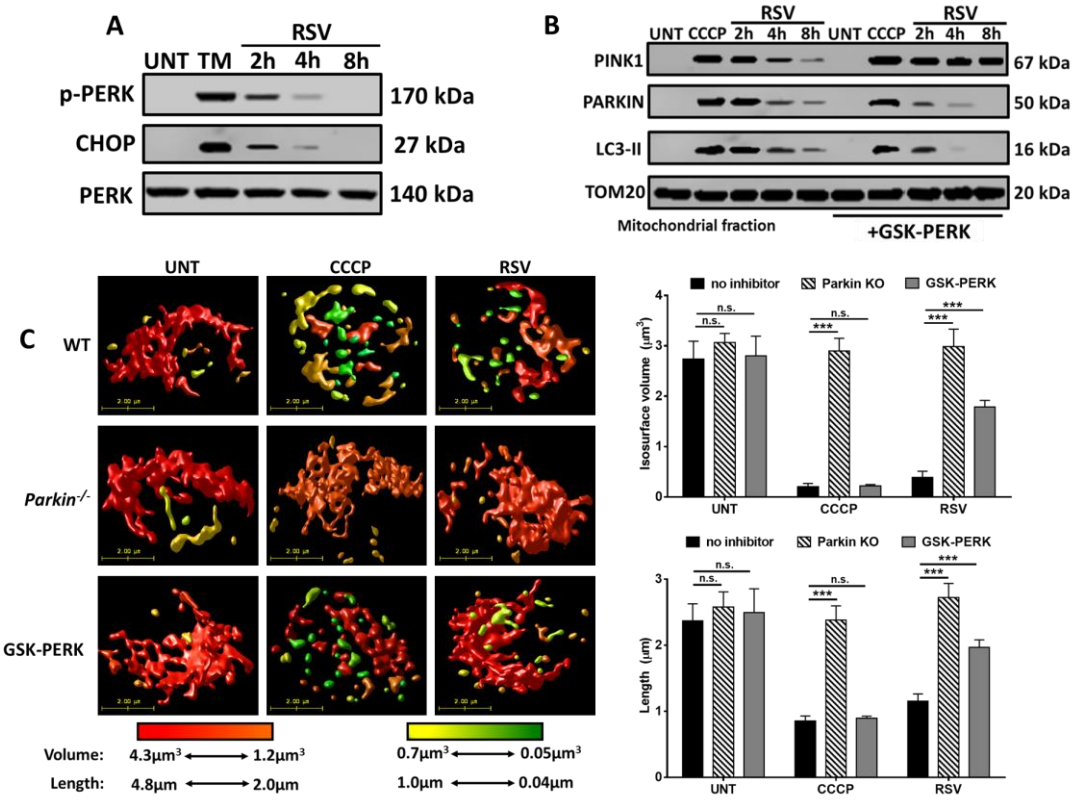

Fig. 4.6: PERK and Parkin mediate RSV-induced mitophagy. (A) PERK phosphorylation and CHOP induction in RSV-infected (MOI 1) BMDM. PERK and TM served as the loading and positive controls respectively. (B) Immunoblot of mitophagy markers PINK1, LC3-II, and PARKIN in the mitochondrial fraction of CCCP and RSV-infected BMDM. TOM20 serves as loading control and mitochondrial marker. C) 3-D reconstruction and quantification of the mitochondrial network labeled with TOM20 (mitochondrial marker, outer membrane protein) of CCCP treated and RSV-infected WT, *Parkin*$^{-/-}$, and GSK2606414-treated BMDM. Colors represent the size of the fragments within the network. Error bars in (A - C) represent mean ±SD of n≥3 independent experiments. ** and *** represent p-values <0.001 and <0.0001 respectively. n.s. = not significant.

We observed mitochondrial fragmentation in RSV-infected BMDM – a phenotype that decreased in GSK-PERK treated and Parkin deficient BMDM (Fig. 4.6C). Moreover, *parkin* transcription decreased in GSK-PERK-treated RSV-infected BMDM (Fig. A23). Parkin deficiency exerted a greater effect on fragmentation than PERK inhibition, suggesting that another inducer of Parkin is involved in RSV-induced mitophagy. Since we observed mitophagy in RSV-infected BMDM, we assessed whether mitophagy was important in regulating inflammasome activation. GSK-PERK treatment and Parkin deficiency led to increased IL-1β production and caspase-1 activation *in vitro* (Fig. 4.7A and Fig. A24A-B). Consistent with our *in vitro* data, we observed increased IL-1β production in RSV-infected mice treated with GSK-PERK (Fig. 4.7B). Taken together, our data identify Parkin-dependent mitophagy as a mechanism by which PERK can suppress ER-stress induced inflammasome activation.

Conclusions

Recent studies have demonstrated that ER stress can trigger mitochondrial dysfunction, as well as aid in autophagy, a process known for preventing accumulation of damaged mitochondria [26]. There is significant evidence showing that mitochondrial dysfunction promotes the progression of neurodegenerative and inflammatory diseases [4, 27, 28]. Although PERK can mediate an antioxidant response [12, 29] and promote autophagy, it has not been linked to inflammasome regulation. In this study, we provide evidence for a model where PERK acts as a suppressor of inflammasome activation by driving Parkin-dependent mitophagy during infection (Fig. 4.8). When mitochondrial damage occurs, whether microbial

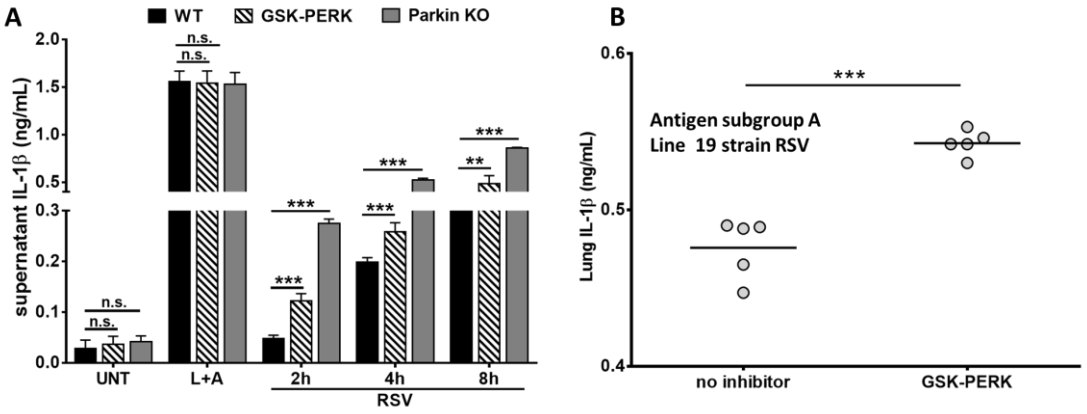

Fig. 4.7: Mitophagy decreases RSV-induced inflammation *in vitro* and *in vivo*. (A) IL-1β ELISA analysis of supernatants from RSV-infected GSK2606414-treated (specific PERK inhibitor, 5 μM) and *Parkin*$^{-/-}$ BMDM. Error bars represent mean ± SD of n≥3 independent experiments. *** represent p-value <0.0001, n.s. = not significant. (B) Lung IL-1β levels in mice treated with 5% DMSO (control n = 5) or GSK2606414 (n = 5) and infected with RSV.

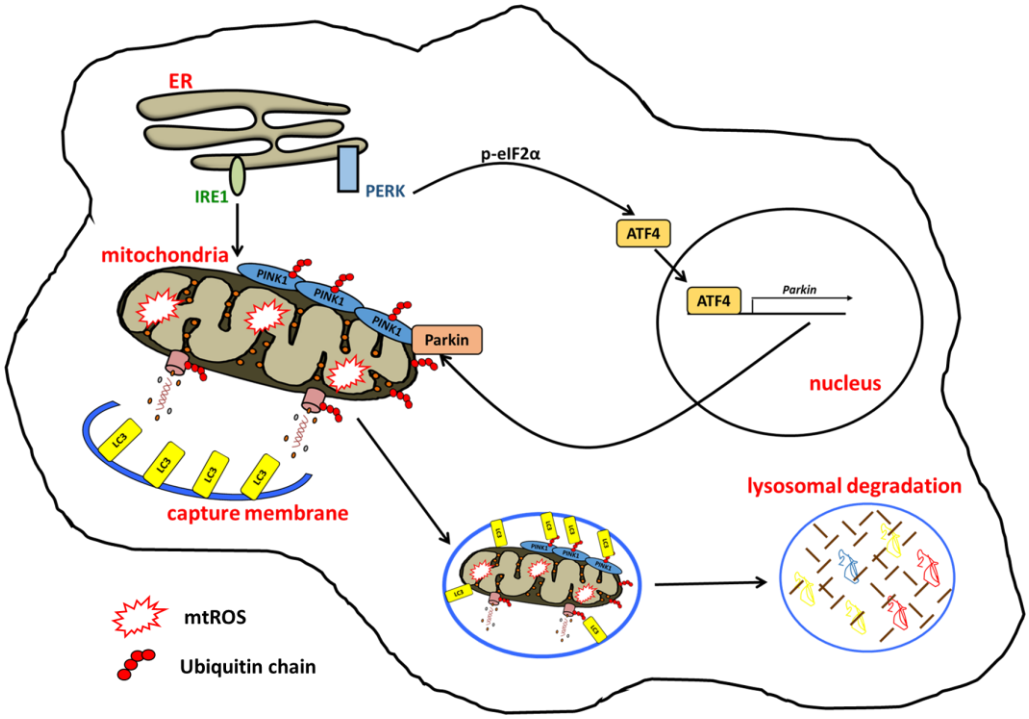

Fig. 4.8: PERK drives Parkin-mediated mitophagy to suppress the inflammasome. IRE1-induced mitochondrial damage and ROS production triggers PINK1 accumulation on the outer membrane of mitochondria. Upon PERK activation, ATF4 translocates to the nucleus and initiates Parkin transcription. Parkin is recruited to damaged mitochondria tagged with PINK1 and ubiquitinates outer membrane proteins. Ubiquitination of mitochondrial proteins triggers fragmentation and allows for capture of dysfunctional mitochondria by the isolation membrane. Once captured, the autophagosome fuses with the lysosome and degrades the damaged mitochondria.

or chemically induced, PINK1 accumulates on the surface serving as a tag for dysfunctional mitochondria. If PERK is activated, it signals ATF4-dependent *parkin* transcription. Parkin is recruited to mitochondria, initiating fragmentation of the network and allowing the capture of damaged mitochondria by autophagosomes. The removal of damaged mitochondria would lead to the observed decrease in mtDAMPs, preventing oligomerization or activation of the inflammasome on the mitochondrial surface and the lack of sustained caspase-1 activation. We previously demonstrated that NLRP3 and caspase-2 are recruited to the mitochondrial network; therefore, it is possible that NLRP3 and caspase-2 are being captured and degraded along with damaged mitochondria. Caspase-2 activation, similar to caspase-1, is not sustained during HK infection – an observation that supports the hypothesis of caspase-2 being captured with damaged mitochondria. Furthermore, we demonstrated that this PERK-dependent inflammasome suppression pathway can be triggered by microbial infections *in vitro* and *in vivo*. Our studies have uncovered a novel role for PERK in controlling inflammasome activity during infection.

Previous studies that implicated mitophagy in inflammasome activation demonstrated that LC3b deficiency increased IL-1β production and caspase-1 activation upon treatment with LPS+ATP and viral infections [7]. Since LC3b is involved in both autophagy and mitophagy, it remained unclear which pathway was involved. Our study now demonstrates that Parkin-mediated mitophagy, distinct from the beclin-1 autophagy pathway, can suppress IL-1β production during microbial infection. Similar to LC3b deficiency, we showed that Parkin deficiency

increased IL-1β production and caspase-1 activation. Inhibition of PERK or ATF4 KD led to higher levels of cytosolic mtDNA, suggesting that damaged mitochondria were accumulating within the cell. More damaged mitochondria in the cell and increased mtDNA levels are consistent with the sustained inflammasome activation we observed.

Activation of PERK by chemical inducers (e.g. tunicamycin) leads to increased transcription of *parkin* by ATF4 [15]. ATF4 induction is controlled by the alpha subunit of eukaryotic initiation factor 2 (eIF2α). Upon phosphorylation, eIF2α reduces general translation while facilitating the preferential translation of ATF4. This eIF2α-ATF4 pathway can be triggered by several kinases in different stress conditions: PERK (ER stress), GCN2 (amino acid deficiency), HRI (heavy metals), and protein kinase R (PKR, viral infection). We found that in HK-infected BMDM, ATF4-induced *parkin* transcription was solely dependent upon PERK whereas in RSV-infected BMDM it was only partially dependent upon PERK. Reports show that RSV can activate PKR leading to phosphorylation of eIF2α [30, 31]. In addition, PKR can induce autophagy leading to viral degradation during infection [32]. These observations suggest the possibility that in BMDM, RSV activates both PERK and PKR thus triggering ATF4-dependent *parkin* transcription. If this is occurring, both PERK and PKR may act to control inflammasome output with the right contextual signals.

Additional evidence has surfaced showing that microbial infections can selectively activate UPR sensors [5]. Most studies indicate that IRE1 is important for triggering inflammatory responses, whereas PERK is critical for suppressing

global translation and triggering cell death. Our work shows that selective activation of ER stress sensors may allow the ER to control the amplitude and kinetics of the inflammatory response. The observation that PERK was able to prevent IRE1-induced mitochondrial damage in microbial infections highlights the fact that ER stress signaling is not limited to initiating inflammation. Viral pathogens are known for exploiting autophagy to increase their chances for replication and preventing cell death [19-21, 33]. RSV might selectively activate PERK as a means of suppressing inflammation and increasing pathogenesis. Understanding the mechanism of selective activation of ER stress sensors may lead to better therapeutic strategies for diseases that involve ER stress and mitochondrial dysfunction.

Materials and Methods

Mice

Humane animal care at the University of Michigan is provided by the Unit for Lab Animal Medicine, which is accredited by the American Association for Accreditation of Laboratory Animal Care and the Department of Health and Human Services. This study was carried out in strict accordance with the recommendations in the Guide for the Care and Use of Laboratory Animals of the National Institutes of Health. The protocol was approved by the Committee on the Care and Use of Animals (UCUCA) of the University of Michigan.

C57BL/6 5% DMSO treated (n = 12), GSK-PERK2606414 treated (n = 12) mice (8 -12 weeks) were injected intraperitoneally (i.p.) with *Brucella abortus* RB51 vaccine strain (1 x 10^8 CFU) in 200 µl of phosphate-buffered saline (PBS). Mice were

matched by sex and age. Mice were treated with DMSO (5% in PBS) and GSK-PERK2606414 (50mg/kg) daily in 200 µl of PBS. Blood was collected by saphenous vein on day -1, 1, and 3 days post infection (p.i.). Serum was extracted from blood by centrifugation for 3 min at 10,000 rpm and used for assessing IL-1β production by ELISA. At day 3 p.i., spleens were removed from euthanized mice, homogenized in 1 ml 0.2% NP-40, and serial dilutions plated onto *Brucella* agar plates to enumerate CFU.

Cell culture and infection

BMDMs were isolated from WT C57BL/6 mice and were differentiated in DMEM (GIBCO) supplemented with 20% heat-inactivated FBS (Invitrogen), 1% L-glutamine (2 mM), 1% sodium pyruvate (1 mM), 0.1% β-mercaptoethanol (55 µM), 30% L-929 conditioned medium, and J2 recombinant retrovirus. BMDMs were cultured in non-TC treated plates at 37°C in 5% CO^2, fed fresh media on day 3, and harvested on day 6. Four million BMDMs were seeded in 6 well plates 18 hr prior to infection. The LPS+ATP samples were pretreated with LPS (200 ng/mL) overnight. The following day, where indicated, cells were pretreated with GSK-PERK2606414 (PERK specific inhibitor, 5 µM) and Mdivi-1 (mitochondrial fission, 20 µM) for 1 hr prior to infection. Untreated and pretreated cells were infected with Live and HK RB51 (MOI 20) for 30 min or after which the inoculum was removed and cells were washed with PBS. Medium containing 50 µg/ml of gentamicin was added to kill extracellular bacteria. To synchronize infection, cells were spun at 1200 rpm for 3 min after adding inoculum. Cells were treated with tunicamycin (10 µg/mL), Carbonyl cyanide m-chlorophenyl hydrazine (CCCP, 20 µM), or ATP

(1mM) for 4 hr. At the indicated times, cells were lysed in RIPA buffer on ice for 15 min and spun at 16,000 x g for 15 min to pellet debris. For mitochondrial fractions, cells were lysed in buffer 1% NP-40 on ice for 15 min and spun at 16,000 x g for 15 min to pellet the insoluble fraction. The insoluble fraction was resuspend in mitochondrial suspension buffer (10mM TrisHCl pH 6.7, 0.15 mM MgCl2, 0.25 sucrose, 1 mM PMSF, 1 mM DTT) and centrifuged at 11,000 x g for 15 minutes at 4ºC to pellet the isolated mitochondria.

Respiratory Syncytial Virus (RSV)

All RSV experiments utilized antigenic subgroup A, Line 19 strain RSV obtained from Dr. N. Lukacs (University of Michigan). The strain was originally isolated from a sick infant in the University of Michigan Health System. Cells were pretreated with GSK-PERK2606414 (PERK specific inhibitor, 5 μM) for 1 hr prior to RSV infection (MOI 1). At the indicated times, cells were lysed in RIPA buffer on ice for 15 min and spun at 16,000 x g for 15 min to pellet debris. For mitochondrial fractions, cells were lysed in buffer 1% NP-40 on ice for 15 min and spun at 16,000 x g for 15 min to pellet the insoluble fraction. The insoluble fraction was resuspend in mitochondrial suspension buffer (10mM TrisHCl pH 6.7, 0.15 mM MgCl2, 0.25 sucrose, 1 mM PMSF, 1 mM DTT) and centrifuged at 11,000 x g for 15 minutes at 4ºC to pellet the isolated mitochondria.

Bacterial strains and reagents

Brucella abortus strain RB51 was obtained from Dr. G. Schurig (Virginia Polytechnic Institute and State University). Aliquots of RB51 were subjected to heat killing by incubating at 70ºC in a water bath for 60 min. HK bacterial

preparations were confirmed to be nonviable by plating aliquots on *Brucella* agar plates and confirming lack of growth following 4 days of incubation. Reagents were obtained from the following vendors: tunicamycin (Sigma-Aldrich), CCCP (Sigma-Aldrich), Mdivi-1 (Fisher), and ATP (Sigma-Aldrich). Antibodies were obtained from the following vendors: anti-PERK (cat#: 3192S, Cell Signaling), anti-p-PERK (cat#: sc-32577, Santa Cruz), anti-ATF6 (cat#: sc-22799, Santa Cruz), anti-caspase-1 (cat#: sc-514, Santa Cruz), PINK1 (cat#: BC100-494, Novus Biologicals), LC3B (cat#: NB100-2331, MBL), PARKIN (cat#: 4211, Cell Signaling), and anti-TOM20 (cat.# sc-11415, Santa Cruz).

siRNA knockdown of ATF4

Immortalized BMDMs were transfected with specific Dharmacon siGENOME ATF4 siRNA (cat# M-042737-01-0005) or non-target siRNA (cat.# D-001206-13-20) using DharmaFECT 4 transfection reagent according to the manufacturer's protocol. Knockdown efficiency was assessed via immunoblot using anti-ATF4 (cat.# sc-200) antibodies (Fig. A25).

ROS measurements

BMDMs were plated in a 96 well plate with black slides and clear bottom. At designated time points, BMDMs were washed with PBS and then incubated with CM-H2DCFDA (Invitrogen) at a final concentration of 2.5 µM in Ringer buffer (155 mM NaCl, 5 mM KCl, 1 mM $MgCl_2$ 6H2O, 2 mM NaH_2PO_4 H_2O, 10 mM HEPES, 10 mM glucose). Cell were incubated for 30 min at 37ºC, washed three times with cold PBS, and incubated for an additional 15 min at 37ºC in warm media for

recovery. After recovery, cells were washed one more time with PBS. Florescence was measured at excitation/emission 485nm/525nm.

Immunoblot Assay

Whole cell and mitochondrial extracts collected at indicated time points (2, 4, and 8 hr pi) were separated by SDS-PAGE, transferred to nitrocellulose membranes (Millipore), blocked with 5% nonfat dry milk in TBS-0.1% Tween20 (TBS-T), and incubated overnight at 4°C with primary antibodies specified above. Membranes were washed with TBS-T and incubated with secondary IRDye 680LT Goat anti-rabbit or IRDye 680LT Goat anti-mouse (1:20,000) at room temperature for 1 hr. Bands were visualized using the Li-Cor Odyssey Infrared Imaging System. Immunoblots shown in the figures are representative of n≥3 independent experiments. All immunoblots shown within an individual panel were analyzed in parallel with identical parameters using the Li-Cor System.

Cytokine Analysis

Culture supernatants were collected at indicated time points from macrophages infected as described. IL-1β levels were determined by sandwich enzyme-linked immunosorbent assay (ELISA) according to the manufacturer's instructions (BioLegend). A minimum of 3 technical replicates per experiment and 3 experimental replicates were analyzed for each condition.

Xbp1 splicing assay

Total RNA (2 µg) extracted from samples was prepared using the RNeasy Mini Kit (Qiagen) and used for cDNA synthesis. Primers encompassing the spliced sequences in xbp1 mRNA (forward 5'-GAACCAGGAGTTAAGAACACG-3' and

reverse 5'-AGGCAACAGTGTCAGAGTCC-3') were used for PCR amplification with GoTaq polymerase (Invitrogen). The thermal cycling profile consisted of 30 cycles at 94°C for 1 min, 60°C for 1 min, and 72°C for 1 min. PCR products were incubated with PstI (Invitrogen) at 37°C overnight. PstI digested products were separated by electrophoresis through a 2.5% agarose gel.

Mitochondrial DNA (mtDNA) release assay

DNA was isolated from 200 µL of the cytosolic fraction using a DNeasy Blood & Tissue Kit (Qiagen). Quantitative PCR was employed to measure mtDNA using Brilliant II SYBR Green with Low ROX (Agilent Technologies) on a Stratagene MX300 QPCR System. The copy number of mtDNA encoding cytochrome c oxidase I was normalized to nuclear DNA encoding 18S ribosomal RNA. The following primers were used: cytochrome c oxidase I (forward 5'-GCCCCAGATATAGCATTCCC-3' and reverse 5'-GTTCATCCTGTTCCTGCTCC-3') and 18S rRNA (forward 5'-TAGAGGGACAAGTGGCGTTC-3' and reverse 5'-CGCTGAGCCAGTCAGTGT-3').

JC-1 staining for mitochondrial membrane potential ($\Delta\psi_m$)

Four million BMDMs were seeded into a 96-well black plate. Cells were treated with 5 µl of JC-1 staining solution (Life Technologies) then treated with CCCP or infected with Live and HK RB51. Fluorescence of JC-1 in treated cells was measured at various time points using the following excitation and emission wavelengths: 560nm/595nm (aggregates) and 485nm/535nm (monomers).

For fluorescence microscopy, 3 x 10^5 cells were seeded in a 60 mm glass-bottom dish. Cells were treated with 100 µl of JC-1 staining then treated with the conditions

stated above. Healthy mitochondria were detected with fluorescence settings designed to detect Texas Red (excitation/emission: 590/610nm).

Parkin qPCR

RNA was isolated from treated BMDM using a RNeasy Midi Kit (Qiagen). cDNA was synthesized from the extracted RNA using the SuperScript III First-Strand Synthesis System (Life Technologies). Quantitative PCR was employed to measure PARKIN transcript levels using Brilliant II SYBR Green with Low ROX (Agilent Technologies) on a Stratagene MX300 QPCR System. The copy number of PARKIN was normalized to Actin. The following primers were used: PARKIN (forward 5'-AAACCGGATGAGTGGTGAGT-3' and reverse 5'-AGCTACCGACGTGTCCTTGT-3').

Confocal microscopy and 3-D reconstruction of mitochondrial network

BMDM were seeded onto square coverslips in 6 well plates at a density of 3×10^5 per well the night before infection. The day of infection, host cells were treated with CCCP (positive control of fragmentation) or infected with Live and HK RB51 as stated above. Coverslips were rinsed using DPBS (+ calcium and magnesium) and fixed in 4% paraformaldehyde. After fixation, coverslips were rinsed three times in TBS+0.1% Triton-X 100 and stained with the mitochondrial marker TOM20 (1:350) for 45 minutes, stained with secondary Cy3 (1:100) for 45 minutes, and counterstained with DAPI (1:1000) for 15 minutes. Coverslips were mounted onto slides using Prolong Gold Anti-Fade (Invitrogen). Cells were imaged at the Microscopy and Image Analysis (MIL) core at the University of Michigan Medical School using an Nikon A-1 inverted fluorescence microscope. Images were

collected using the Nikon Elements software with diode lasers 405 (DAPI) and 561 (Cy3) with a Z-stack step size of 0.200 µm. Z-stacks of images were combined using Metamorph to obtained a single image. The stacked images was processed using a deconvolution algorithm followed by 3-D reconstruction using the Huygens Essentials software. A region of interest (ROI) was drawn around a cell to obtain the isosurface volume and length of the mitochondrial network. Sample size of each condition consist of n = 25 cells.

Statistical Analysis

All p values were generated between identified samples using unpaired two-tailed Student's t-tests and represent analysis of ≥3 replicates per condition. Asterisks denote the following p values: *p<0.05, **p<0.001 and ***p<0.0001.

Author contributions:

DNB and MXDO designed the experiments. DNB performed the experiments. SHM and NWL contributed critical reagents, materials, and discussion. DNB and MXDO analyzed the data and wrote the paper.

Author information:

The authors have declared that no competing interests exist.

Acknowledgements:

We acknowledge members of the O'Riordan lab for many helpful discussions. We thank the staff of the UM Unit for Laboratory Animal Medicine that provided assistance with saphenous vein blood collection. The University of Michigan Microscopy and Image Analysis laboratory and Center for Live-Cell Imaging for providing guidance with confocal microscopy and 3-D reconstruction. We

acknowledge financial support from the University of Michigan Rackham Graduate School (DNB) and Michigan Genetics Training Fellowship (DNB, GM007544). This research was supported by funding from the NIH to MXDO (AI101777), and NWL (HL114858). The funders had no role in study design, data collection and analysis, decision to publish, or preparation of the manuscript.

References

1 Kim, I., Xu, W. & Reed, J. C. Cell death and endoplasmic reticulum stress: disease relevance and therapeutic opportunities. Nature reviews. Drug discovery 7, 1013-1030, doi:10.1038/nrd2755 (2008).

2 Zhao, L. & Ackerman, S. L. Endoplasmic reticulum stress in health and disease. Current opinion in cell biology 18, 444-452, doi:10.1016/j.ceb.2006.06.005 (2006).

3 de Moura, M. B., dos Santos, L. S. & Van Houten, B. Mitochondrial dysfunction in neurodegenerative diseases and cancer. Environmental and molecular mutagenesis 51, 391-405, doi:10.1002/em.20575 (2010).

4 Pieczenik, S. R. & Neustadt, J. Mitochondrial dysfunction and molecular pathways of disease. Experimental and molecular pathology 83, 84-92, doi:10.1016/j.yexmp.2006.09.008 (2007).

5 Martinon, F., Chen, X., Lee, A. H. & Glimcher, L. H. TLR activation of the transcription factor XBP1 regulates innate immune responses in macrophages. Nature immunology 11, 411-418, doi:10.1038/ni.1857 (2010).

6 Cassel, S. L., Joly, S. & Sutterwala, F. S. The NLRP3 inflammasome: a sensor of immune danger signals. Seminars in immunology 21, 194-198, doi:10.1016/j.smim.2009.05.002 (2009).

7 Nakahira, K. et al. Autophagy proteins regulate innate immune responses by inhibiting the release of mitochondrial DNA mediated by the NALP3 inflammasome. Nature immunology 12, 222-230, doi:10.1038/ni.1980 (2011).

8 Shi, C. S. et al. Activation of autophagy by inflammatory signals limits IL-1beta production by targeting ubiquitinated inflammasomes for destruction. Nature immunology 13, 255-263, doi:10.1038/ni.2215 (2012).

9 Rodgers, M. A., Bowman, J. W., Liang, Q. & Jung, J. U. Regulation where autophagy intersects the inflammasome. Antioxidants & redox signaling 20, 495-506, doi:10.1089/ars.2013.5347 (2014).

10 Ricci, J. E., Waterhouse, N. & Green, D. R. Mitochondrial functions during cell death, a complex (I-V) dilemma. Cell death and differentiation 10, 488-492, doi:10.1038/sj.cdd.4401225 (2003).

11 Salvioli, S., Ardizzoni, A., Franceschi, C. & Cossarizza, A. JC-1, but not DiOC6(3) or rhodamine 123, is a reliable fluorescent probe to assess delta psi changes in intact cells: implications for studies on mitochondrial functionality during apoptosis. FEBS letters 411, 77-82 (1997).

12 Avivar-Valderas, A. et al. PERK integrates autophagy and oxidative stress responses to promote survival during extracellular matrix detachment. Molecular and cellular biology 31, 3616-3629, doi:10.1128/MCB.05164-11 (2011).

13 Kouroku, Y. et al. ER stress (PERK/eIF2alpha phosphorylation) mediates the polyglutamine-induced LC3 conversion, an essential step for autophagy formation. Cell death and differentiation 14, 230-239, doi:10.1038/sj.cdd.4401984 (2007).

14 Youle, R. J. & Narendra, D. P. Mechanisms of mitophagy. Nature reviews. Molecular cell biology 12, 9-14, doi:10.1038/nrm3028 (2011).

15 Bouman, L. et al. Parkin is transcriptionally regulated by ATF4: evidence for an interconnection between mitochondrial stress and ER stress. Cell death and differentiation 18, 769-782, doi:10.1038/cdd.2010.142 (2011).

16 Cassidy-Stone, A. et al. Chemical inhibition of the mitochondrial division dynamin reveals its role in Bax/Bak-dependent mitochondrial outer membrane permeabilization. Developmental cell 14, 193-204, doi:10.1016/j.devcel.2007.11.019 (2008).

17 Lupfer, C. et al. Receptor interacting protein kinase 2-mediated mitophagy regulates inflammasome activation during virus infection. Nature immunology 14, 480-488, doi:10.1038/ni.2563 (2013).

18 Kim, S. J., Syed, G. H. & Siddiqui, A. Hepatitis C virus induces the mitochondrial translocation of Parkin and subsequent mitophagy. PLoS pathogens 9, e1003285, doi:10.1371/journal.ppat.1003285 (2013).

19 Kim, S. J. et al. Hepatitis C virus triggers mitochondrial fission and attenuates apoptosis to promote viral persistence. Proceedings of the National Academy of Sciences of the United States of America 111, 6413-6418, doi:10.1073/pnas.1321114111 (2014).

20 Kim, S. J. et al. Hepatitis B virus disrupts mitochondrial dynamics: induces fission and mitophagy to attenuate apoptosis. PLoS pathogens 9, e1003722, doi:10.1371/journal.ppat.1003722 (2013).

21 Xia, M. et al. Mitophagy enhances oncolytic measles virus replication by mitigating DDX58/RIG-I-like receptor signaling. Journal of virology 88, 5152-5164, doi:10.1128/JVI.03851-13 (2014).

22 Borchers, A. T., Chang, C., Gershwin, M. E. & Gershwin, L. J. Respiratory syncytial virus--a comprehensive review. Clinical reviews in allergy & immunology 45, 331-379, doi:10.1007/s12016-013-8368-9 (2013).

23 Munday, D. C., Howell, G., Barr, J. N. & Hiscox, J. A. Proteomic analysis of mitochondria in respiratory epithelial cells infected with human respiratory syncytial virus and functional implications for virus and cell biology. The Journal of pharmacy and pharmacology, doi:10.1111/jphp.12349 (2014).

24 Boyapalle, S. et al. Respiratory syncytial virus NS1 protein colocalizes with mitochondrial antiviral signaling protein MAVS following infection. PloS one 7, e29386, doi:10.1371/journal.pone.0029386 (2012).

25 Segovia, J. et al. TLR2/MyD88/NF-kappaB pathway, reactive oxygen species, potassium efflux activates NLRP3/ASC inflammasome during respiratory syncytial virus infection. PloS one 7, e29695, doi:10.1371/journal.pone.0029695 (2012).

26 Verfaillie, T., Salazar, M., Velasco, G. & Agostinis, P. Linking ER Stress to Autophagy: Potential Implications for Cancer Therapy. International journal of cell biology 2010, 930509, doi:10.1155/2010/930509 (2010).

27 Batlevi, Y. & La Spada, A. R. Mitochondrial autophagy in neural function, neurodegenerative disease, neuron cell death, and aging. Neurobiology of disease 43, 46-51, doi:10.1016/j.nbd.2010.09.009 (2011).

28 Khandelwal, P. J., Herman, A. M., Hoe, H. S., Rebeck, G. W. & Moussa, C. E. Parkin mediates beclin-dependent autophagic clearance of defective mitochondria and ubiquitinated Abeta in AD models. Human molecular genetics 20, 2091-2102, doi:10.1093/hmg/ddr091 (2011).

29 Cullinan, S. B. & Diehl, J. A. PERK-dependent activation of Nrf2 contributes to redox homeostasis and cell survival following endoplasmic reticulum stress. The Journal of biological chemistry 279, 20108-20117, doi:10.1074/jbc.M314219200 (2004).

30 Lindquist, M. E., Mainou, B. A., Dermody, T. S. & Crowe, J. E., Jr. Activation of protein kinase R is required for induction of stress granules by respiratory syncytial virus but dispensable for viral replication. Virology 413, 103-110, doi:10.1016/j.virol.2011.02.009 (2011).

31 Groskreutz, D. J. et al. Respiratory syncytial virus induces TLR3 protein and protein kinase R, leading to increased double-stranded RNA responsiveness in airway epithelial cells. Journal of immunology 176, 1733-1740 (2006).

32 Talloczy, Z., Virgin, H. W. t. & Levine, B. PKR-dependent autophagic degradation of herpes simplex virus type 1. Autophagy 2, 24-29 (2006).

33 Xia, M. et al. Mitophagy switches cell death from apoptosis to necrosis in NSCLC cells treated with oncolytic measles virus. Oncotarget 5, 3907-3918 (2014).

Chapter 5

Perspective

Overview

ER and mitochondrial crosstalk: a regulator of inflammasome activation

Inflammation is a double-edged sword, because it aids in resolution of infection but overexuberant inflammation can cause severe damage to the host. Individually, the ER and mitochondria have been shown to cooperate in triggering inflammation – the ER stress sensor IRE1 drives cytokine upregulation, while mitochondrial DAMPs activate the inflammasome. Although crosstalk frequently occurs between these two organelles, it was unclear whether ER-mitochondrial crosstalk was important for modulating an inflammatory response. Using the attenuated cattle vaccine strain of *Brucella abortus* RB51 as a model pathogen, I discovered that selective activation of host ER stress pathways can have different and profound effects on mitochondria leading to infection-associated proinflammatory signaling, inflammasome suppression, or cell death. Triggering the inflammasome by infection-induced ER stress required signaling through the IRE1-NLRP3-caspase-2-Bid axis upstream of the mitochondria. Suppression of the inflammasome could be mediated by PERK-induced mitophagy. If PERK was not activated then IRE1-mediated inflammation eventually resulted in a unique form of cell death with characteristics of both apoptosis (silent cell death) and pyroptosis (inflammatory cell death).

Novel roles for non-inflammatory proteins

This thesis work has also uncovered surprising roles for proteins that did not have well-established functions in inflammation. Caspase-2 was classified as an apoptotic caspase with ties to metabolism, mitochondrial damage, and ER stress [1]. A previous study reported that caspase-2 could mediate caspase-1 activation during a *Salmonella* macrophage infection [2]. No other study has been published to confirm this finding, and the mechanism by which caspase-2 regulated caspase-1 was not identified. Here I show that caspase-2 does regulate caspase-1 activation by inducing mitochondrial damage, leading to inflammasome activation. Additionally, NLRP3 can regulate caspase-2 activation in response to ER stress. Classically, no other caspase besides caspase-1 is known to interact with NLRP3 – the interaction between NLRP3 and caspase-1 is mediated by ASC with contains both a CARD (caspase-1 interacting domain) and PYD domain (NLRP3 interacting domain). Although caspase-2 contains a CARD domain similar to caspase-1 [1], no reports have ever linked NLRP3 and caspase-2 together especially during inflammatory contexts, and it is intriguing to speculate that NLRP3 may interact with caspase-2 in a complex that is analogous to, but distinct from the canonical inflammasome.

Similar to caspase-2, PERK had not previously been linked to control of inflammation. PERK is best known for its involvement in ER stress-induced cell death and upregulation of antioxidant capacity. A previous study linked PERK to mitophagy, but in a non-infectious context. I discovered that specific microbial signals could activate PERK, which suppressed IL-1β production by triggering

removal of damaged mitochondria and mtDAMPs, ligands that stimulate inflammasome activation. My data are consistent with a suppressive role for PERK signaling during the inflammatory response to microbial infections both *in vitro* and *in vivo*. Since PERK suppresses inflammation, this UPR sensor may be useful as a therapeutic target for inflammatory diseases. By triggering PERK activation, one could reduce inflammation and pathology, thus increasing the health of patients who suffer from mitochondrial dysfunction-mediated diseases such as heart disease, Alzheimer's, and diabetes. My thesis research supports a role for ER as a critical hub for integrating cellular stress and innate immune signaling. Additionally, this work highlights the importance of maintaining the integrity of the mitochondrial network for minimizing inflammation. Even though we now have models that better define the regulatory role of ER-mitochondrial crosstalk in immune regulation, there are still questions that remain to be investigated.

Broader impact of these pathways in infectious and non-infectious conditions

Although I used an attenuated vaccine strain to elucidate the regulatory mechanisms on inflammation licensed by the ER and mitochondria, I was able to demonstrate that these pathways occur during other infectious and non-infectious contexts. I found that in contexts where ER stress is triggered by chemical inducers (Chapter 3), IRE1 was essential for triggering inflammasome activation in a NLRP3/caspase-2/Bid dependent manner. Furthermore, Parkin-dependent mitophagy suppressed RSV- and HK RB51-induced IL-1β production (Chapter 4). The similarity of these pathways in different contexts aligns with previous work demonstrating that numerous stimuli (e.g. infection, irritants, injury, etc.) can elicit

cellular stress; therefore, it is not surprising that these pathways are crucial in different contexts. My thesis work highlights the potential role for ER-mitochondrial crosstalk in the broader context of clinically relevant infections and chronic inflammation. While some of the proteins described here were implicated in various inflammatory diseases, their connection to disease was previously unclear; my thesis research provides a framework and specific mechanisms by which cellular stress programs control inflammation.

Future Areas of Investigation

What is the fate of the damaged mitochondria captured during mitophagy?

Captured cargo from autophagy and autophagy related processes are degraded and recycled for use by the cell [3]. In Chapter 3, I showed that damaged mitochondria fragment from the network and are captured in HK-infected BMDM. I have preliminary data that show these mitochondrial fragments are tagged by LC3 and released by the cell, suggesting that they are not autonomous but are surrounded by an autophagic membrane (Fig. A26). It is unclear if these fragments are intact mitochondria or mitochondrially derived vesicles (MDVs) [4]. Previous studies have illustrated that both mitochondria and MDVs can be released by cells. Released mitochondria are intact (lack signs of damage) and trigger inflammatory responses [5]. MDVs are cargo-selective vesicles that bud off mitochondria in a Parkin-dependent manner [4, 6]. These MDVs are enriched for oxidized mitochondrial proteins and form in response to mitochondrial stress. The cargo (e.g. TOM20 positive or negative) and structure (single or double-membrane) of these MDVs can vary. I speculate that the observed extracellular mitochondrial

fragments are MDVs because these fragments are dependent upon Parkin and are associated with LC3. Intact mitochondria, when released, are not surrounded by a plasma membrane [5]. Although I have observed TOM20 positive fragments, it is unclear if other types of MDVs are being released by HK-infected BMDM. Immunostaining for mitochondrial proteins (PDH –matrix and Complex III – inner membrane) that have been identified in MDVs will further characterize the particles released by HK-infected BMDM. Additionally, I could probe for other proteins that I showed in Chapter 3 (e.g., caspase-2, NLRP3, Bid, etc.) to determine if they associate with these extracellular mitochondria. These vesicles/fragments may be carrying non-mitochondrial proteins that can trigger other cellular processes such as cell death or inflammation. Determining the molecular characteristics of MDVs will elucidate the as yet unknown function of extracellular mitochondrial fragments in the context of infection and inflammation.

Currently, it remains unclear if these mitochondrial fragments would be perceived as pro-inflammatory or anti-inflammatory signals. It is known that apoptotic bodies when engulfed by a neighboring cell can be anti-inflammatory [7]. Since these mitochondrial fragments appear to be surrounded by an autophagic membrane, it is quite possible that, if sensed by recipient cells, they would not trigger the production of pro-inflammatory cytokines. Mitochondrial DAMPs can be detected in the bloodstream of patients suffering from systemic inflammatory response syndrome (SIRS), Acute Respiratory Distress Syndrome (ARDS), and acute lung injury (ALI) [8, 9]. These observations suggest that mitochondria contribute to immune responses and that these mtDAMPs are underappreciated

signaling molecules that may influence the course of disease. The genesis and regulation of mitochondrial vesicle formation has not been fully explored. Therefore, it is of interest to elucidate mechanisms of formation and extracellular release of these mitochondrial DAMPs/vesicles. Further investigation into the mechanisms and impact of these mitochondrial fragments may shed light on how cellular stress pathways exert long-range influence on other cells and organs during an inflammatory response.

Why does mtROS increase when ROS-detoxifying mechanisms exist?

The mitochondrial network is the major production site of ROS, and excessive ROS production can be very toxic for the cell. Recent studies have illustrated that a NAD+ dependent deacetylase, Sirtuin-3 (Sirt3), can aid in detoxifying mtROS. Sirt3 localizes primarily in mitochondria and deacetylates several mitochondrial targets, including acetyl-CoA synthase 2, succinate dehydrogenase, manganese superoxide dismutase (MnSOD), and isocitrate dehydrogenase 2 [10]. Deacetylation of these targets allows Sirt3 to regulate oxidative phosphorylation and prevent oxidative damage. Recently, it was reported that DNA damage could trigger proteasomal degradation of Sirt3 leading to increased ROS production [11].

In Chapter 3, the observation of a rapid and steady increase in ROS in Live-infected BMDM suggested that there might be a deficiency in Sirt3. In Live-infected BMDM, I observed a significant decrease in Sirt3 activity and protein levels suggesting that Sirt3 was being inactivated or degraded (Fig. A27). There is little evidence to support Sirt3 degradation, especially during ER stress conditions.

These observations suggest that ER stress not only aids in the release of mitochondrial contents but can also regulate mitochondrial protein function. Degradation of Sirt3 could be viewed as a release on the inflammatory brake – by removing the brake, the cell can ramp up inflammation quickly and increase the chances of clearing the infection. My preliminary data show that Sirt3 degradation occurs during other types of microbial infections (*Salmonella* and MRSA, data not shown), suggesting that this degradation phenotype is not *Brucella*-specific but rather a broader phenomenon associated with infection. Degradation of Sirt3 could be mediated by (a) the mitochondrial localized proteasome, Lon [12, 13], or (b) exported from the mitochondria and degraded by the cytosolic ubiquitin-proteasome system [14]. Sirt3 binds to heat shock protein 60 (HSP60), an interaction that may be critical for maintaining the presence of Sirt3 in the mitochondrial matrix [15]. During ER stress, there may be signals that destroy the Sirt3-HSP60 interaction thus leading to Sirt3 degradation. Currently, I am investigating whether Sirt3 degradation is mediated by the cytosolic ubiquitin-proteasome system and what triggers Sirt3 degradation (e.g., TLR signaling, TXNIP translocation to mitochondria, calcium flux). Further investigation into what signals Sirt3 degradation is important because deficiency or mutations in SIRT3 lead to increased inflammation in mice [16]. These data suggest that SIRT3 can regulate inflammatory outputs in response to infection and/or cellular stress.

What role does calcium play in inflammation modulation?

Close interactions between the endoplasmic reticulum (ER) and mitochondria are essential for rapid and sustained Ca^{2+} uptake by mitochondria

[17]. VDAC, located in the outer mitochondrial membrane, is responsible for the rapid transfer of Ca^{2+} at mitochondrial-associated membranes (MAMs) or contact sites between ER and mitochondria. Increasing mitochondrial Ca^{2+} concentration activates dehydrogenases, thus increasing the electron flux and ATP production. Under homeostatic conditions, inositol 1,4,5 trisphosphate receptor (IP_3R, located in the ER membrane) allows for regulated calcium transfer to the mitochondria. Interestingly, IP_3R also inhibits autophagy by forming protein complexes with Beclin-1 and Bcl-2 [18]. If calcium transfer is inhibited, Ca^{2+}-dependent stimulation of aerobic metabolism triggers autophagy due to the disruption of the Bcl-2/Beclin-1/IP_3R interaction. Preventing mitochondrial calcium uptake or massive calcium overload can trigger apoptosis. In healthy mitochondria, VDAC interacts with Bax and Bak to prevent the formation of Bak/Bax pores – pores that aid in the release of mitochondrial contents into the cytosol. Following an apoptotic stimulus, BID, a death agonist, is cleaved and binds to the outer mitochondrial membrane (OMM), where it activates Bax and Bak. Activated Bax and Bak promote OMM permeabilization and increase calcium leakage from the ER by interacting with IP_3R [19]. This leads to the release of caspase cofactors into the cytosol thus triggering apoptosis. In addition to the release of proapoptotic factors, mitochondrial danger signals (mtDAMPs) are also released into the cytosol thus leading to inflammation, in particular inflammasome activation.

There are stark differences between the inflammatory response from Live RB51 and HK-infected BMDM. Live infection triggers excessive mitochondrial damage and pyroptosis (Chapters 2 and 3), whereas HK infection triggers

mitophagy (Chapter 4) and does not induce cell death [20]. Early in infection, both Live and HK-infected BMDM look similar; however, at 4h p.i. they begin to diverge. During the first two hours of infection by both Live and HK, there may be an influx of calcium from the ER into mitochondria, thus triggering a decrease in membrane potential and the stabilization of PINK1 on the outer membrane. Since at 4h p.i., Live-infected BMDM cleave Bid leading to outer mitochondrial membrane permeabilization, I hypothesize that mitochondrial damage possibly increases calcium efflux from the ER. This would increase mitochondrial calcium uptake and exacerbate mitochondrial damage. In HK-infected BMDM at 4h p.i., PERK is activated and induces Parkin upregulation. Parkin is recruited to the mitochondrial network and begins to ubiquitinate mitochondrial proteins, like VDAC, on the outer mitochondrial membrane, which would likely prevent further uptake of calcium into the mitochondria. To test this hypothesis, we can now take advantage of available mitochondria-specific calcium probes, including fusion proteins that carried calcium-sensitive photoproteins and GFP-based protein constructs engineered to change fluorescence properties following Ca^{2+} binding. With these tools, we will be able to measure changes in calcium concentration within the ER lumen and mitochondrial matrix, as well as more rigorously assess if differences in calcium flux are the key to modulating ER stress-induced inflammation.

What feature of HK RB51 is essential for PERK activation?

Very little is known about the exact mechanism of ER stress activation by microbial ligands. Recent evidence has shown that activation sensitivity differs between UPR sensors [21]. In Chapter 3, I observed that HK, but not Live,

triggered PERK activation. HK bacteria could be viewed as a collection of microbial ligands. It is quite possible that our heat treatment changes protein structure, thus presenting ligands/epitopes that the cell would not normally see. To investigate whether microbial viability was the key to triggering PERK activation, I heat inactivated a variety of Gram-positive and -negative bacteria and measuring CHOP (a downstream target of PERK) induction. Only HK RB51 and the positive control tunicamycin (ER stress inducer) triggered CHOP induction – even at high MOI neither *Salmonella* (SL1344), *Listeria* (10403S) MRSA (USA300), nor *E. coli* (HB101) could trigger the PERK pathway (Fig. A28). Notably, all of the HK bacteria could trigger robust *xbp1* splicing, indicating activation of the IRE1 ER stress sensor (data not shown). These data suggest that there is another factor responsible for triggering PERK activation.

Brucella abortus RB51 contains a Type 4 secretion system (T4SS) [22, 23], and heat killing RB51 would prevent the secretion of effector proteins into macrophages, because the bacteria are not metabolically active. If Live RB51 is actively suppressing PERK through an effector protein, then Live RB51 lacking a functional T4SS should trigger PERK activation. Infecting BMDM with Live RB51ΔvirB (T4SS) stimulated more PERK phosphorylation than wildtype Live RB51, but less than HK (Fig. A28). This is an interesting observation because virulent *Brucella* strains do induce PERK activation and contain a T4SS [24]. RB51 is an attenuated laboratory strain derived from the virulent S2308 strain that was grown and passaged in media containing the antibiotic Rifampin [25]. Rifampin binds to the β subunit of the DNA-dependent RNA polymerase, and growth in

rifampin yields rough *Brucella abortus* colonies (deficient O antigen). Rifampin treatment also induced additional missense mutations (526 amino acids affected in total) in RB51 [25]. These observations suggest that an effector protein secreted through the T4SS is defective in PERK activation by Live RB51 due to mutations that alter expression or function of the effector protein. A recent study reported that four *Brucella* effector proteins (BspA, BspB, BspD, and BspK) localized to the ER [23]. With these newly identified ER-localized effector proteins, we can detect mutations in these proteins by comparing the sequence of RB51 to its parent strain, S2308. If there are any differences in sequence, we can then investigate whether the mutated effector protein in RB51 is responsible for the lack of PERK activation during Live infection. Additionally, by infecting macrophages with WT RB51 and RB51+WTeffector we could do a co-immunoprecipitation assay to assess interaction between the effector and PERK. If there are differences that interrupt interaction, then we would demonstrate that bacterial effector proteins can modulate ER stress sensors.

Conclusions and Significance of Thesis

This thesis addresses an open question in the innate immunity field of how cellular stress can lead to control of inflammation, specifically the inflammasome. My data show that the partnership between the ER and mitochondria is essential for fine-tuning the immune response during infection. ER stress sensors can either induce mitochondrial damage to trigger an immune response or remove fragments of the mitochondrial network to dampen an immune response. Since ER components can trigger or suppress inflammation depending on the context, it

might be possible to customize immune responses – either increase inflammation to shorten time for microbial clearance (trigger IRE1) or dampen an immune response during disease to decrease tissue damage (trigger PERK). Researchers are now discovering that many pathogens can exploit these cellular stress programs to increase their survival and dampen the immune response – thus providing a strong rationale for a better mechanistic understanding of these stress pathways and their influence on immune responses. Furthermore, these three ER stress sensors have been implicated in promoting insulin secretion, differentiation, lipid biosynthesis, and neurite outgrowth. By selectively activating or deactivating these stress programs using small molecule compounds, it may be possible to modulate cellular function and treat disease where these functions are altered. The results described in this thesis are relevant to understanding how ER stress might influence many diseases. Overall, the molecular context of cellular stress is critical in defining the pathways that govern cellular function, infection and inflammation.

References

1. Krumschnabel, G., et al., The enigma of caspase-2: the laymen's view. Cell Death Differ, 2009. 16(2): p. 195-207.

2. Jesenberger, V., et al., Salmonella-induced caspase-2 activation in macrophages: a novel mechanism in pathogen-mediated apoptosis. J Exp Med, 2000. 192(7): p. 1035-46.

3. Eskelinen, E.L. and P. Saftig, Autophagy: a lysosomal degradation pathway with a central role in health and disease. Biochim Biophys Acta, 2009. 1793(4): p. 664-73.

4. Sugiura, A., et al., A new pathway for mitochondrial quality control: mitochondrial-derived vesicles. EMBO J, 2014. 33(19): p. 2142-56.

5. Maeda, A. and B. Fadeel, Mitochondria released by cells undergoing TNF-alpha-induced necroptosis act as danger signals. Cell Death Dis, 2014. 5: p. e1312.

6. McLelland, G.L., et al., Parkin and PINK1 function in a vesicular trafficking pathway regulating mitochondrial quality control. EMBO J, 2014. 33(4): p. 282-95.

7. Maderna, P. and C. Godson, Phagocytosis of apoptotic cells and the resolution of inflammation. Biochim Biophys Acta, 2003. 1639(3): p. 141-51.

8. Sun, S., et al., Mitochondrial DAMPs increase endothelial permeability through neutrophil dependent and independent pathways. PLoS One, 2013. 8(3): p. e59989.

9. Zhang, Q., et al., Circulating mitochondrial DAMPs cause inflammatory responses to injury. Nature, 2010. 464(7285): p. 104-7.

10. Nogueiras, R., et al., Sirtuin 1 and sirtuin 3: physiological modulators of metabolism. Physiol Rev, 2012. 92(3): p. 1479-514.

11. Iwahara, T., et al., SIRT3 functions in the nucleus in the control of stress-related gene expression. Mol Cell Biol, 2012. 32(24): p. 5022-34.

12. Kaser, M. and T. Langer, Protein degradation in mitochondria. Semin Cell Dev Biol, 2000. 11(3): p. 181-90.

13. Ngo, J.K., L.C. Pomatto, and K.J. Davies, Upregulation of the mitochondrial Lon Protease allows adaptation to acute oxidative stress but dysregulation is associated with chronic stress, disease, and aging. Redox Biol, 2013. 1(1): p. 258-64.

14. Azzu, V. and M.D. Brand, Degradation of an intramitochondrial protein by the cytosolic proteasome. J Cell Sci, 2010. 123(Pt 4): p. 578-85.

15. Yang, Y., K.Y. Chen, and Q. Tong, Murine Sirt3 protein isoforms have variable half-lives. Gene, 2011. 488(1-2): p. 46-51.

16. Hirschey, M.D., et al., SIRT3 deficiency and mitochondrial protein hyperacetylation accelerate the development of the metabolic syndrome. Mol Cell, 2011. 44(2): p. 177-90.

17. Rizzuto, R., et al., Mitochondria as sensors and regulators of calcium signalling. Nat Rev Mol Cell Biol, 2012. 13(9): p. 566-78.

18. Vicencio, J.M., et al., The inositol 1,4,5-trisphosphate receptor regulates autophagy through its interaction with Beclin 1. Cell Death Differ, 2009. 16(7): p. 1006-17.

19. Oakes, S.A., et al., Proapoptotic BAX and BAK regulate the type 1 inositol trisphosphate receptor and calcium leak from the endoplasmic reticulum. Proc Natl Acad Sci U S A, 2005. 102(1): p. 105-10.

20. Chen, F. and Y. He, Caspase-2 mediated apoptotic and necrotic murine macrophage cell death induced by rough Brucella abortus. PLoS One, 2009. 4(8): p. e6830.

21. DuRose, J.B., A.B. Tam, and M. Niwa, Intrinsic capacities of molecular sensors of the unfolded protein response to sense alternate forms of endoplasmic reticulum stress. Mol Biol Cell, 2006. 17(7): p. 3095-107.

22. de Jong, M.F. and R.M. Tsolis, Brucellosis and type IV secretion. Future Microbiol, 2012. 7(1): p. 47-58.

23. Myeni, S., et al., Brucella modulates secretory trafficking via multiple type IV secretion effector proteins. PLoS Pathog, 2013. 9(8): p. e1003556.

24. Smith, J.A., et al., Brucella induces an unfolded protein response via TcpB that supports intracellular replication in macrophages. PLoS Pathog, 2013. 9(12): p. e1003785.

25. Marianelli, C., et al., Genetic bases of the rifampin resistance phenotype in Brucella spp. J Clin Microbiol, 2004. 42(12): p. 5439-43.

Appendix

Purpose

The following section contains figures supplemental to the main chapter discussions. Figures A1-A3 were supplemental material published in the Frontiers of Cellular and Infection Microbiology and are referenced in Chapter 2. Figures A4-A19 were included as supplemental material in the submitted IRE1 manuscript and are referenced in Chapter 3. Figures A20-A25 are supplemental data for the PERK data and are referenced in Chapter 4. Figures A26-A28 represent data that do not form a complete scientific story and are referenced in Chapter 5 as ideas that should be investigated further.

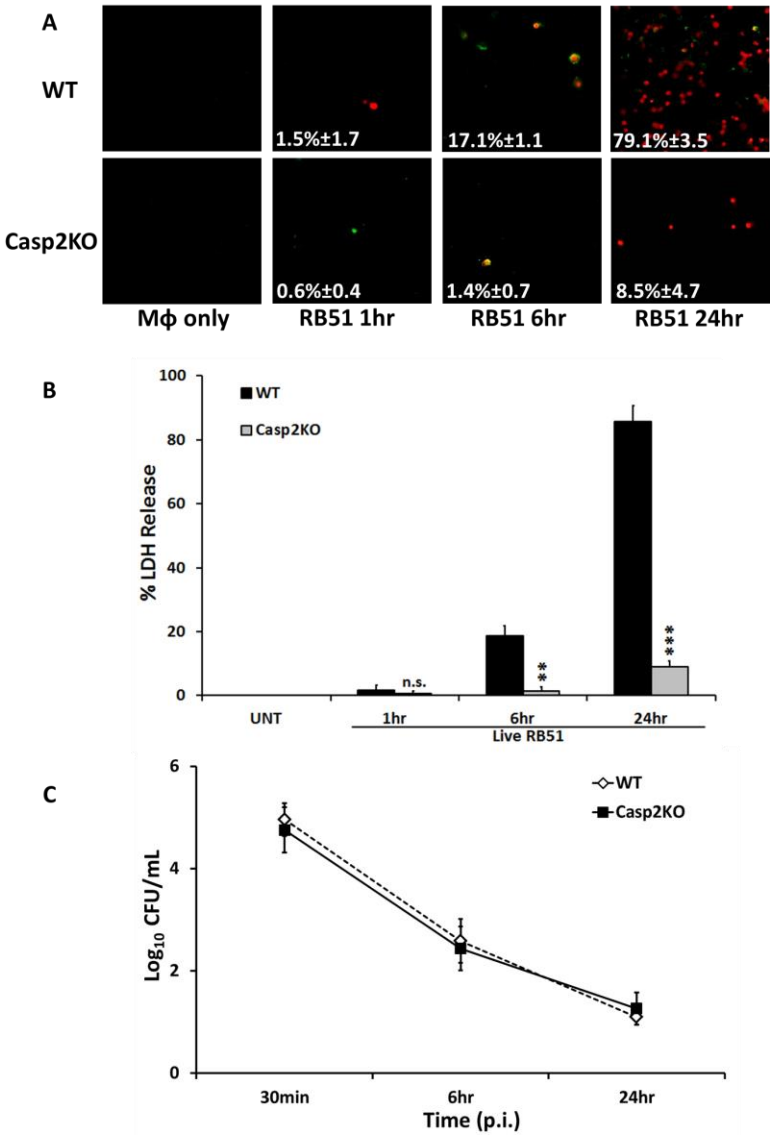

Figure A1: Caspase-2 mediates RB51-induced macrophage cell death. (A) Annexin V/propidium iodide (PI) staining of RB51-infected WT and *casp2*$^{-/-}$ BMDMs at 100X magnification. Images are representatives of n≥3 independent experiments. (B) LDH release in Live RB51-infected WT and *casp2*$^{-/-}$ BMDMs. Cells were counted in randomly selected fields of 100 cells. (C) CFU analysis of RB51 in WT and *casp2*$^{-/-}$ BMDMs, Error bars represent mean ± SD of n≥3 independent experiments. **p < 0.001 and ***p < 0.0001, Student's *t*-test. n.s. = not significant.

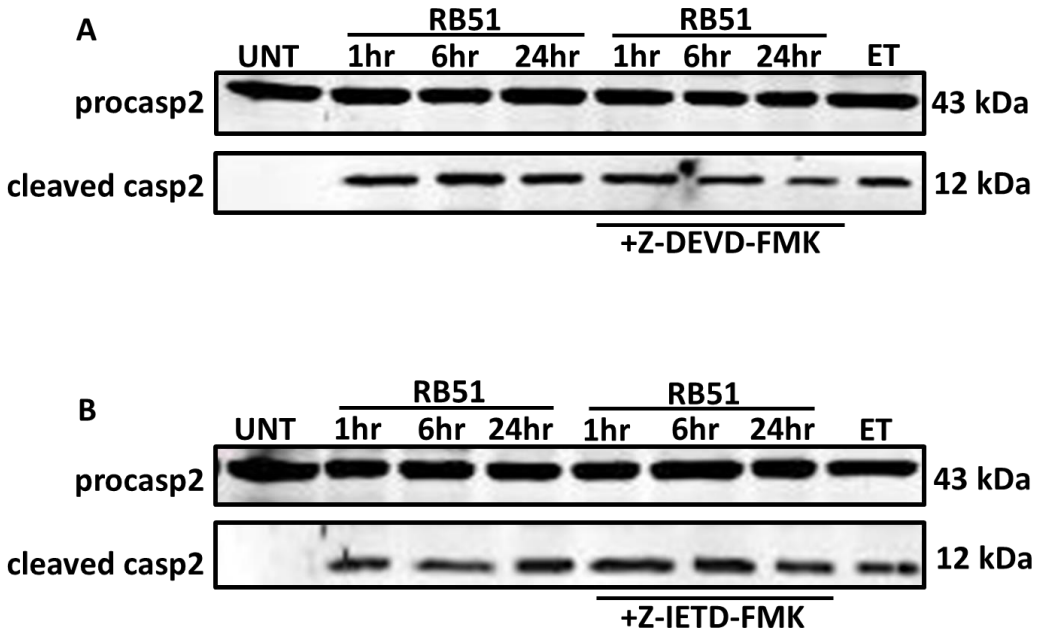

Figure A2: Caspase-3 and -8 are involved in RB51-induced cell death. (A) Caspase-2 cleavage (activation) in Live RB51-infected RAW264.7 macrophages with or without Z-DEVD-FMK (20 µM, Caspase-3 inhibitor). (B) Caspase-2 cleavage (activation) in Live RB51-infected RAW264.7 macrophages with or without Z-IETD-FMK (20 µM, Caspase-8 inhibitor). UNT and ET represent untreated and etoposide (25 µM, 6hr treatment) respectively. Immunoblots are representatives of n≥3 independent experiments.

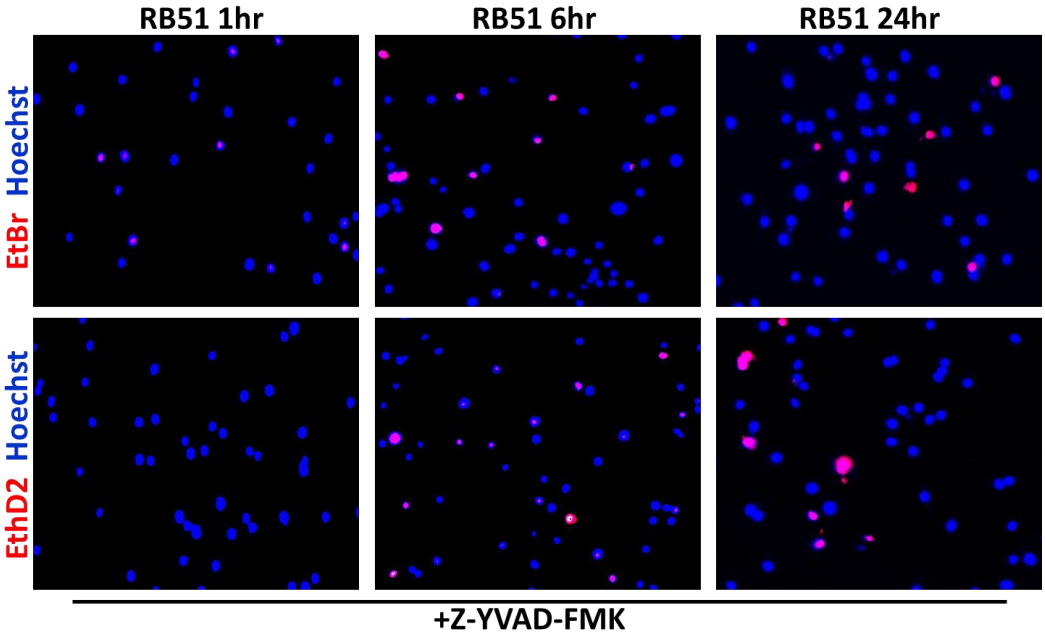

Figure A3: Caspase-1 aids in RB51-induced pore formation. RB51-infected RAW264.7 macrophages treated with Z-YVAD-FMK (20 µM, caspase-1 inhibitor) were stained with the membrane permeable dye Hoechst 33342 (blue) and the membrane impermeant dyes (red), EtBr (MW 394) or EthD2 (MW 1293). Adherent cells were visualized by fluorescence microscopy (100x). Images are representatives of n≥3 independent experiments**.**

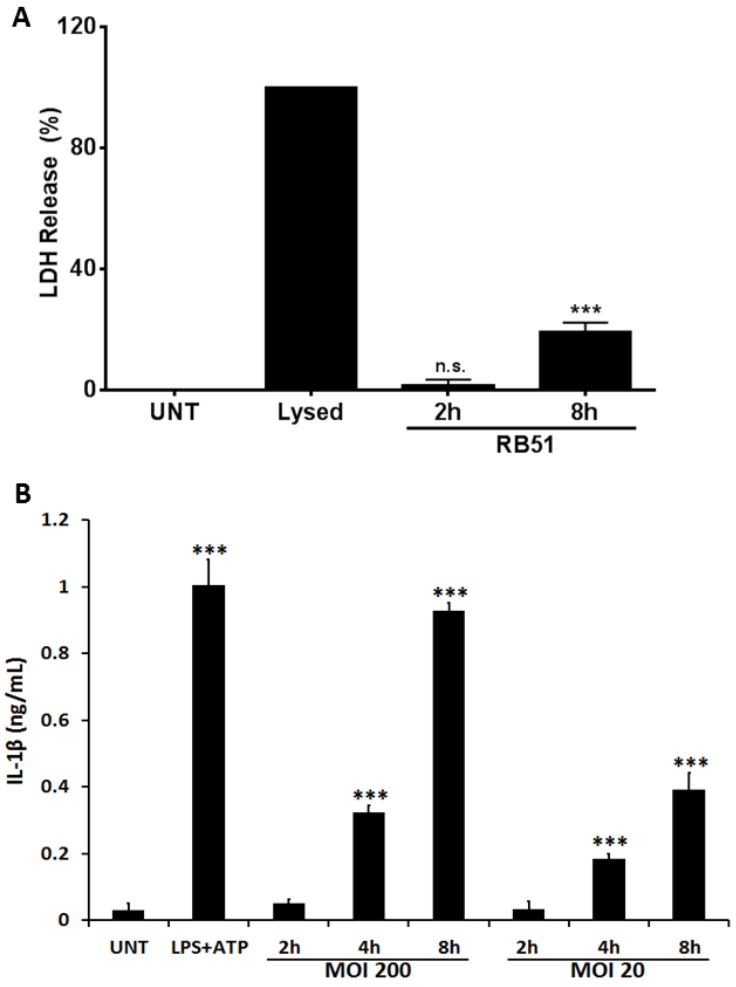

Figure A4: RB51 infection does induce IL-1β production but no cell death. (A) LDH release of RB51-infected (MOI 200) BMDMs. Lysed (Triton-X100 treated) and untreated (UNT) cells served as positive and negative controls respectively. (B) IL-1β levels in macrophages treated with LPS+ATP (200 ng/mL and 1mM respectively) or infected with RB51-infected at MOI 200 or 20. Error bars represent mean ± SD of n≥3 independent experiments. *** represent p-value <0.0001 respectively. n.s. = not significant.

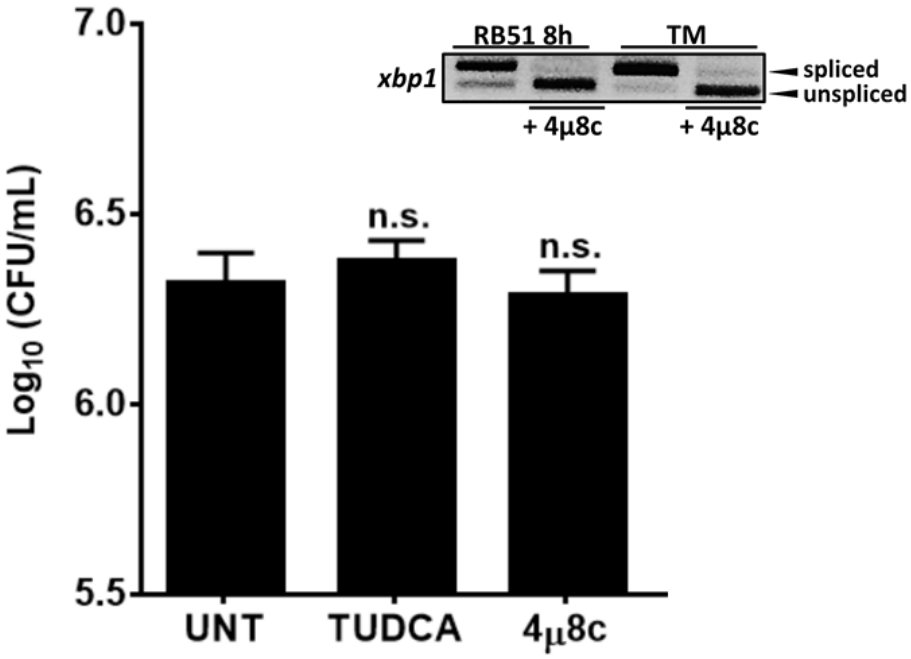

Figure A5: Chemical inhibitors do not affect bacterial uptake. BMDMs were pretreated with TUDCA (chemical chaperone, 300 μM) or 4μ8c (IRE1 inhibitor, 50 μM) for one (1) hour prior to infection. These pretreated BMDMs were then infected with RB51 (MOI 200). One (1) h.p.i BMDMs were lysed to enumerate intracellular CFU. Error bars represent mean ± SD of n≥3 independent experiments. n.s. = not significant. The inset demonstrates the efficacy of 4μ8c inhibiting IRE1-induced *xbp1* splicing in TM (tunicamycin, 10 μg/mL) treated and RB51-infected BMDM.

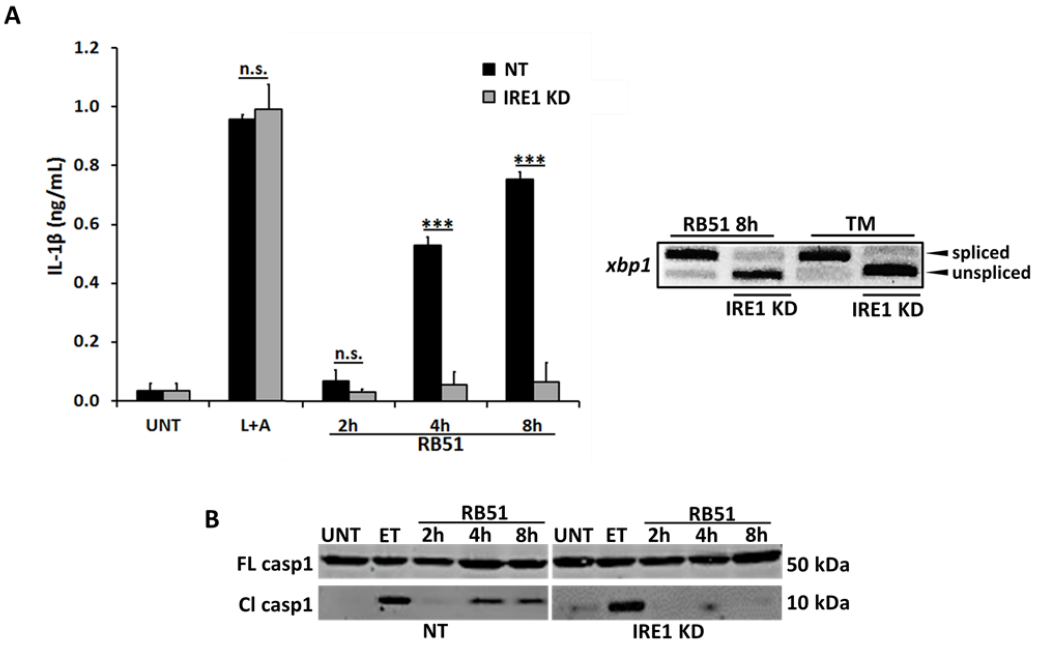

Figure A6: IRE1 is required for RB51-induced inflammasome activation. (A) IL-1β levels and (B) caspase-1 cleavage in RB51-infected non-target (NT) and IRE1KD RAW264.7 macrophages. UNT, L+A, and ET represent untreated, LPS+ATP (positive control for IL-1β 200 ng/mL and 1 mM), and etoposide (positive control for caspase-2 activation and Bid truncation, 25 µM) respectively. Error bars represent mean ± SD of n≥3 independent experiments. *** represent p-value <0.0001, n.s. = not significant. Immunoblots in (B) are representative of n≥3 independent experiments that were performed and imaged in parallel with identical parameters using a LiCor Odyssey imaging system. Full length caspase-1serve as loading controls.

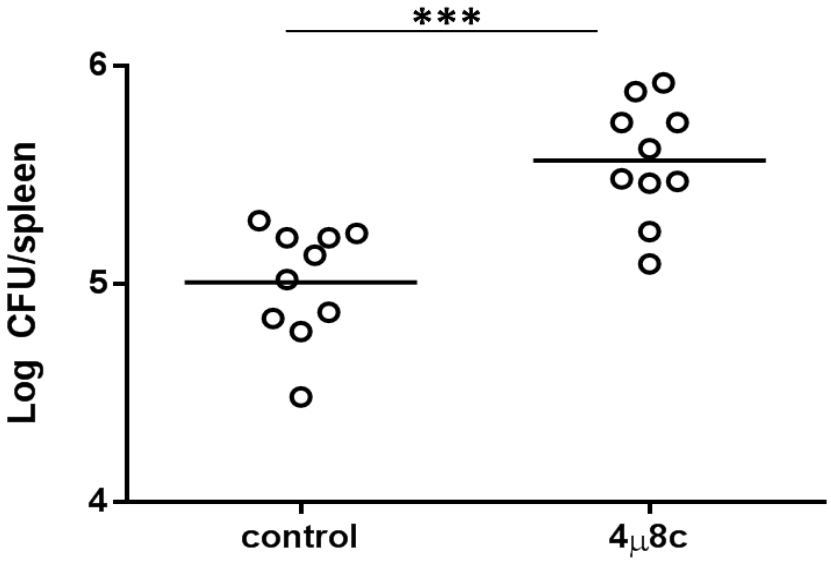

Figure A7: IRE1 inhibition decreases bacterial killing *in vivo*. Mice were intraperitoneally (i.p.) injected with *Brucella abortus* RB51 (CFU 1 x 10^8). Mice were treated with 5% DMSO (n = 10) or 4μ8c (n = 10) on day 0 – 3 post infection. The spleens were collected 3 days post infection and bacterial numbers (CFU/mL) were measured. The data were pooled from 2 separate experiments. *** represent p-value <0.0001.

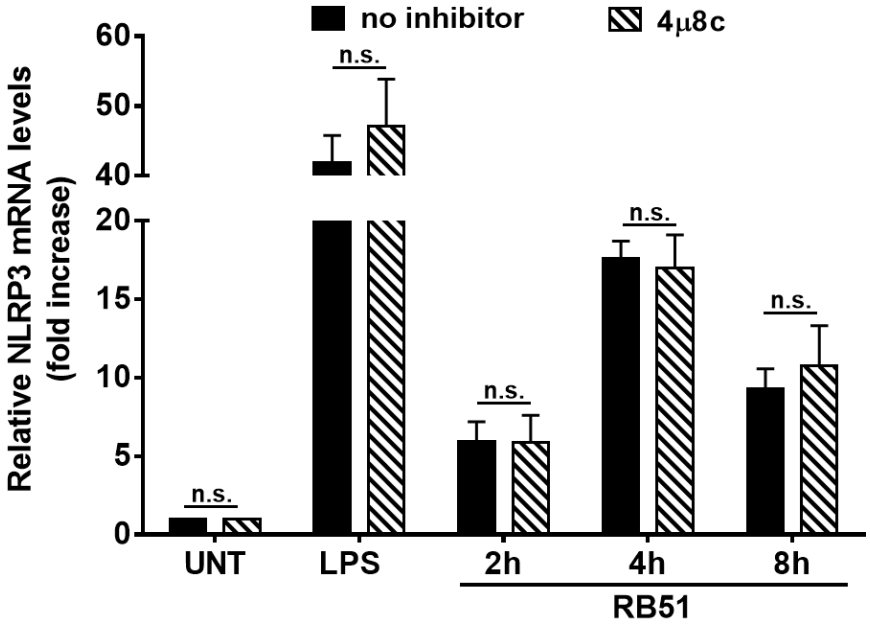

Fig. A8: IRE1 inhibition does not affect priming. qPCR analysis of NLRP3 transcript levels RB51-infected BMDMs in absence or presence of 4μ8c.

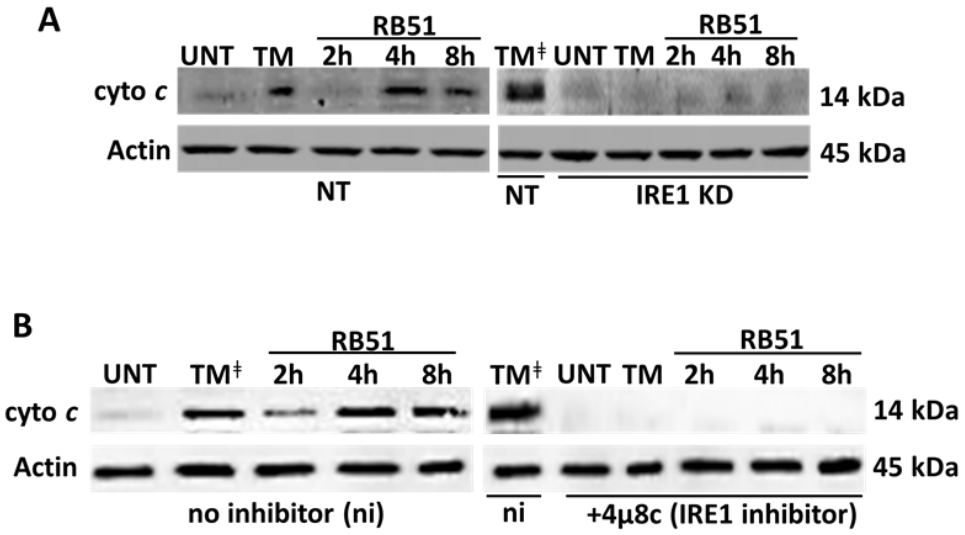

Figure A9: IRE1 is required for RB51-induced cytochrome *c* release. Immunoblot analysis of cytochrome *c* (cyto *c*) in cytosolic extracts from RB51-infected BMDMs in (A) non-target or IRE1 KD RAW264.7 macrophages or in (B) the absence or presence of 4μ8c (IRE1 inhibitor, 50 μM) – TM‡ denotes the same control TM-treated sample. The blots were probed with anti-actin antibody as a loading control. Immunoblots are representative of n≥3 independent experiments that were performed and imaged in parallel with identical parameters using a LiCor Odyssey imaging system. UNT and TM represent untreated and tunicamycin (10 μg/mL, positive control for ER stress activation respectively.

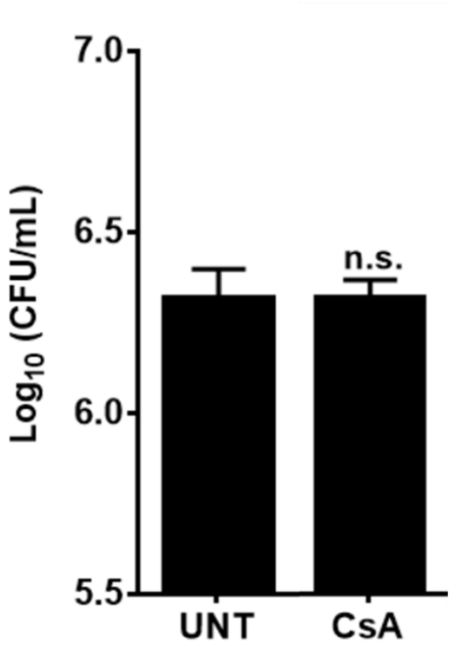

Figure A10: Cyclosporin A treatment has no effect on bacterial uptake. BMDMs were pretreated with cyclosporin A (CsA, inhibitor of MPTP opening 10 μM) for one (1) hour prior to infection. These pretreated BMDMs were then infected with RB51 (MOI 200). One (1) h.p.i BMDMs were lysed to enumerate intracellular CFU. Error bars represent mean ± SD of n≥3 independent experiments. n.s. = not significant

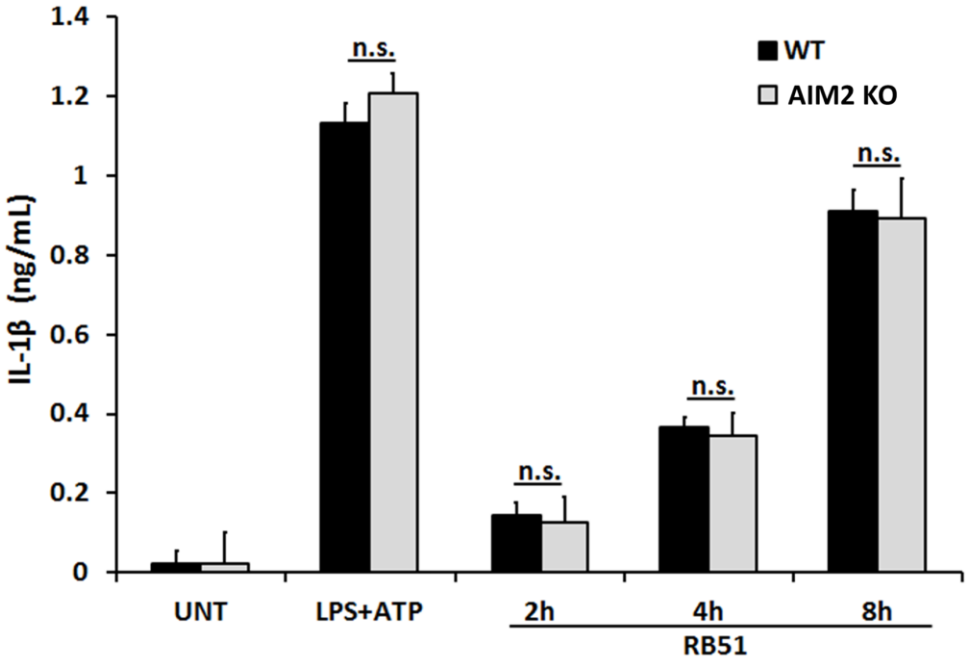

Figure A11: AIM2 is not required for ER stress-induced IL-1β production. ELISA analysis of IL-1β levels in the supernatant of WT and *aim2*$^{-/-}$ RB51-infected BMDMs. Error bars represent mean ± SD of n≥3 independent experiments. n.s. = not significant. UNT (untreated) and LPS+ATP (trigger of IL-1β production, 200ng/mL and 1mM) respectively.

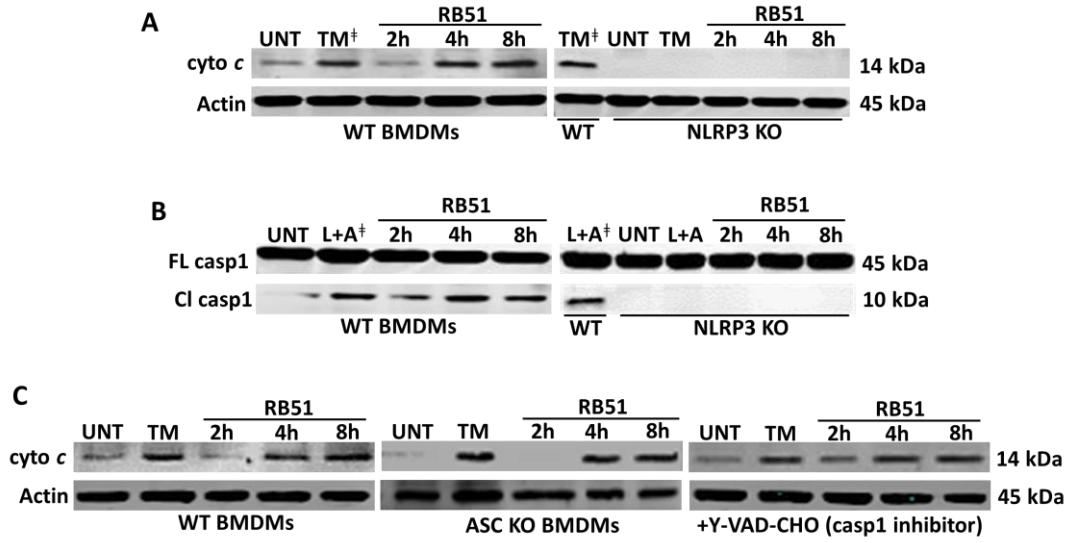

Figure A12: NLRP3, not ASC or caspase-1, is essential for RB51-induced mitochondrial dysfunction. (A) Immunoblot analysis of cytochrome *c* (cyto *c*) in cytosolic extracts from RB51-infected WT and *nlrp3*$^{-/-}$ BMDMs – TM‡ indicates duplicate lanes of the same sample. (B) Immunoblot analysis of caspase-1 in RB51-infected WT and *nlrp3*$^{-/-}$ BMDMs – L+A‡ indicates duplicate lanes of the same sample. (C) Immunoblot of cytochrome c in WT, *asc*$^{-/-}$, and Y-VAD-CHO (caspase-1 inhibitor, 2 μM) treated BMDMs. Actin and full length (FL) caspase-1 serve as a loading control. The cleaved active form (Cl) was detected on the same blot as FL.

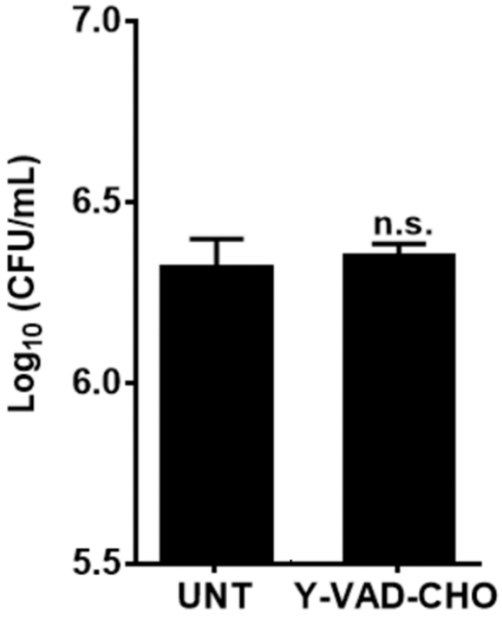

Figure A13: Inhibition of caspase-1 has no effect on bacterial uptake. BMDMs were pretreated with Z-YVAD-CHO (caspase-1 inhibitor, 2 µM) for one (1) hour prior to infection. These pretreated BMDMs were then infected with RB51 (MOI 200). One (1) h.p.i BMDMs were lysed to enumerate intracellular CFU. Error bars represent mean ± SD of n≥3 independent experiments. n.s. = not significant

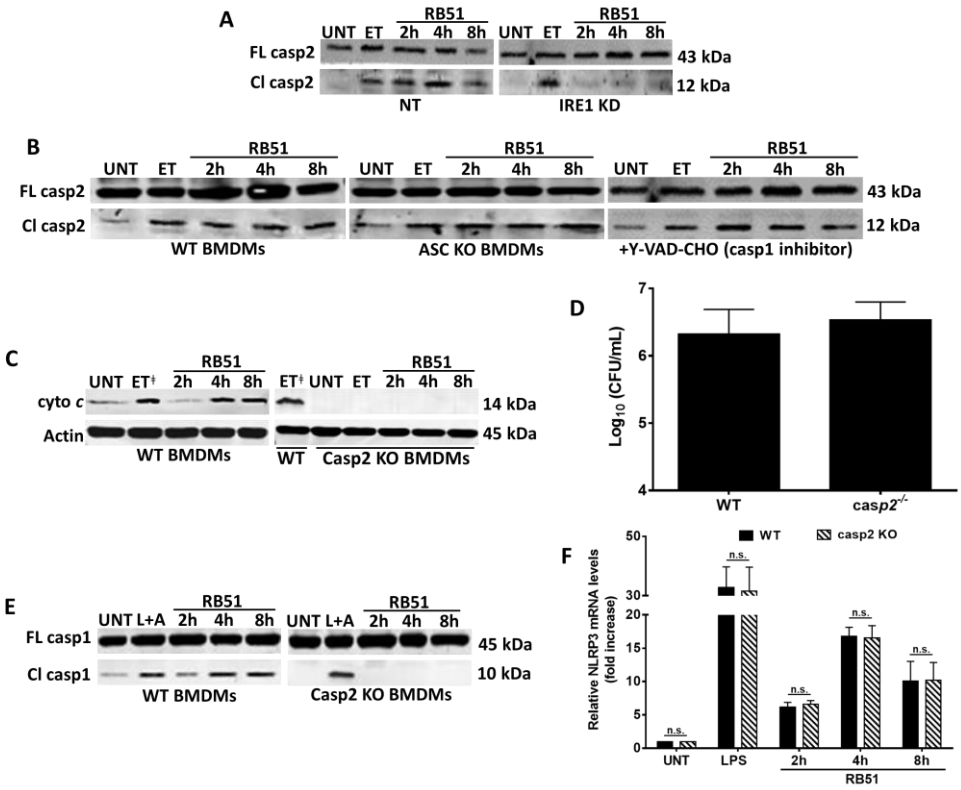

Figure A14: Caspase-2 triggers mitochondrial damage via IRE1 and NLRP3. Caspase-2 activation in (A) non-target (NT) and IRE1 KD or (B) WT, *asc*$^{-/-}$, and Y-VAD-CHO (caspase-1 inhibitor, 2 μM) treated BMDMs. (C) cytochrome c release in WT and *casp2*$^{-/-}$ BMDMs infected with RB51. (D) Bacterial uptake in WT and *casp2*$^{-/-}$ BMDMs 1 hour post infection. (E) Immunoblot of caspase-1 cleavage (activation) in WT and *casp2*$^{-/-}$ BMDMs infected RB51. UNT, ET, and L+A represent untreated, etoposide (inducer of caspase-2 activation, 25 μM), and LPS+ATP (trigger of IL-1β production, 200ng/mL and 1mM) respectively. (F) qPCR analysis of NLRP3 transcript levels RB51-infected WT and *casp2*$^{-/-}$ BMDMs. Immunoblots are representative of n≥3 independent experiments that were performed and imaged in parallel with identical parameters using a LiCor Odyssey imaging system. Actin and full length (FL) caspase-2 serve as loading controls.

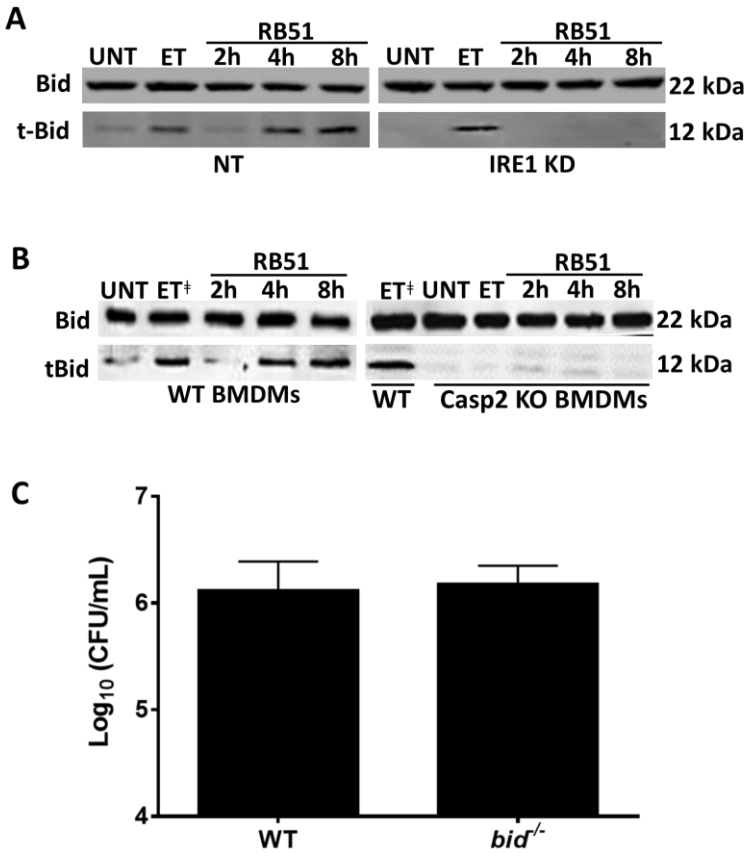

Figure A15: ER stress-induced caspase-2 mediates Bid truncation. Immunoblot analysis of Bid truncation in (A) non-target and IRE1KD RAW264.7 macrophages or (B) WT and *casp2*$^{-/-}$ BMDMs infected with RB51 – ET‡ identifies duplicate lanes of the same sample. UNT and ET represent untreated and etoposide (inducer of caspase-2 activation, 25 µM) respectively. (C) Bacterial uptake in WT and *bid*$^{-/-}$ BMDMs 1 hour post infection. Immunoblots are representative of n≥3 independent experiments that were performed and imaged in parallel with identical parameters using a LiCor Odyssey imaging system. Full length (FL) Bid serves as loading controls.

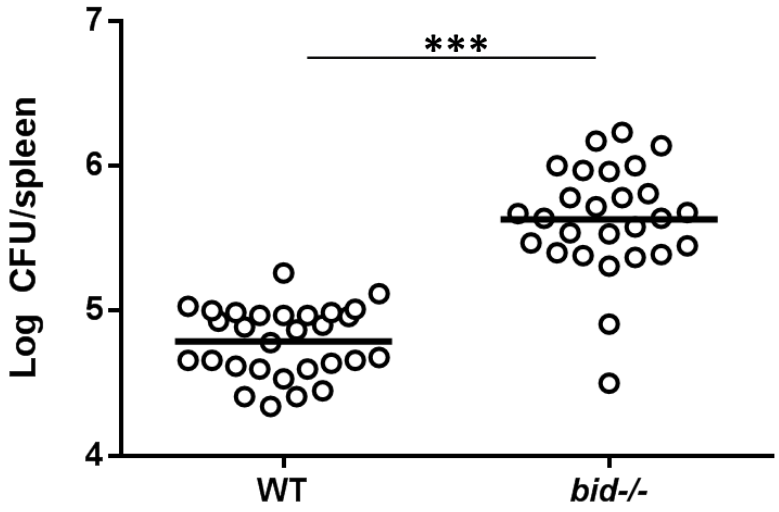

Figure A16: Bid is required for bacterial killing *in vivo*. WT (n=29) and *bid*$^{-/-}$ (n = 30) mice were intraperitoneally (i.p.) injected with *Brucella abortus* RB51 (CFU 1 x 10^8). The spleens were collected 3 days post infection and bacterial numbers (CFU/mL) were measured. The data was pooled from 2 separate experiments. *** represent p-value <0.0001.

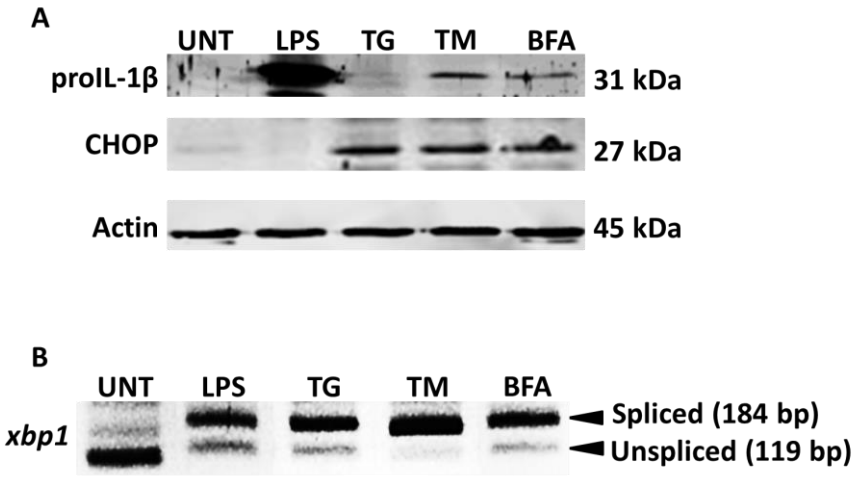

Figure A17: ER stress triggers weak priming of proIL-1β. (A) ProIL-1β and (B) *xbp1* splicing in BMDMs after 4 hour treatment with LPS, as well as ER stress inducers thapsigargin (TG, 10 μM), tunicamycin (10 μg/mL), and brefeldin A (BFA, 20 μM). CHOP serves as a marker of ER stress and actin serves as a loading control. Immunoblots in (A) are representative of n≥3 independent experiments that were performed and imaged in parallel with identical parameters using a LiCor Odyssey imaging system.

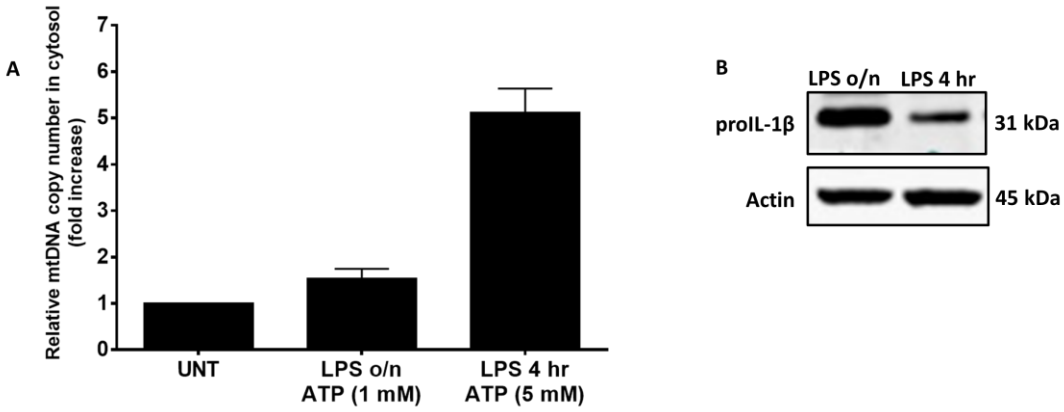

Figure A18: Amount of stress determines route of inflammasome activation. (A) Amount of mtDNA released into the cytosol when treated with two different L+A treatment protocols. (B) Immunoblot of proIL-1β protein levels in cell treated with LPS (200 ng/ml) overnight (o/n) or for 4 hrs prior to ATP treatment.

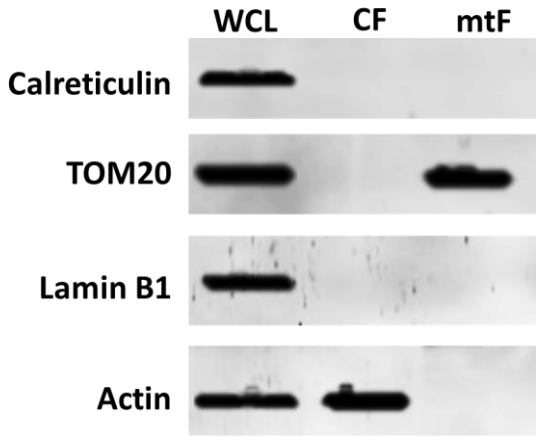

Figure A19: Purity of mitochondrial fraction. Whole Cell lysate (WCL), cytosolic fraction (CF), and mitochondrial fraction (mtF) are assessed for the presence of different cellular markers: Calreticulin (ER marker), TOM20 (mitochondrial marker), Lamin B1 (nuclear marker), and Actin (cytosolic marker).

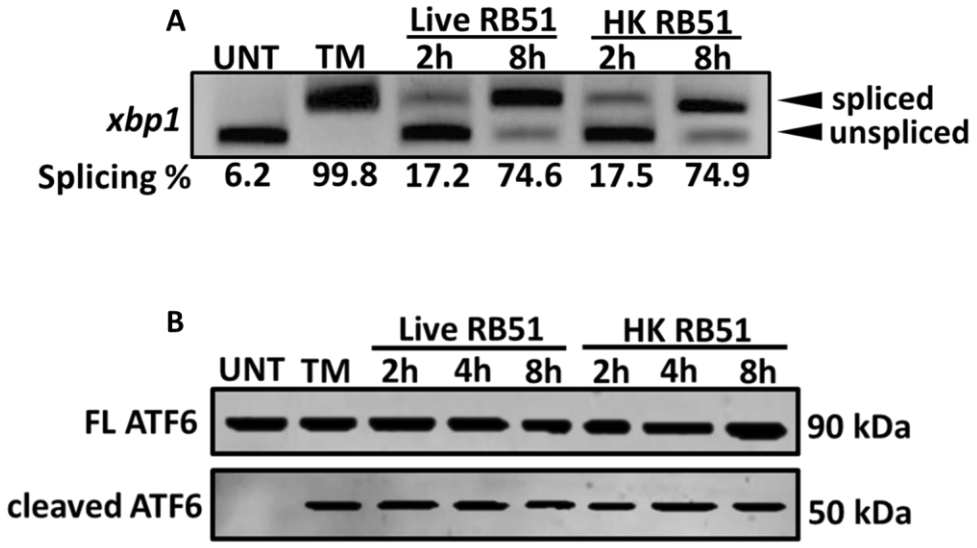

Figure A20: Both Live and HK RB51 induce IRE1 and ATF6 activation. (A) *xbp1* splicing, in Live and HK RB51-infected (MOI 20) BMDM**.** qRT-PCR samples were treated with PstI to distinguish between spliced (184 bp) and unspliced variants (119 bp following PstI digestion). (B) Immunoblot of ATF6 cleavage in Live and HK RB51-infected BMDM. UNT and TM represent untreated and tunicamycin (10 µg/mL, positive control for ER stress activation).

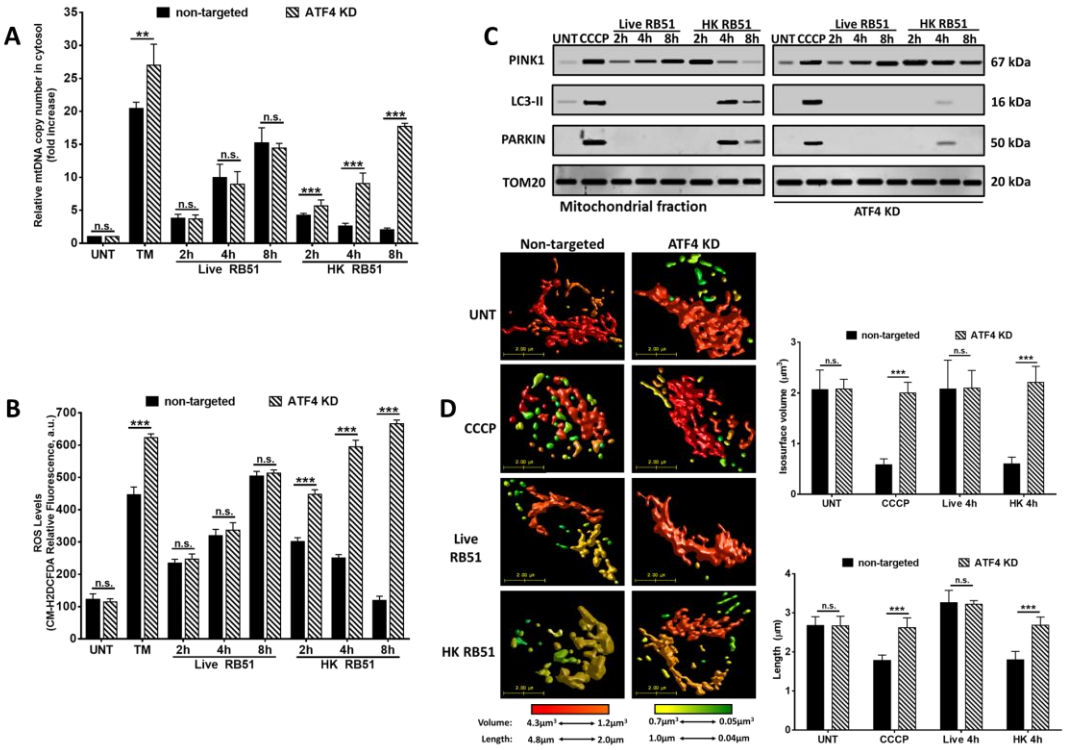

Figure A21: Deficiency in ATF4 leads to increased mitochondrial damage. (A) Amount of mtDNA released into the cytosol by Live and HK-infected BMDM in the presence of non-target or ATF4 specific siRNA. (B) CM-H2DCFDA was used to measure ROS levels in non-target or ATF4 siRNA treated BMDM infected with Live and HK-RB51. (C) Immunoblot of mitophagy markers PINK1, LC3-II, and Parkin in the mitochondrial fraction of CCCP and Live/HK-infected BMDM in the presence of non-target or ATF4 siRNA. (D) 3-D reconstruction and quantification of the mitochondrial network labeled with TOM20 (mitochondrial marker, outer membrane protein) with or without ATF4 siRNA in CCCP and Live/HK-infected BMDM. Colors represent the size of the fragments within the network. Error bars in (A, B, and D) represent mean ±SD of n≥3 independent experiments. ** and *** represent p-values <0.001 and <0.0001 respectively. n.s. = not significant. UNT, CCCP, and TM represent untreated and Carbonyl cyanide m-chlorophenyl hydrazine (20 μM, positive control for mitophagy induction), and tunicamycin (10 μg/mL, positive control for ER stress-induced mitochondrial damage).

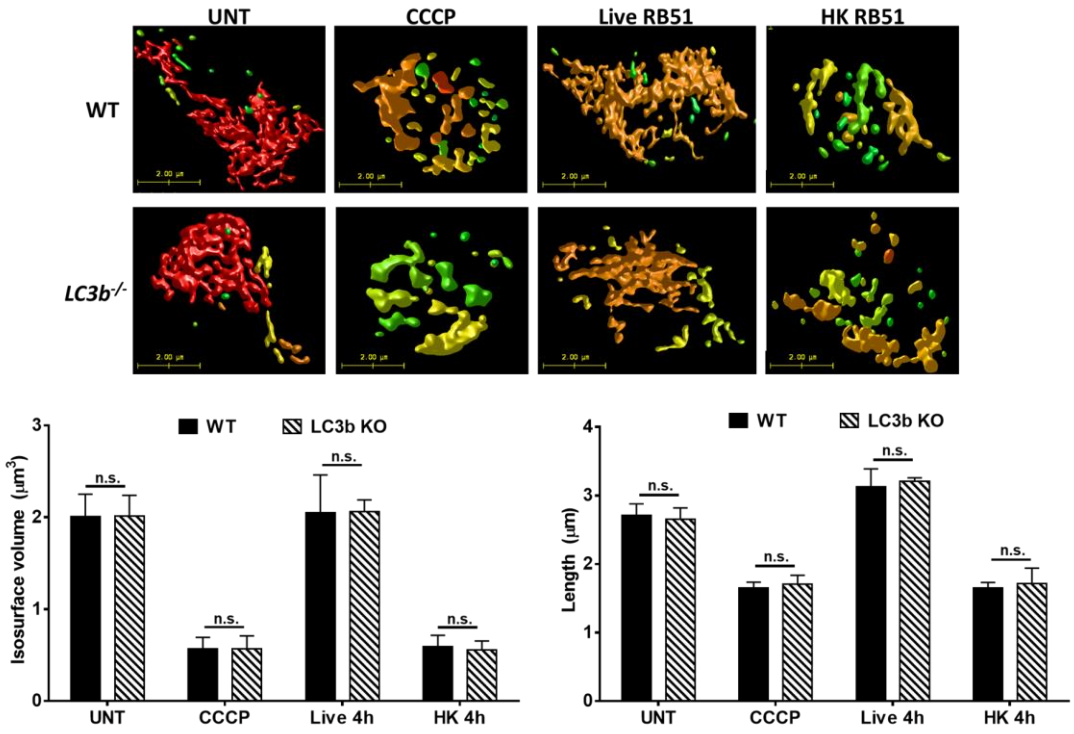

Figure A22: LC3b deficiency does not prevent mitochondrial fragmentation. 3-D reconstruction and quantification of the mitochondrial network labeled with TOM20 (mitochondrial marker, outer membrane protein) in CCCP and Live/HK-infected WT or *lc3b*$^{-/-}$ BMDM. Colors represent the size of the fragments within the network. Error bars in represent mean ±SD of n≥3 independent experiments where n.s. = not significant. UNT and CCCP, represent untreated and Carbonyl cyanide m-chlorophenyl hydrazine (20 µM, positive control for mitophagy induction).

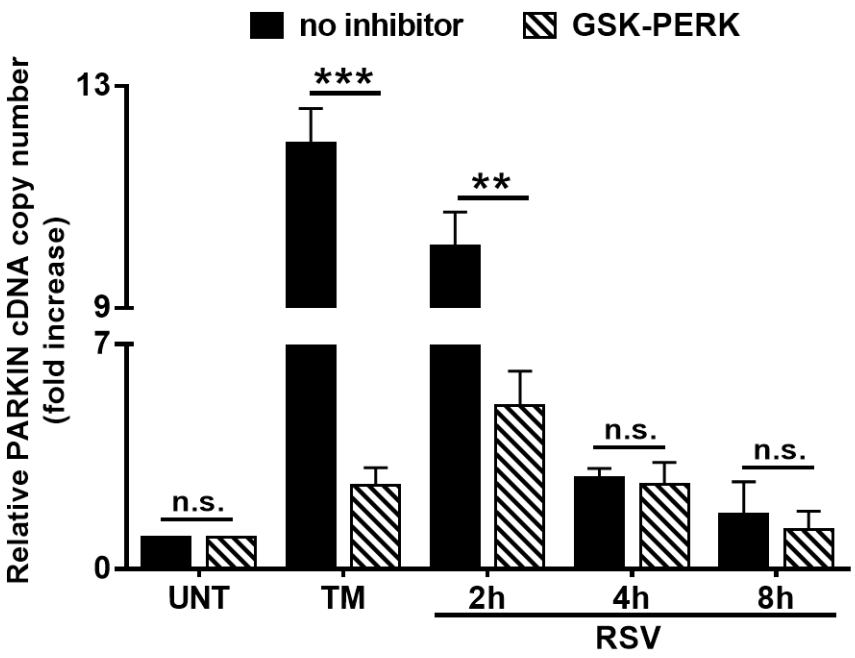

Figure A23: PERK inhibition decreases Parkin transcription in RSV-infected BMDM. qPCR analysis of Parkin transcription during RSV BMDM infection (MOI 1) in the absence or presence of GSK-PERK (GSK2606414, 5 µM). Tunicamycin (TM) serves as a positive control for PARKIN induction. Error bars represent mean ± SD of n≥3 independent experiments. ** represents p-values of <0.001, n.s. = not significant.

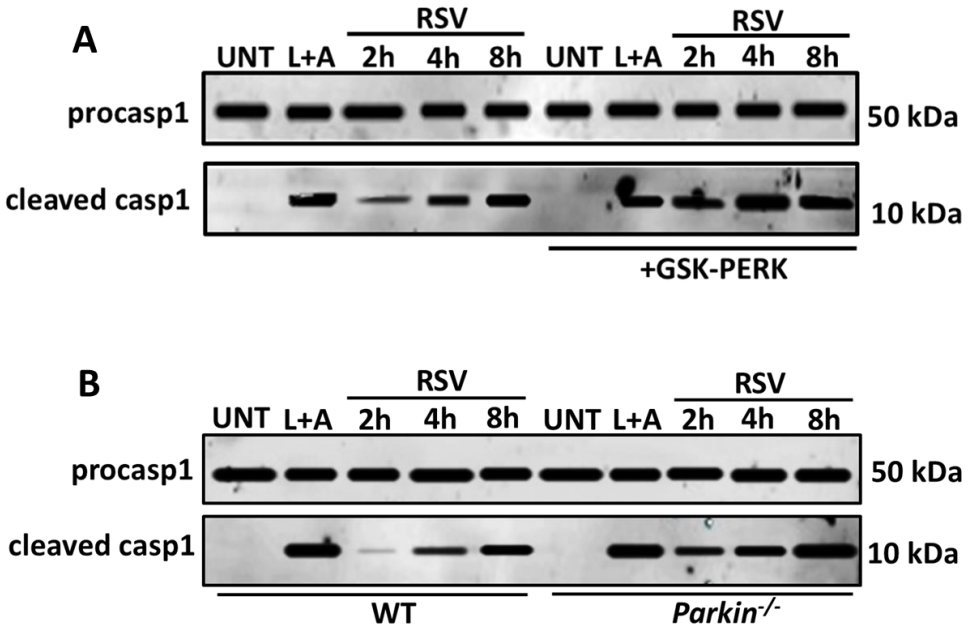

Figure A24: PERK and Parkin suppress RSV-induced caspase-1 activation. Caspase-1 cleavage during RSV (MOI 1) infection (A) in absence or presence of GSK-PERK (5 μM) or (B) WT and *parkin*$^{-/-}$ BMDM. Immunoblots in (A) and (B) are representative of n≥3 independent experiments performed and imaged using a LiCor Odyssey imaging system. UNT and L+A represent untreated and LPS+ATP (200 ng/mL and 1mM respectively; positive control for inflammasome activation).

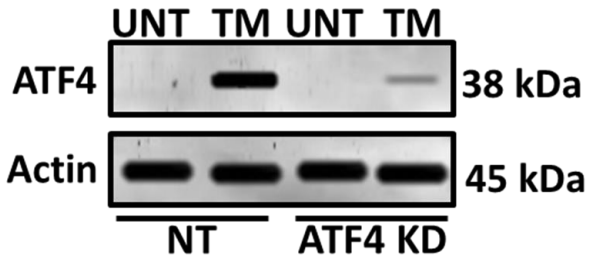

92.2% KD efficiency in n≥3

Figure A25: ATF4 knockdown efficiency in BMDM. Non-target and ATF4 siRNA BMDM were treated with TM to induce ATF4. Knockdown of ATF4 was assessed during each experiment and percent of knockdown efficiency was normalized to Actin. Immunoblot is representative of n≥3 independent experiments performed and imaged using a LiCor Odyssey imaging system.

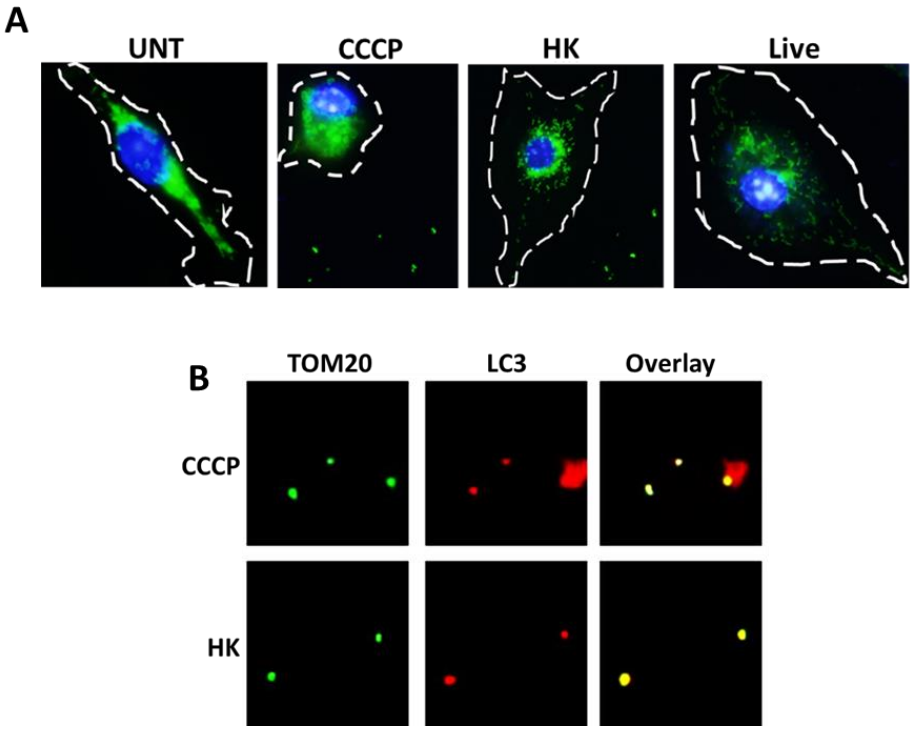

Figure A26: HK-infected BMDM release mitochondria into media. (A) BMDM were immunostained with TOM20 (mitochondrial marker) and DAPI (nuclear marker). Cells were counterstained with Phallodin to determine the outline of the cell (denoted by white dashed line). (B) Extracellular mitochondrial fragments from CCCP treated and HK-infected (MOI 20) BMDM were stained with TOM20 and LC3 (autophagy marker). (All images in A-C are representative of n≥3 independent experiments.

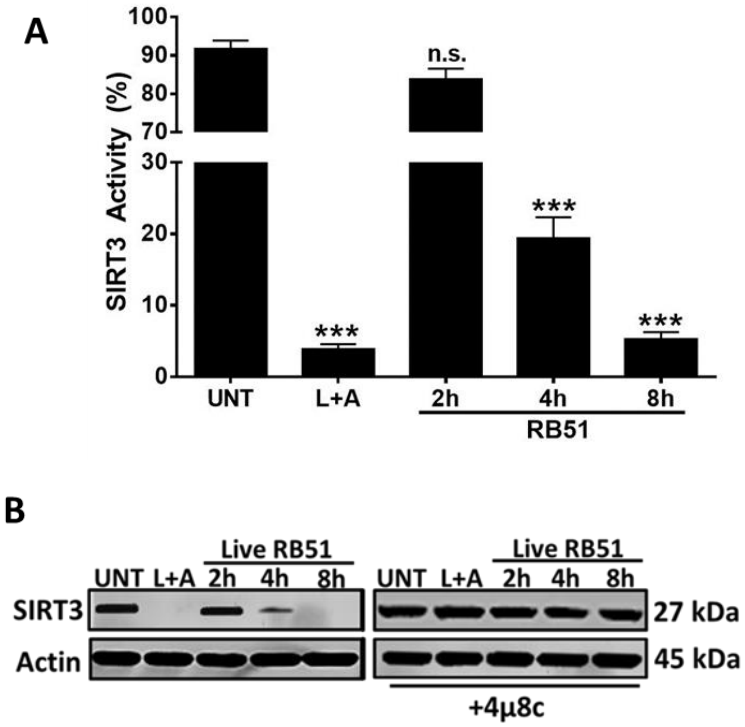

Figure A27: Live RB51 induces Sirt3 degradation. (A) Lysates of Live-infected BMDM were used to measure Sirt3 activity via fluorescence. Percent activity was determined by comparing infection fluorescence values to untreated fluorescence values. (B) Immunoblot of Sirt3 in L+A treated or Live infected BMDM in the presence or absence of Epoximicin (proteasome inhibitor, 5 μM) or 4u8c (IRE1 specific inhibitor, 50 μM. Immunoblots are representative of n≥2 independent experiments performed and imaged in parallel with identical parameters using a LiCor Odyssey imaging system.

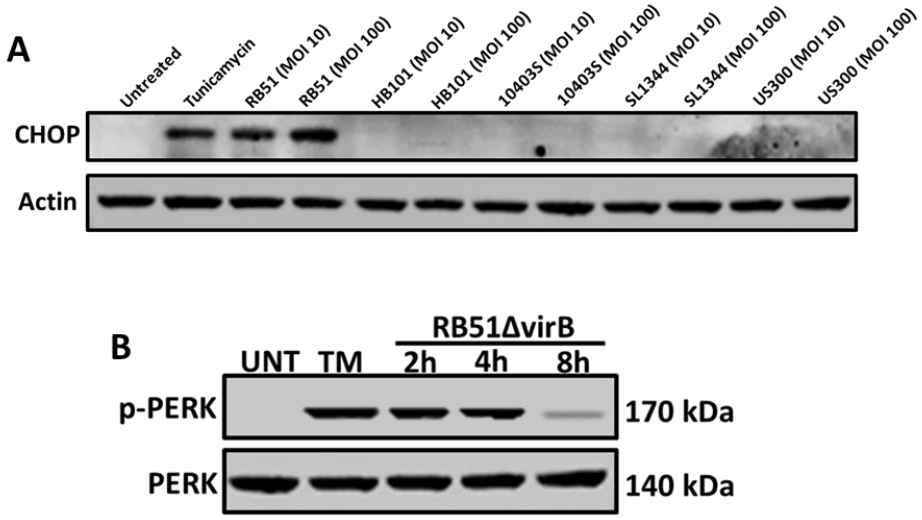

Figure A28: Secretion system not viability mediates PERK activation. (A) Immunoblot of CHOP in the presence of *Brucella* (RB51), *E. coli* (HB101), *Listeria*(10403S), *Salmonella* (SL1344), and MRSA (US300). Tunicamycin (TM) serves as a positive control for CHOP induction. (B) PERK phosphorylation in RB51ΔvirB-infected (Type 4 secretion system mutant, MOI 20) BMDM. PERK and TM served as the loading and positive controls respectively. Immunoblots are representative of n≥3 independent experiments performed and imaged in parallel with identical parameters using a LiCor Odyssey imaging system.